united nations
educational, scientific
and cultural
organization

international atomic
energy agency

the
abdus salam
international centre for theoretical physics

SMR.1135 - 4

THIRD WORKSHOP ON
THIN FILMS PHYSICS AND TECHNOLOGY
(8 - 24 MARCH 1999)
including
TOPICAL CONFERENCE ON
MICROSTRUCTURE AND SURFACE MORPHOLOGY
EVOLUTION IN THIN FILMS
(24 - 26 MARCH 1999)

"Solar Selective Coatings"

Kasturi CHOPRA
Indian Institute of Technology
Thin Film Laboratory
Department of Physics
Haus Khas
110016 New Delhi
INDIA

These are preliminary lecture notes, intended only for distribution to participants

Reviews of Renewable Energy Resources Volume 2
Edited by M. S. Sodha, S. S. Mathur and M. A. S. Malik
Wiley Eastern Limited, London (1984)

3

Solar Selective Coatings*

K.L. CHOPRA, D.K. PANDYA AND L.K. MALHOTRA

1. INTRODUCTION

The interaction of electromagnetic radiations with matter is determined by the response of its electronic structure and lattice dynamics. The uniqueness of the electronic and lattice structures of a material produces a characteristic

*In collaboration with Drs. G.B. Reddy, S.N. Kumar and K. Muralidharam.

response in the form of its reflectance, transmittance and absorption spectra with an associated frequency dependence (dispersion). Thus, all materials exhibit a sort of natural or intrinsic optical selectivity. The response depth of the interacting radiation depends on its frequency and the optical constants of the medium. In the case of absorbing and/or reflecting media, this depth is confined near the surface/interface of the material. Since the response is due to the optically mismatched interface, a significant change of this response is possible by modifying the interface by adding more interfaces in the form of thin films/coatings/layers (these three words being used interchangeably and synonymously in literature) of other materials. Consequently, the optical properties of a material can be changed and even tailor made to produce literally any desired spectral response. Surfaces, thin films or coatings (single or multilayer) which yield a desired and selective suppression or enhancement of the spectral dependence of reflectance, transmittance or absorptance are termed "selective".

Selective surfaces/films/coatings form the basis of a wide range of very useful optical coatings and interference filters with very precisely defined wavelength regions of transmittance or reflectance. The physics and technology of "optical coatings" is one of the most well established fields, both scientifically and industrially. The energy crisis and, therefore, intensive efforts to find ways and means to convert solar energy efficiently have led to the development of solar selective surfaces/coatings. The primary purpose of these coatings is to provide the useful part of the solar spectrum for conversion by a given device as in the case of solar cells. In the case of photothermal conversion of solar energy, the selective coatings provide high absorptance of the solar spectrum, attended by a low emittance or radiation of the absorbed energy.

The subjects of optical coatings and selective surfaces/coatings are treated in various text books and review articles (Chopra 1969; Heavens 1965; Macleod 1969; Koltun 1981; Agnihotri and Gupta 1981; Chopra and Kaur 1982; Seraphin 1979; Meinel and Meinel 1976; Seraphin and Meinel 1976; Lampert 1979; Pandya and Chopra 1981; Tabor 1967). However, these references do not present a complete and up-to-date review of the rapidly evolving status of the research and development of selective coatings. This review provides a comprehensive status report on the basic understanding, theoretical modelling, technology and applications of a variety of selective coatings.

2. BASIC CONCEPTS

As a result of the interaction of the radiation with the surface or bulk of the material, the incident light is partly reflected (and scattered), partly transmitted and partly absorbed. Since the total energy has to be conserved

$$R_\lambda + T_\lambda + \alpha_\lambda = 1 \qquad (2.1)$$

Here, R_λ, T_λ and a_λ are the total values of reflectance (sum of diffuse and specular), transmittance and absorptance of the interacting material/surface for a given wavelength. The above equation is valid for an optically passive medium at each wavelength and at any temperature. A part of the absorbed energy is radiated and the net energy radiated per unit area by the material surface at a temperature T_1, into an ambient at T_2 is given by the Stefan-Boltzmann law

$$W = \epsilon\sigma(T_1^4 - T_2^4) \tag{2.2}$$

where σ is the Stefan-Boltzmann constant and ϵ is termed as the "effective" thermal emittance (or emissivity, though not an appropriate terminology).

Under the condition of thermodynamical equilibrium, total emitted energy must be equal to the total absorbed energy. This yields the well known Kirchhoff's law

$$\epsilon_\lambda = a_\lambda \tag{2.3}$$

which is valid for every wavelength at a given temperature. If the material or its surface coating is non-transparent ($T_\lambda = 0$), Eqs. (2.1) and (2.3) yield

$$\epsilon_\lambda = a_\lambda = 1 - R_\lambda \tag{2.4}$$

Thus, selectivity in the reflectance spectrum of a material will also be reflected in the selectivity of its absorptance and emittance spectra.

In order to appreciate the requirements of selectivity for utilizing the solar energy, let us examine the solar spectrum. The emission spectrum of the sun outside the earth's atmosphere (AMO) corresponds approximately to that of a black body emitting at 5800 K and is given by Planck's law

$$W_\lambda = \epsilon_\lambda \frac{C_1\lambda^{-5}}{\exp(C_2/\lambda T) - 1} \tag{2.5}$$

where ϵ_λ can be taken equal to unity (the value for a black body) and c_1 and c_2 are constants. The atmosphere of the earth significantly modifies this AMO solar spectrum due to the presence of absorption bands of water vapour, carbon dioxide and ozone. The extent of modification (absorption) is a function of the angle at which radiation is received at the earth's surface. The AM2 solar spectrum incident on the surface of earth at an angle of 60° is shown in Fig. 1. Also shown in this figure are the AM2 spectra at various solar concentrations which would be required to obtain higher absorber temperatures. If we compare this AM2 spectrum with that of a black body held at 100, 300 and 700°C (also shown in Fig. 1), we note the following features:

(1) The solar spectrum is primarily confined to 0.3 to 2.5 μm range.

(2) The emission shows a peak at $\lambda_{max} = \frac{2898}{T}$ microns (called Wien's law).

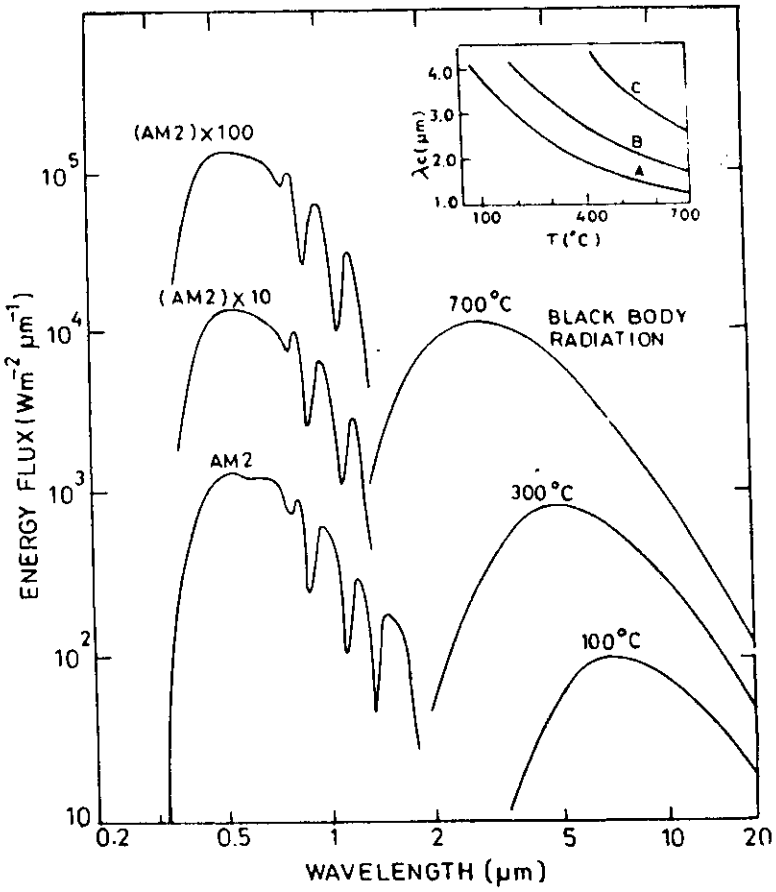

Fig. 1. Spectral distribution of solar flux at the surface of the earth under AM2 conditions for various solar concentration factors compared to thermal flux radiated by a black body at 100, 300 and 700°C. The inset shows the variation of cut-off wavelength as a function of absorber temperature and solar concentration. $A = 1$ sun; $B = 10$ suns and $C = 100$ suns.

(3) About 25% of the emitted energy is below λ_{max} and 75% above it. Only 1% of the total energy is emitted at wavelength below 0.5 λ_{max}.

(4) There is very little overlap between the solar spectrum and that emitted by a terrestrial source at a lower temperature. The wavelength, called the cut-off wavelength (λ_c), at which solar flux is equal to the radiated flux from a material held at $T°K$ shifts towards shorter wavelengths with increasing temperature and solar concentration as shown in the inset of Fig. 1.

As already pointed out, the ability of a surface or coating to absorb and emit radiations is expressed by the absorptance (α) and emittance (ϵ) parameters respectively. Since, in this review, we are primarily interested in the interaction of the solar spectrum with the surface coatings, it is necessary to define "solar absorptance". The parameter is simply given as the ratio of the absorbed energy flux to that of incident energy flux. Thus,

$$\alpha_s = \frac{\int_{0.3\,\mu m}^{2.5\,\mu m} \alpha(\lambda) I_s(\lambda)\, d\lambda}{\int_{0.3\,\mu m}^{2.5\,\mu m} I_s(\lambda)\, d\lambda} \tag{2.6}$$

Here $I_s(\lambda)$ is the spectral solar irradiance and the limits of integration are confined to the limits of the solar spectrum i.e. 0.3 to 2.5 μm. Since for an opaque body $\alpha(\lambda) = 1 - R(\lambda)$, α_s could be calculated from the R_λ data.

The hemispherical thermal emittance (ϵ_T) is defined as the ratio of the energy radiated per unit area at a given temperature to that radiated by the unit area of a black body surface at the same temperature. Hence

$$\epsilon_T^H = \frac{\int_0^\infty \epsilon(\lambda,T) W_B(\lambda,T)\, d\lambda}{\int_0^\infty W_B(\lambda,T)\, d\lambda} \tag{2.7}$$

Here $\epsilon(\lambda,T)$ is the spectral hemispherical emittance at a temperature T and $W_B(\lambda, T)$ is the black body irradiance at the same temperature T. The practical limits of integration depend on the temperature of the emitting surface. For $T < 1000$ K, practical limits are 0.5 to 50 μm. In the case of an opaque body, $\epsilon(\lambda, T)$ can be replaced by $[1 - R(\lambda, T)]$ and therefore ϵ_T^H could be calculated from the $R(\lambda, T)$ data. It should be noted that $R(\lambda,T)$ is the total (specular + diffuse) reflectance. For convenience, the suffixes in the terms α_s and ϵ_T^H are dropped in the following text.

3. IDEAL SELECTIVE SURFACES

As already pointed out, all materials exhibit some sort of optical selectivity. Which optical property is to be selectively enhanced or suppressed, and in what frequency or wavelength range and to what extent it is desired depends on the application we have in mind. For example, interference filters show very high selectivity of reflectance or transmittance (as the case may be) in a very narrow, or broad range of wavelengths. For thermal energy applications, four types of selective surfaces are of technical interest. The ideal form of selectivity in these cases is shown in Fig. 2.

Type (a) represents a selectively absorbing surface/coating called a "dark mirror" with solar absorptance of unity in 0.3-2.5 μm range and a thermal emittance of zero beyond 2.5 μm. This type of selectivity is ideally suited

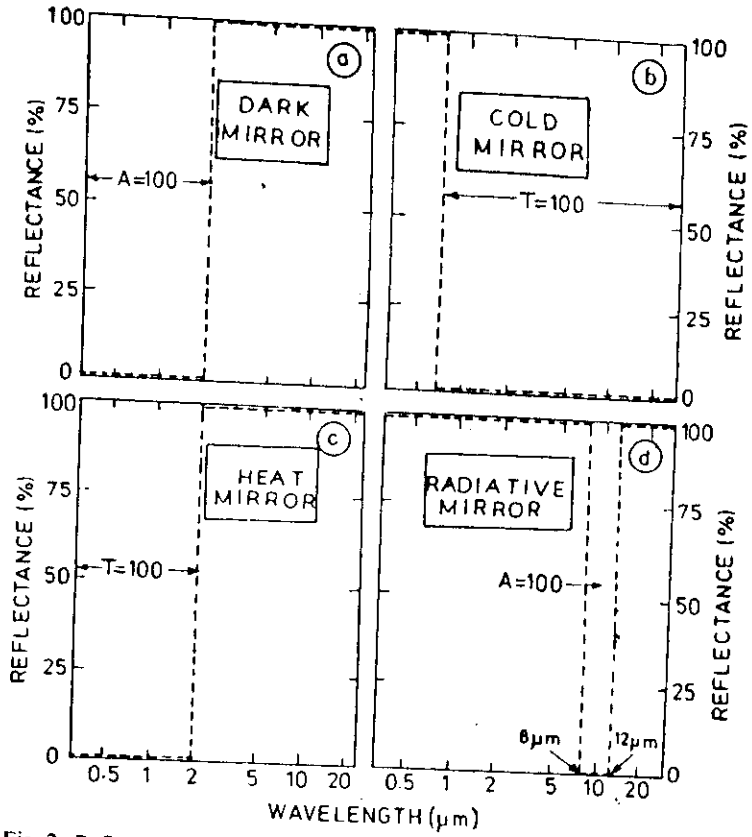

Fig. 2. Reflectance profiles of different ideal selective surfaces: (a) selective absorber; (b) cold mirror; (c) heat mirror; and (d) radiative cooling surface. $A = 100$ and $T = 100$ respectively indicate the wavelength region in which the incident energy is either fully absorbed or fully transmitted.

for conversion of solar energy into thermal energy. Type (b) exhibits unity reflectance in the visible part of the solar spectrum and unity transmittance for wavelengths greater than about 0.8 μm. Such a selective surface is called a "cold mirror" and is commonly used to separate the visible from the IR radiation. The process allows the solar spectrum to be effectively utilized for hybrid photo-voltaic-photothermal conversion. This procedure could also be adopted in a green house, such that the visible radiations are utilized by the plants and the IR is used to heat the environment. Type (c), commonly called a "heat mirror", has a transmittance of unity in the visible part of the solar spectrum and unity reflectance beyond about 0.7 μm. It has a major application in the area of solar architecture designed to keep out the thermal

part of radiation of the solar spectrum (also called passive cooling). In conjunction with a non-selective absorber, the resultant set-up behaves like a "dark mirror". For this application, the heat mirror should have unity transmittance for 0.3 to 2.5 μm and unity reflectance beyond this region. The same heat mirror with λ_c at about 2.5 μm could be used in winter/cold conditions to prevent ambient thermal radiations from escaping through windows (passive heating). Type (d) exhibits zero absorptance between 0.3 to 8 μm, unity absorptance from 8 to 13 μm and zero absorptance from 13 to 50 μm. Such a surface undergoes radiative cooling at or below room temperature by emitting selectively into the ambient (atmospheric window). This process offers interesting possibility of emissive cooling below the ambient temperature.

4. SELECTIVE STRUCTURES

As we will see in the following section, an ideal selectivity of the type described in the preceding cannot be obtained by using a single surface or interface of any known material. In fact, it is essential to use two or more surfaces/interfaces to obtain nearly ideal selectivity. Basically, selective surfaces/coatings/structures can be classified in three groups:

(a) Single interface (or a surface)
(b) Double interface (or a single layer on a substrate)
(c) Multiple interface (or multilayers on a substrate).

Each type has several variations which are described in the following sections.

4.1 Single Interface

(a) *Smooth Surface*: Metal surfaces show high reflectivity in the visible and infrared due to the presence of high concentration of free electrons. The free electron gas exhibits plasma resonance at a frequency

$$\omega_p = \sqrt{\frac{4\pi Ne^2}{m^* \epsilon_\infty}}$$

where N is the carrier concentration, e is the electronic charge, m^* is the electron effective mass and ϵ_∞ is the optical dielectric constant. For $\omega > \omega_p$, the radiation propagates through the medium. The magnitude of the energy reflected at the air/medium interface is given by the well known relation

$$R = \frac{(n-1)^2 + k^2}{(n+1)^2 + k^2} \tag{4.1}$$

For $\omega < \omega_p$, the radiation energy does not propagate through the medium and is completely reflected. Between these two extremes of frequency, the optical behaviour is complex and depends on the details of the electronic band structure of the metal. This point is illustrated in Fig. 3 by the reflectance curves of several metals.

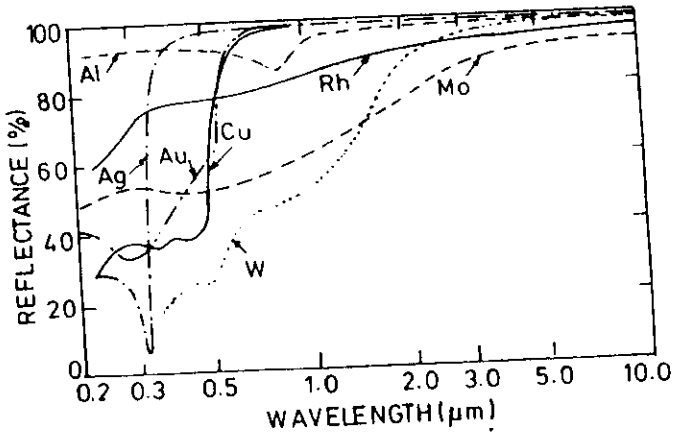

Fig. 3. Spectral reflectance behaviour of polished metal surfaces of different metals showing high reflectivity regions due to plasma resonance (Hahn and Seraphin, 1978).

Knowing the reflectance spectrum (or the corresponding optical constants), the thermal emittance can be calculated. Values of emittance for a number of metals range from 0.02 to 0.08. The emittance of a metal depends on the d.c. resistivity and carrier density (Sievers 1978). For a Drude metal, in the relaxation frequency approximation, the normal emittance is given by

$$\epsilon = \frac{1.269 \times 10^{-2} \rho(T)}{(r_s/\beta)^{3/2}} \tag{4.2}$$

where $\rho(T)$ is the resistivity at temperature T, r_s is the radius of free electron Fermi sphere which gives a measure of the free electron density and β is the linear thermal expansion coefficient. Thus, the emissivity varies linearly with temperature (since the resistivity does so) as shown in Fig. 4.

In the case of semiconductor surfaces, absorption contributions arise from electrons in various bands depending on the photon energy. A typical absorption spectrum is shown in Fig. 5. Its main features are high absorptance above the band gap energy, free carrier absorption at long wavelengths, multiphonon and lattice vibrational mode absorption at longer wavelengths. The band gap absorptance depends on whether the optical transitions are direct or indirect. The infrared transparency region is determined by the strength of the lattice absorption processes. If the plasma resonance condition is satisfied at a certain wavelength, λ_p, high reflectance is observed at wavelengths longer than λ_p. Thus each semiconductor has a distinctive absorption spectrum.

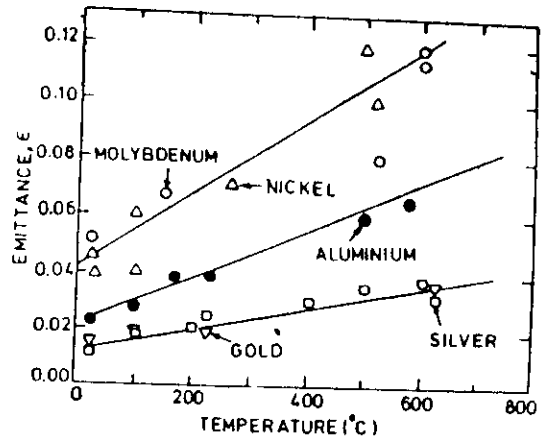

Fig. 4 Experimentally measured variation of emittance with temperature for different metals (Hahn and Seraphin, 1978).

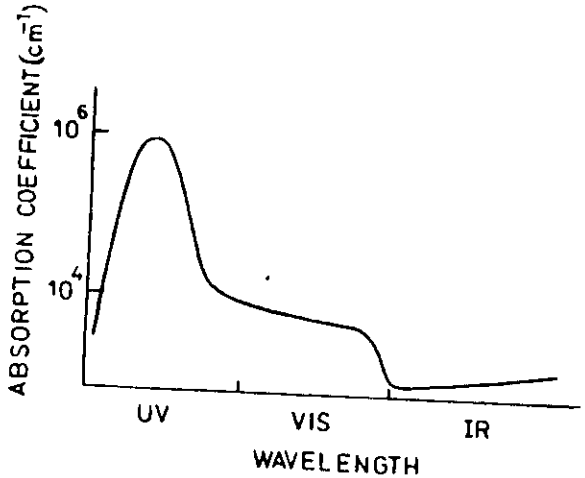

Fig. 5. A typical qualitative variation of absorption coefficient of a semiconductor in different ranges of spectrum.

The absorption in the case of a dielectric surface is due to the band gap transitions (which means near visible and deep UV), electronic polarization (deep UV) and atomic polarization (infrared). Generally speaking, large band gap insulators including optical glasses are highly transparent in the visible with reflectance determined by the refractive index as given by Eq. 4.1. Because of small value of n, and k being zero, the IR reflectance is weak and thus the emittance is high.

We have seen that most single and smooth surfaces exhibit intrinsic optical selectivity of limited technical interest. There are, however, a few examples of useful surfaces. For example HfC and LaB_6 (Meinel and Meinel 1976) show a fairly good selective absorber behaviour (Fig. 6). Increased absorption in such cases is possible by modifying the plasma edge which occurs very early in the solar spectrum. This is achieved by creating internal scattering centres as in MoO_3 (Gesheva et al., 1980, 1981), by hybridization of d band electrons of transition metals with sp electrons of carbon or nitrogen as in HfC (Williams 1957; Allword et al., 1975) and localization of d band electrons by combining with oxygen as in WO_3 and ReO_3 (Feinleib et al., 1968). The shift of the plasma resonance edge is also conveniently achieved by appropriate dopants in degenerate semiconductors as shown in Fig. 7 in the case of Sb-doped SnO_2 films (Shanthi et al., 1981).

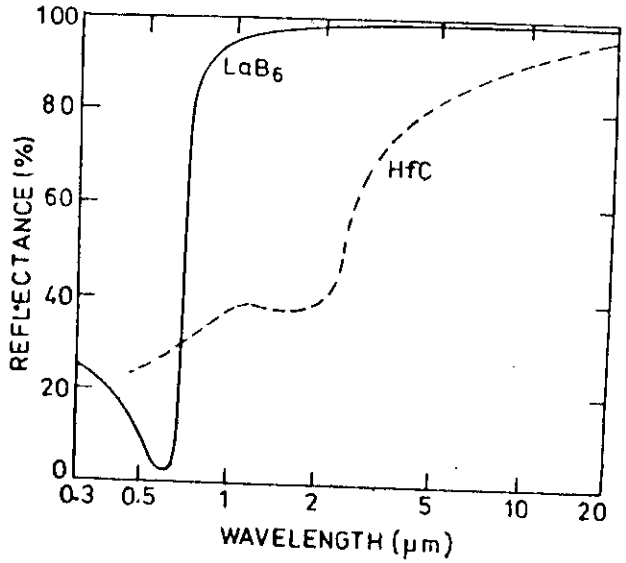

Fig. 6. Measured reflectance profile of LaB_6 and HfC intrinsic selective surfaces.

(b) *Textured Surfaces:* Absorption of a single surface can also be enhanced considerably by texturing a surface (B eucherie 1980) in such a way that multiple reflections take place as shown in Fig. 8. Among the different V grooves, the best shape for multiple reflections is "Gothic Vee" obtained by taking the crest of the groove as centre of the curve of the opposite face. This construction ensures double reflections for all rays including the very oblique ones. A sand blasted surface can also yield multiple reflections. If the texture is dimensionally tailored, spectral selectivity can also be obtained

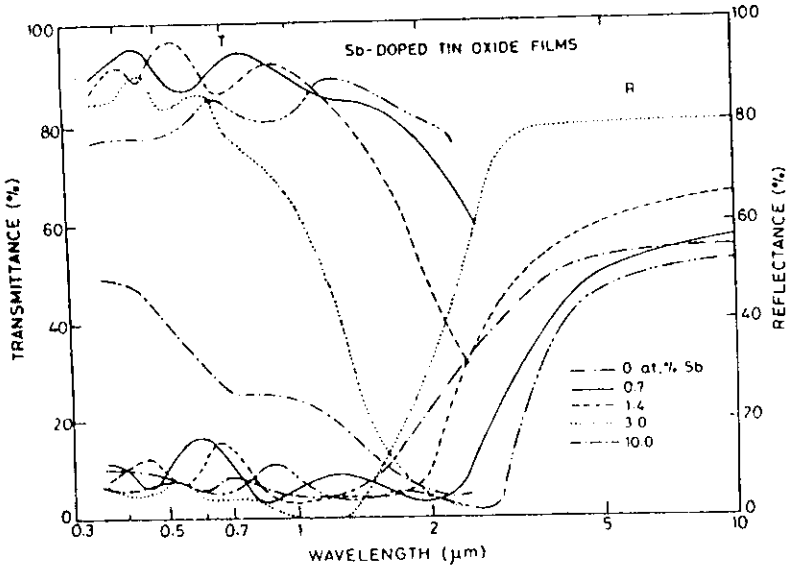

Fig. 7. Reflectance (near normal) and transmittance spectra of antimony doped SnO_2 coating showing the shift of plasma resonance edge with doping concentration (Shanthi et al., 1981).

in normally non-selective surfaces. The enhanced absorptance, α_e, depends on the number (n) of reflections and is given by $\alpha_e = (1 - R^n) = 1 - (1 - \alpha)^n$.

A waveguide method of obtaining selectivity as proposed by Horwitz (1974) is to employ an array of deep holes in a metal. Light of wavelengths greater than the hole diameter will not resolve the holes and hence will see the reflecting surface. Shorter wavelengths will propagate through the holes as in a waveguide.

A dendritic textured surface can be created by employing suitable thin film deposition techniques. Coumo et al. (1975) have deposited tungsten films by CVD process in the form of a dense forest of aligned needles whose diameters are of the order of visible wavelength, with spacings between the needles of several wavelengths. The absorption here is dominated by the geometrical factors. The emittance is the property of the material but it is increased due to increased effective surface area. Other materials like Ni (Grimmer 1978), stainless steel (Beucherie 1980) and Rhenium (Seraphin 1979) with dendritic structures have also been produced.

4.2 Double Interface (Tandem Structures)

By depositing an homogeneous or inhomogeneous thin film/coating of a semiconductor on a metallic substrate, a high level of selectivity can be obtained. It should be pointed out here that the optical properties of thin films

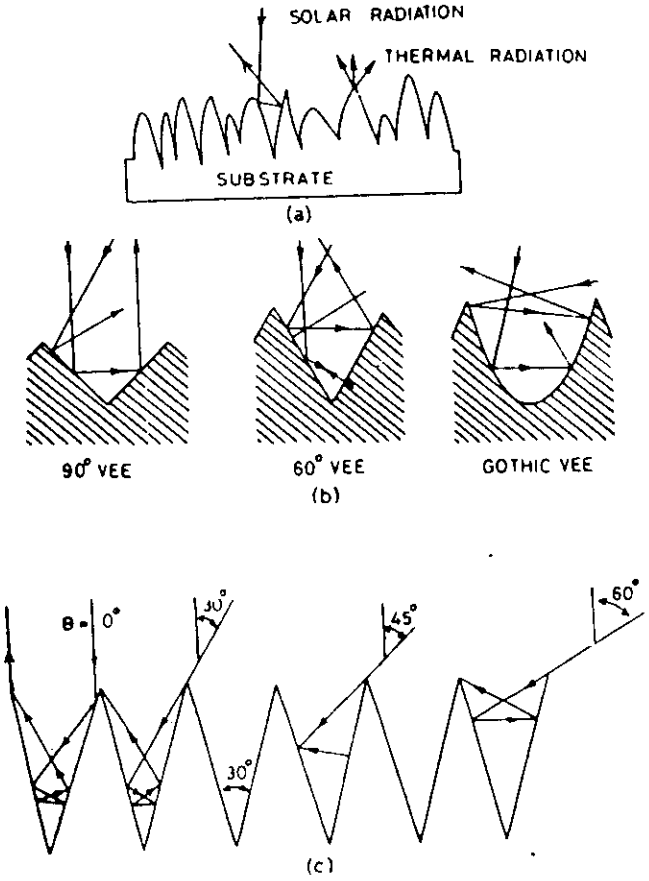

Fig. 8. Schematic diagram of optical trapping: (a) in the random contours of surface roughness; (b) in texturized V-grooves of various shapes, and (c) in 30°-V-grooves as a function of angle of incidence.

are sensitively dependent on microstructure and hence deposition conditions. Therefore, thin-film optical constants rather than those of bulk must be kept in mind for practical structures. Moreover, in the case of ultra-thin films (~20 Å for metals and ~ 100-500 Å for semiconductors), quantum size effects can modify the absorptance of these films considerably due to plasma resonance effects. For example, such effects have been reported in Ag and InSb films (Payan and Rasigni 1964; Giaquinta and Mancini 1978).

Let us now examine the various combinations of coatings on surfaces.

(a) *Semiconductor/Metal Structure*

In this "tandem" structure the absorption is provided by the homogeneous semiconducting coating which is transparent in IR so that long wavelength radiations see through and get reflected from the metallic substrate. Semiconductors having band gap in the range 0.2 to 0.9 eV are best suited as absorbers. This condition is satisfied by the elemental semiconductors Ge and Si and several transition metal carbides, nitrides, oxides and sulphides.

Due to high refractive index of the semiconductor film of appropriate band gap, the tandem structure suffers from high reflection losses. The refractive index and the band gap E_g are related by an empirical relation

$$n^4 E_g \simeq 77 \tag{4.3}$$

The reflection losses are given by Eq. 4.1. Ritchie et al. (1977) have calculated the integrated solar reflectance for normal incidence as a function of n and k. These results are shown in Fig. 9. It is clear from these results that ideal absorber coating should have low (< 1.5) n along with moderate k (0.2 to 0.8) values. Most dielectrics and metals satisfy this requirement of n but dielectrics have low k (< 0.2) and metals have high k (> 0.8) values. On the other hand, many semiconductors have a moderate k but a high n (> 2). Thus, naturally occurring materials do not satisfy optimum conditions of n and k for an ideal absorber.

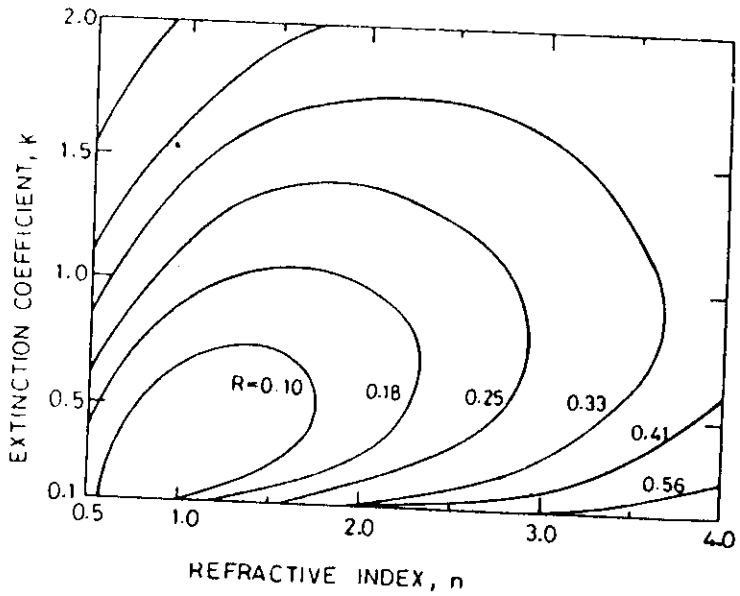

Fig. 9. Normal incidence solar averaged reflectance (R) contours as a function of real and imaginary parts of refractive index, n and k for a thick film of uniform thickness on aluminium substrate (Ritchie and Window, 1977).

As shown in Fig. 4 the emittance of metals increases linearly with temperature. The metal/semiconductor tandem structure also shows a similar variation of the emittance with temperature as shown in Fig. 10 for different metals coated with the same thickness of a semiconductor having ideal n and k values (Trotter et al., 1979). The solid lines further show that there exists a minimum emittance value that can be obtained for such a tandem structure at a particular temperature.

Among the practical tandem absorbers are Fe_2O_3 on stainless steel, nickel oxide on galvanized steel, spray pyrolysed blacks of Co and Cu on stainless steel, magnetron sputtered carbon/stainless steel/Cu films on glass, sputtered

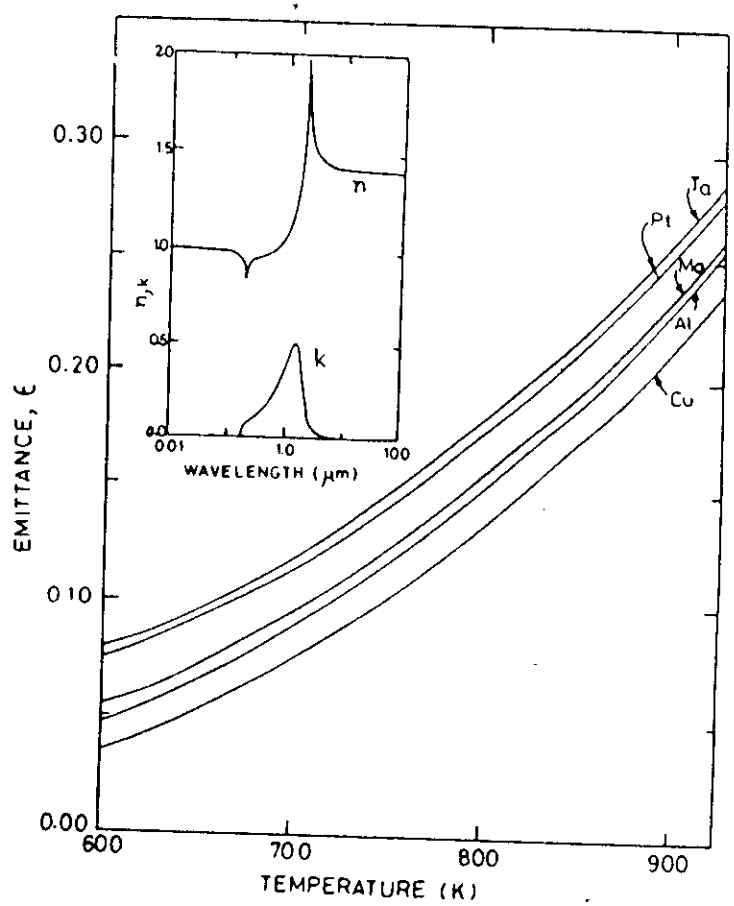

Fig. 10. Variation of emittance with temperature for ideal selective absorber coated metal substrates. Inset shows the n and k variation for the material of the ideal selective absorber (Trotter and Slovers, 1979).

metal carbides and nitrides on metal substrates, electroplated and chemically converted sulphides of copper, cobalt and nickel on metal substrates. The α and ϵ values of these structures are listed in Table 1. The absorption in these structures is mainly intrinsic. As an example of an intrinsic absorption, Fig. 11 shows the reflectance spectrum and an Auger depth profile

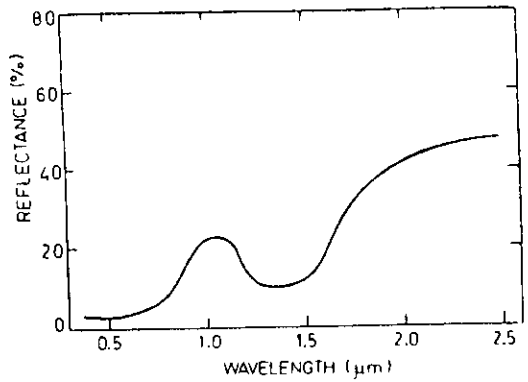

(a)

Fig. 11(a). Total reflectance spectrum of spray pyrolysed CoO on stainless steel.

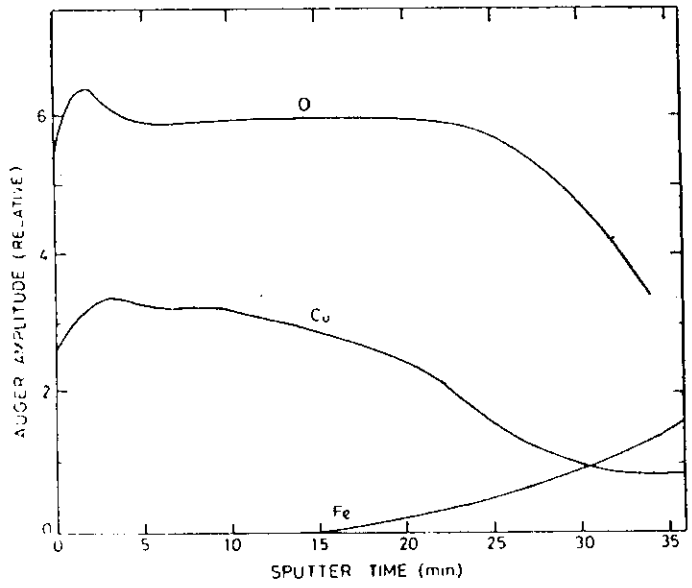

(b)

Fig. 11(b). Auger depth profile of the above coating showing the variation of cobalt and oxygen. The onset of Fe signal indicates the beginning of the substrate interface (Chidambaram et al., 1982).

of spray pyrolysed black cobalt on stainless steel (Chidambaram et al., 1982). The depth profile shows that the coating consists mainly of CoO. The bulk of the absorption is due to CoO and the metal substrate dominates the emittance characteristics. The hump at 1.05 μm in the reflectance spectrum is an intrinsic character of the material. This tandem structure has $\alpha = 0.92$ and $\epsilon_{100} = 0.15$ and is stable up to 600°C.

Table 1

Summary of selective surfaces

Materials	Fabrication technique	Absorptance	Emittance (T°C)	Ref.
1	2	3	4	5
SINGLE SURFACE (INTRINSIC)				
Eu_2O_3				Seraphin (1979)
				Lampert (1979)
ReO_3				Seraphin (1979)
HfC	Sputtering	0.65	0.1(100)	"
V_2O_3				"
LaB_6				"
DOUBLE INTERFACE (HOMOGENEOUS SEMICONDUCTOR ON METAL)				
a-Si	CVD	0.77	0.1	Booth and Seraphin (1979)
a-Si	Sputtering and chemical etching	0.94	0.5	Messier et al. (1980)
a-Ge	Sputtering and chemical etching	0.94	0.55	Swab et al. (1980)
Si - Si_3N_4	CVD + Vac. evap.	0.76	0.07(500)	Donnodieu and Seraphin (1978)
Si - ITO	Spray pyrolysis	0.80	0.05(100)	Goldner and Haskel (1975)
CuO	Chem. conv.	0.91	0.16(100)	Mattox (1975)
	Chemical etching	0.93	0.11	Driver and McCormick (1978)
	Anodization	0.95	0.2	Potdar et al. (1981)
	Spray pyrolysis	0.93	0.11(80)	Hottel and Unger (1959)
Cu_2O	Thermal oxidation	0.85		Aveline and Bonilla (1981)
CoO	Anodization	0.93	0.24(260)	Gillette (1960), Kokoropoulas et al. (1959)
	Thermal oxidation	0.87	0.07(60)	Smith et al. (1980), Kruidhoff and van der Leij (1980)
	Electroplating	0.95	0.2	Smith et al. (1980), Kruidhoff and van der Leij (1980), McDonald (1980)

(Contd.)

-8-

1	2	3	4	5
	Spray pyrolysis	0.92	0.14	McDonald (1980), Chidambaram et al. (1981), Choudhary and Sehgal (1982)
CoO + Fe_2O_3	Thermal oxidation	0.90	0.3(140)	Kruidhoff and van der Leij (1980)
	Spray pyrolysis	0.90	0.20(100)	Chidambaram et al. (1983)
ZnO	Chem. Conv.	0.93	0.08	McDonald (1980)
	Anodization	0.95	0.08	van der Leij (1978)
WO_3	Sputtering	0.83	0.07	Hom-haul et al. (1981)
CoO : CoS	Spray pyrolysis	0.93	0.30	van der Leij (1978)
CoS	Electroplating	0.97	0.20	Chidambaram et al. (1982)
Cu_2S	Chem. conv.	0.79	0.2(200)	Smith et al. (1980)
	Spray pyrolysis	0.89	0.25	Mattox (1975)
PbS	Vac. evap.	0.98	0.2(240)	Gadgil et al. (1981)
	Spray pyrolysis	0.92	0.21	McMohan and Jasperson (1974), Marchini and Gandy (1978), Mattox and Kominaik (1975)
FeC, Black	Sputtering	0.80	0.02(150)	Gupta et al. (1981)
Nickel	Electroplating	0.95	0.18	van der Leij (1978)
	Chem. conv.	0.94	0.15	Tabor (1967), Peterson and Ramsey (1975), Pettit and Sowell (1976), Gogna and Chopra (1978, 1979) Gogna and Chopra (1979), Kumar et al. (1980)
Black Molybdenum	CVD	0.82	0.08	Carver (1979)
	Electroplating	0.85	0.11	Potdar et al. (1982)
Black Enamel/SnO_2	Spray pyrolysis	0.92	0.15	Simonis et al. (1979)
DOUBLE INTERFACE (INHOMOGENEOUS SEMICONDUCTOR ON METAL)				
Al_2O_3-Ni	Vac. evap.	0.94	0.10(150)	Niklasson and Granqvist (1979), Craighead et al. (1979)
	Electroplating	0.93	0.20	Anderson et al. (1980), Kumar et al. (1982)

(Contd.)

1	2	3	4	5
Al_2O_3-Pt	Vac. evap.	0.94	0.07(150)	Craighead et al. (1979)
Al_2O_3-Au	Sputtering	0.95	0.025	Craighead et al. (1979)
Al_2O_3-Cu	Sputtering	0.90	0.045	Mckenzier (1979)
Al_2O_3-Cr	Gas evap.			Niklasson and Granqvist (1978), Granqvist and Niklasson (1977)
Al_2O_3-Co	Electroplating	0.94	0.31	Kumar et al. (1982)
Cr_2O_3-Cr		0.92	0.08	Fan and Sprua (1977)
		0.95	0.07	Lampert and Washburn (1979), Window et al. (1978), McDonald (1975), Gogna and Chopra (1979)
	Plasma spray	0.90	0.5(80)	Mattox (1975)
	Ebonizing	0.90	0.50	Vaidyanathan et al. (1981)
SiO_2-Fe	Sputtering	0.90	0.03	McKenzie (1979)
MgO-Au	Sputtering	0.93	0.09	Fan and Zavracky (1976)
Cr_2O_3-MoO_2	Electroplating	0.96		Smith and Ignatiev (1981)
CuO-Cu	Sputtering	0.94	0.04(120)	Harding (1982)
CaF_2-Si	Sputtering	0.64	0.06	Gittleman et al. (1979)
CaF_2-Ge	Sputtering	0.72	0.10	Gittleman et al. (1979)
Cr, Fe, Mo, SS, Ta, Ti, W-Silicides	Sputtering	0.85	0.02	Harding (1978)
Cr, Fe, Mo, Ni, Ta, W-carbides	Sputtering	0.90	0.06	Harding (1978, 1979), Harding and Craighead (1981)
Ni-NiC	Sputtering	0.90	0.12	Sikkens (1981, 1982)
DOUBLE INTERFACE (TEXTURAL EFFECTS)				
Tungsten dendrite	CVD	0.99	0.26	Coumo et al. (1975)
Steel dendrite	CVD	0.89	0.47(260)	Pettit et al. (1978)
Nickel dendrite	CVD	0.95	0.6(100)	Grimmer et al. (1978)
Rhenium	Vac. evap. CVD	0.70	0.35	Beucherie (1980) Seraphin and Meinel (1976)

(Contd.)

1	2	3	4	5
Gold Smoke Conducting micromesh	Gas evap.	0.99	0.1(100)	O'Neill et al. (1977) Horwitz (1974)
Sn doped In_2O_3 grids	rf sputt.			Fan et al. (1976)
Al PbS SiO	Vac. evap.	0.89	0.02(100)	Flordal and Kivaisi (1977)
Ni/PbS/SiO	Vac. evap.	0.93	0.043(100)	Flordal and Kivaisi (1977)
SiO,Cr SiO	Vac. evap.	0.88	0.1	Mattox (1975)
MgF_2/Mo	Vac. evap.	0.95	0.07	Schmidt and Park (1965)
CeO_2/Mo				
MgF_2/Mo/ MgF_2/Mo	Vac. evap.	0.89	0.07	Schmidt and Park (1965)
SiO_2/Mo/ Sio_2/Mo	Vac. evap.	0.86	0.08	Li et al. (1977)
Ag/Al_2O_3	CVD	0.95	0.04	Meinel et al. (1975)
PbS/ZnS	Vac. evap.	0.75	0.027(100)	Pasquetti (1975)
PbS Al_2O_3	Vac. evap.	0.71	0.032(100)	Pasquetti (1975)
PbS/ZrO	Sputtering	0.82	0.02	Martin et al. (1981)
WO_3/Al_2O_3	Sputtering	0.93	0.09	van der Leij (1978)
PbS CdS	Soln. growth	0.92	0.12	Reddy et al. (1981)
PbS/SnO_2	Soln. growth+j spray	0.92	0.16	Reddy et al. (1982)
MULTIPLE INTERFACE (INTERFERENCE)				
Al_2O_3 Mo Al_2O_3	Vac. evap.	0.95	0.34(100)	Peterson and Ramsey (1975)
	Sputtering	0.95	0.12	Thornton et al. (1980)
Al/Ge SiO	Vac. evap.	0.79	0.012(100)	Flordal and Kivaisi (1977)
Ni Ge SiO	Vac. evap.	0.88	0.035(100)	Flordal and Kivaisi (1977)
Cr Ge SiO	Vac. evap.	0.93	0.11(100)	Flordal and Kivaisi (1977)
PAINTS				
PbS in PP	Spray	0.92	0.89	Martin et al. (1981)
PbS in EPDM	,,	0.91	0.68	-do-
CdTe in EPDM	,,	0.88	0.80	Lin and Zimmer (1977)
Sb_2Se_3 in EPDM	,,	0.80	0.53	-do-
Si in EPDM	,,	0.79	0.56	-do-
Cu-CrO. in EPDM	,,	0.92	0.36	-do-
FeMnCuO. in EPDM	,,	0.90	0.27	-do-
FeMnCuO. in PP	,,	0.95	0.90	-do-
FeMn-CuO. in EP	Spray	0.92	0.36	Lin and Zimmer (1977)
CuCrMn oxide in silicone	,,	0.92	0.68	-do-
CoFeMn oxide in silicone	,,	0.91	0.60	-do-
Polyurathane lacquer with pigmented soot	,,	0.90	0.03	Lofving (1981)

(*Contd.*)

We should point out that by providing an antireflection (AR) coating, the reflectance losses can be minimized. For example, the absorptance of Si increases from $\sim$ 0.6 to 0.76 with the help of Si_3N_4 AR coating and that of PbS from 0.6 to 0.82 by providing ZrO_2 AR coating. Al_2O_3 on WO_3 has been used both as AR coating and for improving the stability of the coating. These are, of course, examples of multilayer coatings which are discussed later.

By providing a transparent conducting coating on a semiconducting substrate, one obtains an inverse tandem structure. Nonstoichiometric SnO_2 and In_2O_3 films on Si substrates yield selective surfaces.

Semiconductor absorber layer on metal can be replaced by a layer of specially treated commercial black paint to obtain partial selectivity. Using stoving black paints such layers have been prepared on different metal substrates in the author's laboratory by the dip technique described in Section 7. By controlling the thickness of the paint layer, through a control on the paint-thinner ratio and pulling speed, α and ϵ can be controlled. $\alpha = 0.87$ and $\epsilon_{100} = 0.32$, have been obtained by this technique.

Partially selective and selective paints can also be obtained by mixing powders of semiconductor (Williams et al. 1963; Tabor 1967; Pettit and Sowell, 1976) inorganic metal oxide (Mar et al. 1976) coated metal (Gupta et al. 1979) and organic black (Lin and Zimmer 1977) with organic and inorganic binders such as polyethylene, polypropylene, ethylene-propylene, ethylene-propylene-diene and silicone resins. Coating thickness and pigment volume concentration are the key parameters for achieving better optical efficiency.

(b) *Inhomogeneous Absorbing Coating on a Metallic Surface*

As already mentioned, optimized optical coatings of the absorber layer can be obtained if the film is a composite or cermet consisting of metal particles suspended in a dielectric matrix. The optical properties of such a composite

can be varied over a wide range by changing the microstructure and composition of the composites. The optical absorption is mainly due to resonant scattering between particles which are small compared to wavelength of the radiation to be absorbed and are spaced far enough to act as independent scatterers. The optical constants of such composite structures can be calculated by an appropriate "Effective Medium Theory" (EMT) described in Section 6.2.

The well known and commercially exploited example of this type of coating is the black chrome (Lampert, 1978) which is a composite of the Cr particles in a matrix of Cr_2O_3 produced by electroplating. The film consists of three regions:

(1) a thin Cr_2O_3 top layer

(2) an intermediate Cr_2O_3-Cr cermet

(3) a Cr rich Cr-Cr_2O_3 cermet dominated by Cr and the Ni substrate. An Auger depth profile of this coating shown in Fig. 12 provides a direct evidence for the proposed structure.

In black chrome the top oxide layer acts as an AR coating. Absorption takes place in the intermediate layer by resonant scattering. This layer is transparent to IR so that the lower metal rich layers and particularly the substrate give rise to high IR reflectivity. The reflectance spectrum of such a coating is also shown in Fig. 12. Values of α as high as 0.98 and emittance as low as 0.08 have been obtained. It should be pointed out that optical

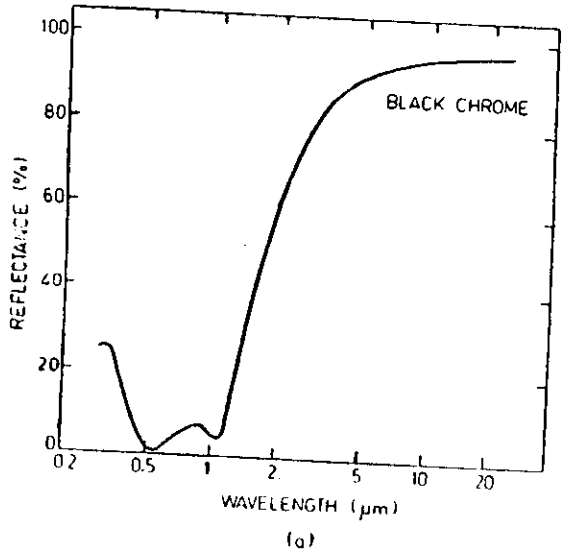

(a)

Fig. 12(a). Total reflectance spectrum of electroplated black chrome on nickel plated copper.

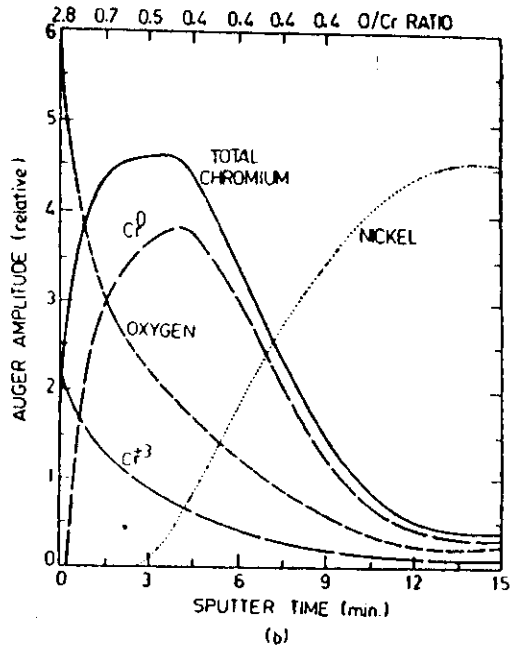

(b)

Fig. 12(b). Auger depth of the above coating showing the variation of total chromium, free metallic chromium Cr°, chromium in Cr_2O_3 as Cr^{+3} and oxygen. Scale at the top shows the variation of oxygen to chromium ratio. The onset of nickel signal indicates the beginning of substrate interface (Lampert, 1978).

properties of black chrome are strongly dependent on local concentration of ionic species in the bath during electroplating, layer conductivity, local field gradients, electroplating parameters and substrate topology.

Similarly black nickel (Tabor 1967; Pettit 1976; Gogna 1979), consisting of NiS and ZnS, is a well known commercially used composite coating. The behaviour of electroplated black Ni is similar to that of black chrome. Apart from mettalic particles of Ni and Zn, the coating consists of the oxides and sulphides of Ni and Zn. The depth profile studies (Gogna 1979) show that the concentration of Zn is maximum at surface and continuously decreases while that of Ni increases. Since ZnO and Zns have $E_g > 3$ eV, the top layer consisting of these compounds acts as a transparent AR layer. NiO and NiS possess semiconducting behaviour and in combination with metallic inclusion of Zn and Ni are responsible for solar absorption. Such coatings with $\alpha = 0.94$ and $\epsilon_{100} = 0.10$ have been obtained on various metal substrates like aluminium, GI, and nickel plated copper.

-11-

The above mentioned black chrome and black nickel coatings are stable only upto ~300°C. For high temperature applications, other cermets such as Au-MgO (Fan 1976), Au-Al_2O_3 (Craighead 1979) Cu-Al_2O_3 (McKenzie 1979) and Fe-SiO_2 (McKenzie 1979) have been prepared by sputtering onto metallic or dielectric (e.g. glass) substrates. The optical properties of such cermet films are dependent on the volume fraction of the metal particles and the micro-structure of the components. High (> 0.9) absorptance and low (~0.1) emittance values with a thermal stability of upto 500°C have been obtained. It should be possible to improve the performance further by incorporating refractive index gradient in the cermet films.

(c) *Graded Index Coatings*

Another practical and effective way of reducing the high reflectance of the absorbing layer in a tandem structure is to grade its refractive index to match with that of interface medium. In principle it is possible to have zero reflectance if the refractive index can be varied gradually from the bulk material value at the bottom to that of air (or the transparent dielectric layer, as the case may be) at the top. In practice, this is not possible since the coating has a limited thickness and further the emittance would increase with thickness. It is, therefore, necessary to optimise the refractive index grading profile (Ritchie et al., 1977) to get minimum reflectance. The optical constants may be graded by mixing different volume fractions of two or more materials. Ritchie et al. (1977) have calculated reflectance spectra of coating with different gradients of their optical constants as shown in Fig. 13. It is clear that the linearly graded coating gives the best performance. Note that sublinear gradients produce little effect on the absorptance. By assuming linear grading to air at the interface, the reflectance contours for different n and k values may be calculated and these results are shown in Fig. 14. A comparison of this data with that of Fig. 9 for a tandem structure without a gradient shows clearly that grading provides a much larger range of n and k values to obtain absorptance values greater than 0.9. For example, a metal surface graded linearly to the optical constants of Al_2O_3 yields $\alpha = 0.9$ which increases to 0.95 if the surface index is graded to air. Similarly, by grading Si surface index linearly to air increases α from 0.7 to α values greater than 0.99.

Pigmented (with Ni or Co) anodized aluminium surface (Granqvist et al., 1979; Kumar et al., 1982) is a good example of graded index selective coating. According to Andersson et al. (1980), the surface of the Al substrate in this case is covered with a thin layer of Al_2O_3 followed by a porous Al_2O_3. These pores are cylindrical in shape. The pigmented metal such as Ni or Co fills the lower part of the pores. The gradient of optical constants is achieved by varying the concentration with depth of metallic particles in the pores. The metal rich bottom layer combined with the substrate ensure high IR reflectance. Structural and metallurgical studies by Kumar et al.

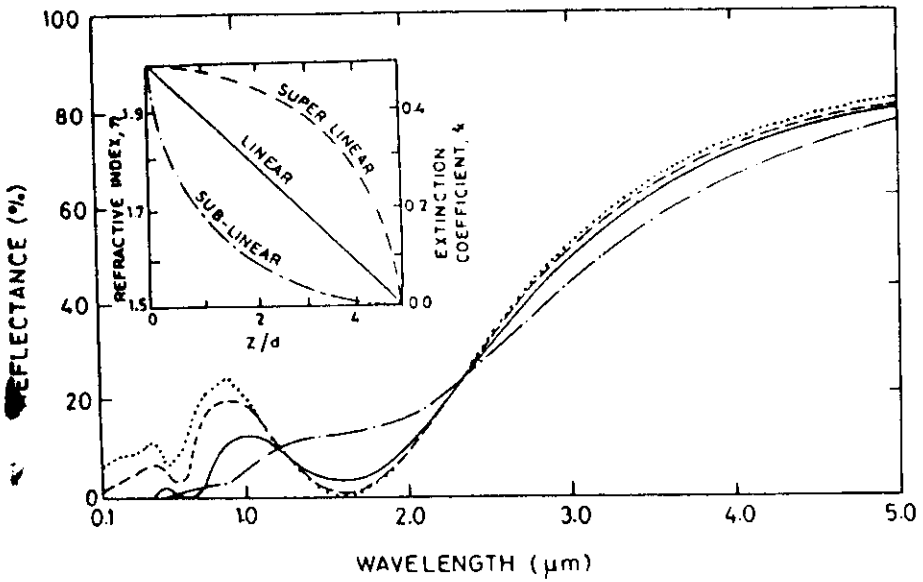

Fig. 13. Calculated reflectance profiles of sublinearly (– – –), linearly (--) and superlinearly (—·—) graded single layer interference coatings compared to that of a uniform coating (...). Thickness is set for each coating such that the first interference minimum is positioned at $\lambda = 1.6$ μm. The inset shows the grading profiles of the refractive index and extinction coefficient for the three type of gradings (Ritchie and Window, 1977).

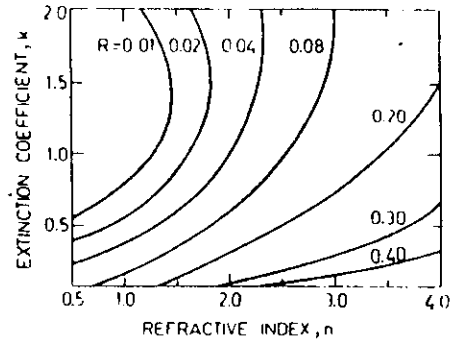

Fig. 14. Normal incidence solar averaged reflectance (R) contours as a function of real and imaginary parts of refractive index n and k for a linearly graded film graded to air. Thickness of the film is always kept such that the first interference minimum occurs at 1.6 μm (Ritchie and Window, 1977).

(1982) have established these results. The magnitude of α and ϵ are controlled by the geometrical distribution of pores and the amount of Ni pigment. Values of α as high as 0.92 and ϵ as low as 0.11 have been obtained by tailor making the gradient of optical constants. A typical depth profile of the composition of one such coating along with its reflectance behaviour is shown in Fig. 15.

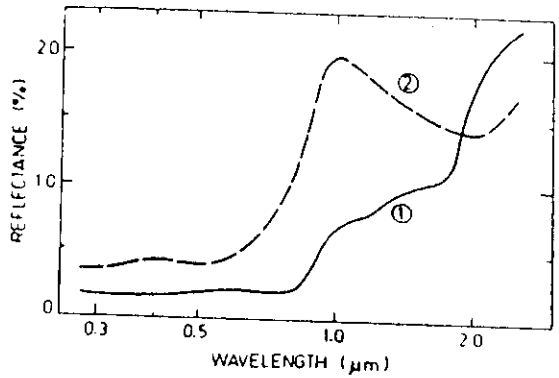

(a)

Fig. 15(a). Total reflectance spectra of Ni pigmented anodized aluminium coatings. 1—Kumar et al. (1983) (2) – – – Anderson et al. (1980).

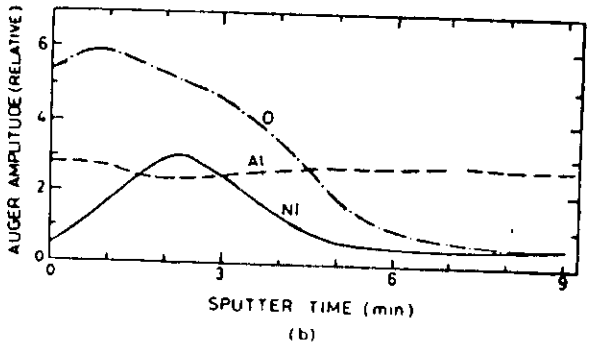

(b)

Fig. 15(b). Auger depth profile of the coating(1) showing the variation of Ni metal in anodized aluminium. The termination of oxygen signal indicates the beginning of the pure aluminium substrate.

(d) *Textured Coating*

We have already mentioned that the absorptance of semiconductors such as Si, Ge and PbS is low because of their high refractive index. The reflectance can be reduced by using an AR coating or by texturing the surface. Texturing may be obtained by roughening the surface, by producing a dendritic or columnar structure using the technique of oblique deposition, or by obtaining a porous film by depositing it in poor vacuum. Surface roughening has to be at a scale to yield multiple reflections in the visible region. Gas evaporation of Si and Ge (Mattox et al., 1975) has been utilized to obtain coatings of high absorptance ~ 0.95. Similarly, porous Ge and "black" gold coatings (Neill et al., 1977) of high absorptance have been obtained. Columnar films of Si and Ge obtained by oblique deposition and also by post-deposition etching of sputtered Si and Ge (Messier et al., 1980; Swab et al., 1980) yield high α values.

A novel method of controlled texturing employed by Fan et al. (1976) is to produce a crossed grating or grid pattern in SnO_2 films coated on glass by lithographic techniques. By controlling the physical dimensions of the pattern, the desired reflectance spectrum can be obtained.

4.3 Multiple Interfaces

By depositing additional layers on the first layer on a metallic substrate, each new layer produces an additional interface between materials of different optical constants. When light is incident on such a stack, it gets reflected at each interface and the phases of all the reflected radiations will depend on the optical thickness of each layer. Hence by adjusting the optical thicknesses, we can either have a constructive or destructive interference. In the following we discuss how such interference stacks can be used as selective surfaces. The materials used for constructing such a stack can be dielectric, semiconductor or metal.

(a) *All Dielectric System*

The use of dielectric films in optical systems for high transmission and high reflection over a wide or narrow band of well defined wavelengths is well known. For a two layer system of indices n_0, n_1, n_2, n_3 (for incident medium, say air, first layer, second layer and substrate) of equal optical thickness i.e. $n_1t_1 = n_2t_2 = \lambda/4$, $3\lambda/4$... the reflectance is given by (Chopra, 1969)

$$R_{\lambda/4} = \left(\frac{n_2^2 n_0 - n_1^2 n_3}{n_2^2 n_0 + n_1^2 n_3}\right)^2 \tag{4.4}$$

$$R = 0 \text{ if } n_0 n_2^2 = n_1^2 n_3 \text{ and } n_1^3 = n_0^2 n_3;\ n_2^3 = n_0 n_3^2$$

The above equation shows that single or double zero reflectance can be obtained by having materials of proper refractive index and optical thickness. Zero reflectance can also be obtained by double layer combination, consisting of high index films thinner than $\lambda/4$ and low index films thicker than $\lambda/4$. Figure 16 gives a comparison of the spectral reflectances of three types of

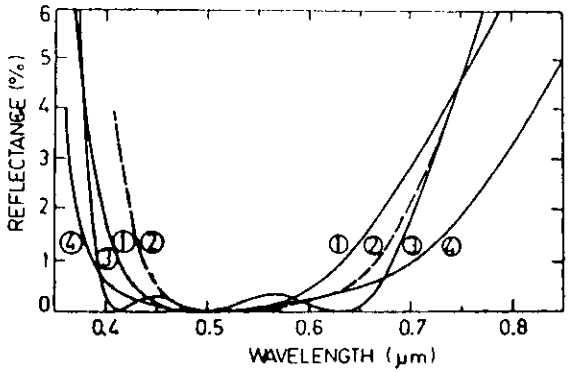

Fig. 16. Calculated reflectance as a function of wavelength of three types of triple layer coatings:
(1) quarter-quarter-quarter
(2) quarter-half-quarter
(3) quarter-half-three quarters.
The observed reflectance of a quarter-half-quarter coating:
(4) consisting of MgF_2 ($n_3 = 1.38$) / CeO_2 ($n_2 = 2.35$) / CeF_3 ($n_1 = 1.7$) is shown by dotted curve (Chopra, 1969).

triple layers on glass and shows that quarter-half-quarter combination is the best choice.

As the number of layers increase, the mathematical analysis becomes more complex. Extending the above treatment to a stack of dielectric layers having alternate high (H) and low (L) indexed odd number of $\lambda/4$ thick films, reflectances very close to 100% can be obtained. The calculated maximum reflectance at $\lambda/4$ for z number of layers in air is given by

$$R = \left[\frac{n_H^{z+1} - n_L^{z-1} n_0}{n_H^{z+1} + n_L^{z-1} n_0}\right]^2 \tag{4.5}$$

where subscripts H and L stand for high and low refractive index and n_0 is the index of the substrate.

If a complicated reflectance profiles is required, then such a filter can also be designed (Liddell 1981) by using different numerical methods (Section 6.1). Using such methods and codeposition/sequential deposition techniques involving different materials it is possible to produce filters with almost any desired spectral transmission properties (Dobrowlski 1966). The inaccuracy arises due to imperfection of the layers and an inadequate knowledge of their optical constants and controlling of the desired profile of refractive index.

(b) *Semiconductor/Dielectric System*

All dielectric systems are transparent in the visible region. An absorbing layer like a semiconductor or a metal must be incorporated in it to obtain selectively absorbing coating. The semiconductor should have an appropriate absorption edge. For example, in the system of PbS/CdS (Reddy et al. 1981) developed in the author's laboratory by solution growth technique, PbS has absorption edge at ~3 μm so that it absorbs all wavelengths below it and CdS deposited on top of PbS with absorption edge at 0.52 μm transmits all wavelengths greater than 0.52 μm. The emittance is still dominated by the metal substrates. The reflectance spectrum and the Auger depth profile of this system is shown in Fig. 17. High reflectance of CdS top layer is decreased by adding a final AR layer of SnO_2 on PbS/CdS combination and thus a higher absorptance is achieved (Reddy et al. 1982).

(c) *Metal/Dielectric System*

Figure 18 shows a schematic diagram of a four layer metal/dielectric stack. The first metallic layer ensures that the reflectance in infrared region is high. The second layer is a dielectric and its thickness is tuned so that the reflection minima of this two layer dielectric/ metal occurs at the desired wavelength. As the reflectance at air/dielectric interface is weak, this interference effect is also weak. Then a second reflective, partially transparent metallic layer is added to strengthen the reflected wave and maximize the internal interference in dielectric layer. This is usually a thin metallic layer ~50 Å and its optical properties are very different (Chopra 1969) from those of bulk. The performance of this layer depends greatly on the deposition conditions. The second dielectric layer is used to broaden the high absorption region through the suppression of the high reflectance of metal. As an example the reflectance spectrum for Al_2O_3-Mo-Al_2O_3 (AMA) (Peterson et al. 1975) coating prepared by evaporation is shown in Fig. 18.

On the basis of this design Meinel et al. (1977) have studied the reflectance of metal/dielectric stacks using a wide range of metals like Cu, Ag, Au, Al, Cr and Mo and dielectrics like MgF_2, SiO, Al_2O_3, CeO_2.

(d) *Antireflecting Coatings*

The condition for a layer to act as an antireflecting (AR) layer on a given surface of refractive index, n_2 is $n_1 = \sqrt{n_0 n_2}$ where n_1 is the refractive index of the AR layer, and n_0 is the index of incident medium. The effectiveness of a single layer AR coating is limited by the available materials. Moreover, zero reflectance can be obtained at only one wavelength, in a narrow wavelength region. These difficulties can be overcome by using multilayer (two or more) structures with properly selected layer thicknesses and refractive indices. Such layers would provide a broad reflectance minima and thus are useful to suppress the high reflectance of a high index top semiconductor

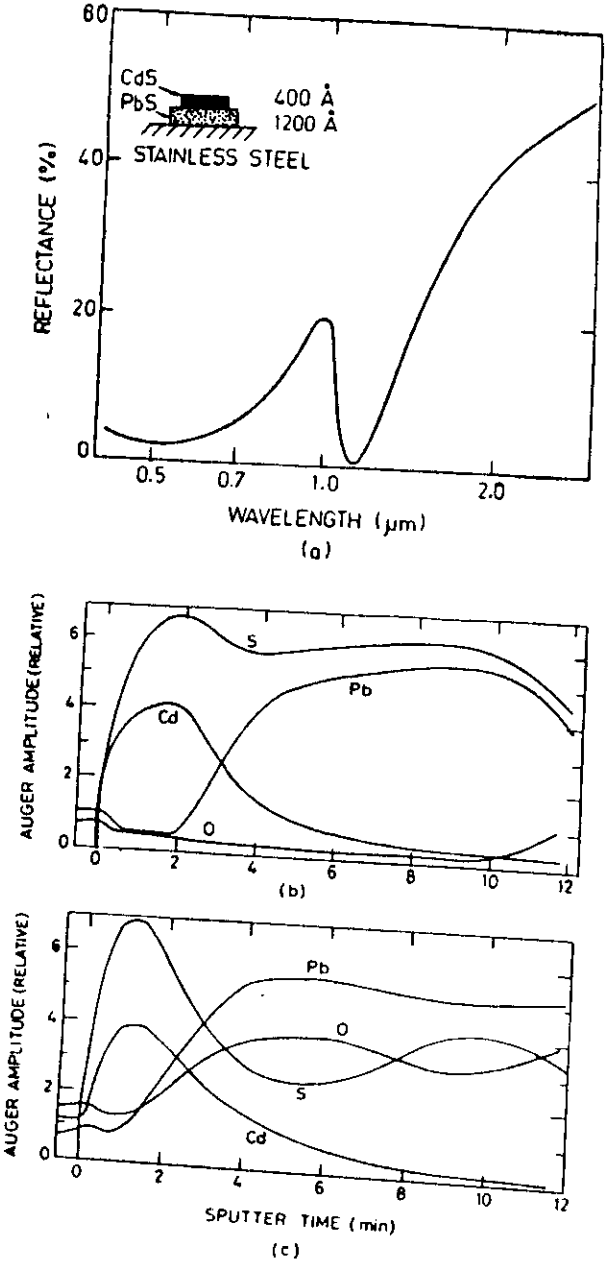

Fig. 17. Total reflectance spectrum of solution growth PbS/CdS two layer selective surface on stainless steel substrate. Auger depth profile of the above coating is shown in (b) as deposited and (c) after annealing at 400°C for 12 hrs (Reddy et al., 1982).

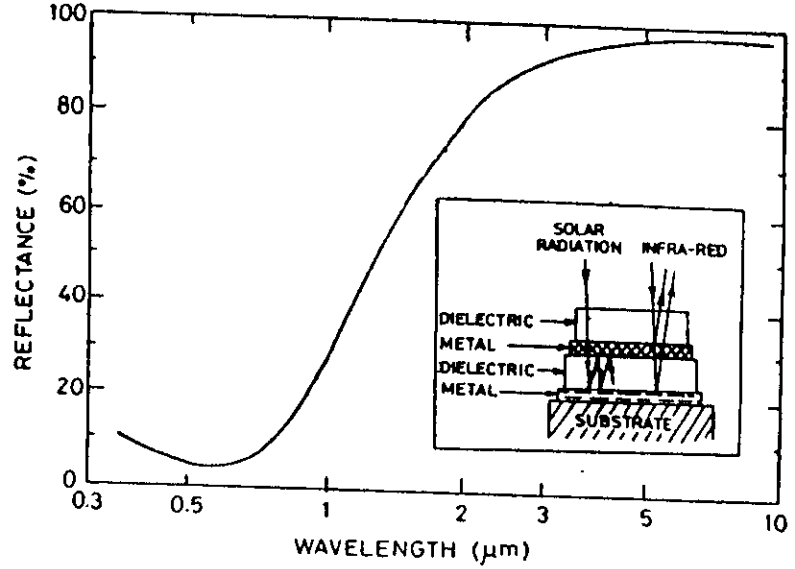

Fig. 18. Spectral reflectance of Al_2O_3-Mo-Al_2O_3 (AMA) coating on Molybdenum substrate (Peterson and Ramsay, 1975). Inset schematically shows the cross-section of such a three layer dielectric-metal-dielectric system.

layer in selective absorbers. As a consequence, propagation of the incident energy into the semiconductor layer is enhanced. Both, all-dielectric and semiconductor-dielectric AR coatings are discussed in literature (Cox and Hass 1964; Macleod 1969).

The necessary condition for zero reflectance in a double layer system is

$$\frac{n_1}{n_0} = \frac{n_2}{n_1} = \frac{n_3}{n_2} \tag{4.6}$$

Combining Eqs. 4.4 and 4.6, one obtains the indices of the two layers for a given set of n_0 and n_3.

For example for Ge surface ($n_{Ge} = 4.0$) we need $n_1 = 1.59$ and $n_2 = 2.50$. Thus, n_1 may be selected from the materials like SiO, Al_2O_3, didymium fluoride, CeF_3, while n_2 could be a layer of CeO_2, ZnS, TiO_2 or Si. Both the layers must be quarter wavelength thick so that $n_1t_1 = n_2t_2 = \lambda_{min}/4$ (λ_{min} is the wavelength at which $R = 0$ is to be obtained). Combinations of SiO + ZnS and didymium fluoride + Si on Ge and $MgF_2 + CeO_2$ on Si have been used as AR layers.

An easier but less effective approach to obtain AR layers for high index materials like Si, Ge and PbS is to follow the inequality relation $n_1 \geq \sqrt{n_0 n_3} \geq n_2$. In this relation, there is no upper limit to n_1 (which is the index of outermost layer) and n_2 is one of the low index materials. Examples of this

system are Ge + MgF_2 on Ge and ZnS + MgF_2 on Si. The double layer AR coatings have the advantage of being less absorbing since the thicknesses of the individual layers and the total optical thickness of the double-layer coating are less than quarter wavelength at the wavelength at which $R = 0$ is desired. In Ge + MgF_2 coating on Ge, Ge has $n_1 t_1 = \lambda/4$ at 0.61 μm and MgF_2 has $n_2 t_2 = \lambda/4$ at 1.03 μm for $R = 0$ at 2.7 μm.

The condition given by Eq. 4.6 can be extended to

$$\frac{n_1}{n_0} = \frac{n_2}{n_1} = \frac{n_3}{n_2} = \frac{n_4}{n_3}$$

for three layer AR coatings with $n_1^4 = n_0^3 n_4$, $n_2^4 = n_0^2 n_4^2$ and $n_3^4 = n_0 n_4^3$ with each layer being a quarter wavelength. An example of this system is $MgF_2 + CeO_2$ + Si coating on Ge which is antireflecting in the range 2 to 7 μm.

To conclude this section, we present in Table 1 the compiled data on useful selective surfaces prepared by various techniques.

5. ABSORPTION PROCESSES

We have described in the preceding section a variety of selective structures which utilize various physical phenomena to yield highly selective spectral response of their optical properties. As we have already noted, some coatings depend on multiple absorption processes for their selectivity. The physical processes involved can be classified as follows:

(a) *Intrinsic:* The metallic and semiconductor surfaces and thin films of oxides and sulphides of various transition metals and of HfC and LaB_6 fall in this category of electronic absorption.

(b) *Geometrical Trapping:* Textured roughened surfaces, and dendritic and porous films utilize geometry based multiple scattering process.

(c) *Optical Matching:* Graded index films exploit this process to produce selectivity.

(d) *Multiple Interference:* A variety of multilayer films utilize multiple interference effects to yield any desired spectral response.

(e) *Plasma Resonance:* Controllably doped degenerate semiconductor films such as transparent conducting oxides based on Sn, In, Zn and Cd exploit this property for selectivity.

(f) *Resonant Scattering:* Inhomogeneous and cermet type of particulate coatings utilize resonant scattering processes taking place between the absorbing particles. Such coatings also utilize intrinsic and geometrical (and in some cases, plasma resonance) effects.

6. OPTICAL MODELLING

The optical modelling of selective surfaces helps in designing and tailor making of the coatings. To maximise the solar absorptance, one has to calculate the reflectance values of given system from known optical constants data. In the case of single surface or single layer, it can be done easily. But in multilayer structures, the number of layers, their order and thicknesses determine the reflectance spectrum. It is generally advisable to design theoretically the optimum number of layers, their arrangement and thicknesses prior to deposition. In this section, we mention some of the standard methods for this purpose. In case of the composite or graded structures, one has to divide the coating into a number of layers with such thicknesses that no significant change in the composition of individual layers occurs. The effective optical constants of these individual layers can be calculated using one of the applicable effective medium theories described in this section.

6.1 Single and Multilayer Coatings

The theoretical calculations of single layer or a multilayer system can be performed using the simple matrix multiplication method (Macleod, 1969; Liddell, 1981; and Macdonald, 1971). The optical behaviour of a stack of layers can be represented by a 2×1 matrix, which can be obtained by multiplying m characteristic (2×2) matrices M_j for each layer and a 2×1 matrix M_s for substrates in the same sequence. That is,

$$M = \prod_{j=1}^{m} M_j \times M_s \tag{6.1}$$

where

$$M_j = \begin{bmatrix} \cos \delta_j & i \sin \delta_j / N_j \\ i N_j \sin \delta_j & \cos \delta_j \end{bmatrix} \tag{6.2}$$

where $\delta_j = 2\pi N_j d_j / \lambda$

d_j = Thickness of the jth layer

λ = wavelength

$N_j = n_j - ik_j$, complex refractive index of the jth layer.

and

$$M_s = \begin{bmatrix} 1 \\ N_s \end{bmatrix} \tag{6.3}$$

N_s = complex refractive index $(n_s - ik_s)$ of the substrate at λ.

The specular (normal) reflectance (R) and transmittance (T) are given by

$$R = \left(\frac{n_0 M_{11} - M_{21}}{n_0 M_{11} + M_{21}}\right)\left(\frac{n_0 M_{11} - M_{21}}{n_0 M_{11} + M_{21}}\right)^* \tag{6.4}$$

where n_0 is the refractive index of the medium of incident radiation* denotes the complex conjugate of the bracketed value.

$$T = \frac{4N_s n_0}{(n_0 M_{11} + M_{21})^2} \tag{6.5}$$

The matrix multiplication method is widely used in design of multilayer optical coatings.

Multilayer Optical Filter Design

As discussed in Section 4.3, using multilayers of all dielectrics or metal-dielectric layers, one can fabricate a coating with any specified optical characteristics. The basic designing process of such a coating consists of two steps:

(1) *Analysis:* This involves the computation of the spectral characteristics of multilayers whose optical constants and thicknesses are known.

(2) *Synthesis:* This involves the determination of the optical constants and thicknesses of multilayer to give some specified spectral response. The analysis can be carried out using a number of available simple methods like matrix multiplication method or graphics method (Liddell, 1981). In designing terminology, the methods which can be used to carry out the first part are termed as "analytical techniques". Liddell (1981) has explained a number of such methods. The techniques which have been developed to carry out synthesis are generally known as "refining techniques". Most of these techniques are based on analytical methods.

Depending on the methods of designing, there exist three classes of refining techniques. (1) The first is based on the merit function concept (Liddell, 1981; Dobrowolski, 1966), where we start with a set of designing parameters and finally get the optimized values by iterative process. After each modification in any of the designing parameter, the merit function—defined as the integrated difference between the required profile and that of calculated—is calculated and is used to make next correction in the right direction. (2) In the Fourier transform method (Dobrowolski and Lowe, 1978, and Pegis, 1961) the reflectance or transmittance of n layers can be represented as Fourier series which can be integrated and used to obtain the optimized refractive index profile. (3) Finally, the refining can be done by standard electrical filter designing techniques (Seeley et al., 1973; Liddell, 1981).

6.2 Composite Coatings

The optical properties of heterogeneous systems consisting of a metal and a dielectric or two dielectrics have been studied for over a century. Faraday introduced the concept of an effective dielectric constant of a heterogeneous dielectric. The most quoted paper on the subject published by Maxwell Garnett in 1904 derived the well-known Clausius-Mossotti-Lorentz-Lorenz relation for a glass system containing small metal regions. A new approach to the effective medium theory (EMT) was given by Bruggeman (1935). Both

the Maxwell Garnett (MG) and Bruggeman (Br) theories have been revised to incorporate the size, concentration, shape and distribution of the metallic particles. The physical basis of the validity of different EMTs has been brought out by the works of Smith (1977, 1979), Bergman (1978, 1979), Stroud (1975), Hori and Yonezawa (1977), Milton (1980, 1981a, b, c) and Lamb et al. (1978, 1980). An excellent review of a comparative analysis of the theories is provided by Landauer (1978) and Granqvist and Hunderi (1977). The derivation of EMTs with a unified approach due to Smith (1977, 1979) and Lamb et al. (1978, 1980) is described briefly in the following section.

6.2.1 Unified Approach EMTs

Heterogeneous materials can have a variety of microstructures. The commonly known microstructures of composite materials are of four types as shown schematically in Fig. 19. One is a separated grain structure in which particles of material A are dispersed in a continuous host of material B. The second refers to an aggregate structure being a space filling random mixture of the two constituents. The separate grain structures can be represented by a random unit cell being a coated sphere consisting of a core with dielectric permeability ϵ_A surrounded by a shell with permeability ϵ_B. The volume ratio of the concentric sphere is chosen so as to correspond with the overall filling factor of the inhomogeneous material. This random unit cell forms the basis of the MG theory.

The aggregate structure, on the other hand, corresponds to a random unit cell with structural equivalence of the two constituents. Therefore, this cell is taken to be a sphere whose dielectric permeability is ϵ_A with probability f, and ϵ_B with probability $(1-f)$. This random unit cell leads to the Bruggeman theory.

The following variations of the above mentioned microstructures are interesting and have been treated theoretically.

The coated sphere microstructure (MG theory) may show spatial variation of the ratio of two materials. In some regions, material A may be covered with B and in other places, B material is completely covered by A as shown in Fig. 19. The effective dielectric constant of such a system has been derived by Ping Sheng (1980a, b).

If the material A is always covered with a shell, whose dielectric constant is influenced by the core material, the microstructure (Fig. 19) is intermediate to that of the MG and Bruggeman theories. The theoretical expression for such a system has been obtained by Hanai (1960).

The effective medium may be defined as follows. The effective medium is that in which the embedded random unit cell should not be detectable in an experiment using electromagnetic radiation confined to a specified wavelength range. In other words, the extinction of the random unit cell should

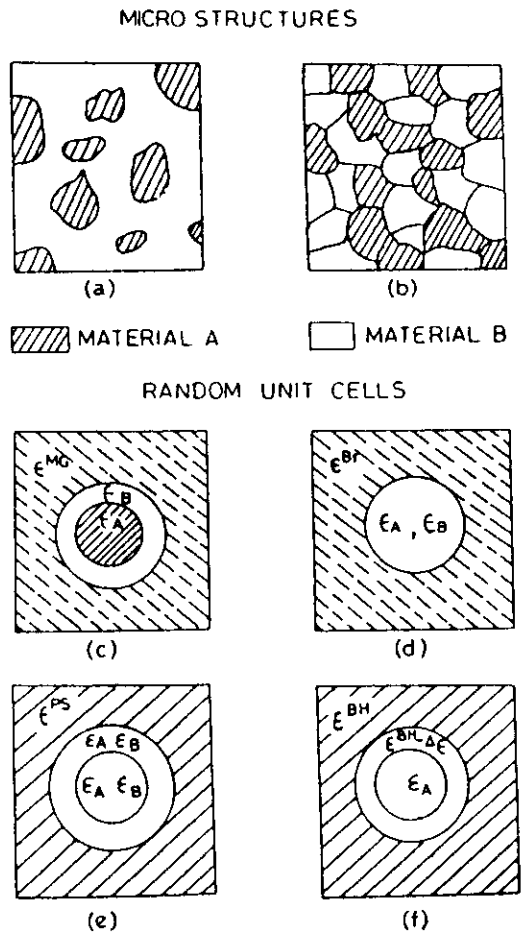

Fig. 19. Schematic diagrams of the microstructures and corresponding unit cells of inhomegoneous two phase systems composed of two materials A and B. Figures (a) and (b) respectively show the microstructures where A is surrounded by B and where A and B are distributed randomly. Figures (e) and (f) show the random unit cells for the modified models of Ping Sheng and Bruggeman-Hanai theory (Niklasson, 1982).

be the same as if it were replaced with a material with the effective dielectric permeability.

The extinction C_{ext}, is related to the amplitude function $S(\theta)$ by the following equation (Kerker 1969).

$$C_{ext} = 4\pi \text{ Re } [S(\theta)/k^2] \tag{6.6}$$

where $k = 2\pi\tilde{\epsilon}^{1/2}/\lambda$, $\tilde{\epsilon}$ is the effective dielectric constant of the medium and θ is the angle of scattering. For forward direction, $\theta = 0°$, so that

$$C_{ext} = 4\pi \text{ Re } [S(0)/k^2] \tag{6.7}$$

From the definition of an effective medium, it follows that

$$C_{ext} = 0, \quad \text{so that}$$
$$S(0) = 0 \tag{6.8}$$

which states the fundamental property of an effective medium. Fresnel's equations then apply at the boundaries of the effective medium. The derivation of the expression for dielectric constant in the above mentioned theories has been done in the same way. That is, the forward scattering amplitude function, $S(0)$, for different unit cell (coated sphere, heterogeneous sphere etc.) has been obtained and equated to zero.

Maxwell Garnett Theory

Guttler (1952) has developed a series approximation for the scattering coefficient of the coated sphere (CS) by expanding the Bessel functions in power of their arguments. The assumption in this derivation is that both the dielectric constants (ϵ_A and ϵ_B) and the particle dimensions are sufficiently small so that these series can be terminated after one or two terms. The scattering amplitude function for coated sphere is given by (Kerker 1969)

$$S_{(0)}^{CS} = i\,(kb)^3\, P_1' + 0\,[(kb)]^5 + \cdots \tag{6.9}$$

where

$$P_1' = \frac{(\epsilon_B - \epsilon^{MG})\,(\epsilon_A + 2\epsilon_B) + f_A\,(2\epsilon_B + \epsilon^{MG})\,(\epsilon_A - \epsilon_B)}{(\epsilon_B + 2\epsilon^{MG})\,(\epsilon_A + 2\epsilon_B) + f_A\,(2\epsilon_B - 2\epsilon^{MG})\,(\epsilon_A - \epsilon_B)}$$

$f_A = \left(\frac{a}{b}\right)^3$ where a is the radius of the inner sphere in the random unit cell and b is that of the complete sphere. The accuracy of calculated values depends on the number of terms we consider in Eq. 6.9. The higher order terms in Eq. 6.9 can be replaced by a quantity δ^{MG}, which is a measure of the accuracy (Niklasson 1981). Thus, this equation becomes

$$S_{(0)}^{CS} = i\,(kb)^3\, P_1' + \delta^{MG} \tag{6.10}$$

As an example, if the δ^{MG} value is of the order of 0.015, the corresponding error in ϵ^{MG} would be $\simeq 10\%$.

By neglecting δ^{MG} and using Eqs. 6.3 and 6.5, we get $P_1' = 0$. Therefore

$$\frac{(\epsilon_B - \epsilon^{MG})\,(\epsilon_A + 2\epsilon_B) + f_A\,(2\epsilon_B + \epsilon^{MG})\,(\epsilon_A - \epsilon_B)}{(\epsilon_B + 2\epsilon^{MG})\,(\epsilon_A + 2\epsilon_B) + f_A\,(2\epsilon_B - 2\epsilon^{MG})\,(\epsilon_A - \epsilon_B)} = 0 \tag{6.11}$$

which yields

$$\frac{\epsilon^{MG} - \epsilon_B}{\epsilon^{MG} + 2\epsilon_B} = f_A \frac{\epsilon_A - \epsilon_B}{\epsilon_A + 2\epsilon_B} \tag{6.12}$$

Solving for ϵ^{MG}, we get

$$\epsilon^{MG} = \epsilon_B \frac{(\epsilon_A + 2\epsilon_B) + 2f_A(\epsilon_A - \epsilon_B)}{(\epsilon_A + 2\epsilon_B) - f_A(\epsilon_A - \epsilon_B)} \tag{6.13}$$

An analogous formula for the inverted structure can be obtained by replacing A with B and vice versa.

Bruggeman Theory

The random unit cell in this case being a heterogeneous sphere (HS), the forward scattering ($\theta = 0°$) amplitude can be written as a series

$$S_{(0)}^{HS} = i(kb)^3 \frac{\epsilon - \epsilon^{Br}}{\epsilon + 2\epsilon^{Br}} + 0(kb)^5 \tag{6.14}$$

We can replace ϵ with ϵ_A or ϵ_B, with corresponding fill factors. Again, by considering small metallic sphere particles, we have

$$S_{(0)}^{HS} = i(kb)^3 \frac{\epsilon - \epsilon^{Br}}{\epsilon + 2\epsilon^{Br}} + \delta^{Br} \tag{6.15}$$

From the definition of the effective medium theory $S^{HS}(0) = 0$, so that neglecting δ^{Br} we get

$$\frac{\epsilon - \epsilon^{Br}}{\epsilon + 2\epsilon^{Br}} = 0$$

and

$$f_A \frac{\epsilon_A - \epsilon^{Br}}{\epsilon_A + 2\epsilon^{Br}} + (1 - f_A) \frac{\epsilon_B - \epsilon^{Br}}{\epsilon_B + 2\epsilon^{Br}} = 0 \tag{6.16}$$

This equation yields the effective dielectric constant of a binary mixture

Ping Sheng Theory

This theory is a symmetrical generalization of the MG theory and takes account of pair-cluster interactions. In this case, the coating material A is surrounded by material B at some places and at other places it is the reverse. The relative occurrence of these two types of random unit cells was determined by Ping Sheng (1980a, b) by counting the number of equally possible configurations corresponding to different positions of the inner sphere in the random unit cell. For a sphere of material A surrounded by a shell of material B, this number V_1 is given by

$$V_1 = (1 - f_A^{1/3})^3 \tag{6.17}$$

For the reverse case,

$$V_2 = (1 - (1 - f_A)^{1/3})^3 \tag{6.18}$$

is obtained. Taking the small sphere limit as in case of the MG theory (Eq. 6.9), we get

$$V_1 \frac{(\epsilon_B - \epsilon^{PS})(\epsilon_A + 2\epsilon_B) + f_A(2\epsilon_B + \epsilon^{PS})(\epsilon_A - \epsilon_B)}{(\epsilon_B + 2\epsilon^{PS})(\epsilon_A + 2\epsilon_B) + 2f_A(\epsilon_B - \epsilon^{PS})(\epsilon_A - \epsilon_B)}$$

$$+ V_2 \frac{(\epsilon_B - \epsilon^{PS})(\epsilon_B + \epsilon_A) + (1 - f_A)(2\epsilon_A + \epsilon^{PS})(\epsilon_B - \epsilon_A)}{(\epsilon_A + 2\epsilon^{PS})(\epsilon_B + 2\epsilon_A) + 2(1 - f_A)(2\epsilon_A - \epsilon^{PS})(\epsilon_B - \epsilon_A)} = 0 \tag{6.19}$$

This is clearly a symmetrization of the MG theory which approaches the Maxwell Garnett result when f approaches 0 and 1.

Bruggeman-Hanai Theory

This theory is applicable for a system having a microstructure intermediate between that of the Bruggeman and MG cases. From Eq. 6.9, we obtain

$$\Delta\epsilon\,(\epsilon_A + 2\epsilon^{BH} - 2\Delta\epsilon) + f^*(3\epsilon^{BH} - 2\Delta\epsilon)(\epsilon_A - \epsilon^{BH} + \Delta\epsilon) = 0 \tag{6.20}$$

where f^* is the ratio of the volumes of the inner sphere to the whole random unit cell. The filling factor of the cell is f_A and that of the shell is $(f_A - \Delta f)$. Here $\Delta\epsilon$ and Δf are the contributions to the shell due to the influence of the core cell. Thus, we obtain

$$f_A = (f_A - \Delta f)(1 - f^*) + f^* \tag{6.21}$$

which is equivalent to

$$f^* = \frac{\Delta f}{1 - f_A + \Delta f}$$

Since $\Delta\epsilon \ll \epsilon^{BH}$ and $\Delta f \ll f_A$, Eq. 6.20 yields

$$\frac{\Delta\epsilon\,(\epsilon_A + 2\epsilon^{BH})}{3\epsilon^{BH}(\epsilon_A - \epsilon^{BH})} = \frac{\Delta f}{1 - f_A} \tag{6.22}$$

By integrating this equation, we obtain the Bruggeman-Hanai (1960) equation.

$$\frac{(\epsilon_A - \epsilon^{BH})}{(\epsilon_A - \epsilon_B)} = (1 - f_A)\left(\frac{\epsilon^{BH}}{\epsilon_B}\right)^{1/3} \tag{6.23}$$

6.2.2 Fundamental Limits of the EMTs

(a) *Size Limit*

The incorporated particle size must be sufficiently large so that the macroscopic dielectric properties can be applied. But it should not be so large that it approaches the wavelength of interest. The former condition allows the metal particles to be represented by a frequency dependent dielectric constant, while the latter condition assumes the existence of a dielectric constant for an ensemble of particles.

(b) *Filling Factor Limit*

In principle, the filling factor can vary from 0 to 1.0. However, for sufficiently large filling factors, one may reach a point where the detailed geometrical configuration of the interacting particles in heterogeneous material starts to play a significant role. The practical limitation of the filling factor is governed by the grain size, dielectric constants of the ingradient materials and the required accuracy of calculations (discussed later).

(c) *Particle Shape*

The preceding theoretical treatments are based on the assumption that the particles are spherical in shape. In practical systems, the shape of the particles may be ellipsoidal, a mixture of ellipsoidal and spherical, cylindrical or conical. The presence of different shapes in a particular system effects the dielectric properties. The variation in the shape can be accounted for by modifying Eqs. 6.9 and 6.14. For example, the MG theory for ellipsoidal particles (Cohen et al., 1973) yields

$$\frac{\epsilon^{MG}-\epsilon_B}{\epsilon^{MG}-2\epsilon_B}=\frac{1}{3}f\frac{\epsilon_A-\epsilon_B}{L_m\epsilon_A(1-L_m)\epsilon_B} \tag{6.24}$$

The particles are assumed to be identical in shape and orientation with characteristic depolarization factor L_m. Similarly, for cylindrical shapes (Cohen et al., 1973), one obtains

$$\epsilon^{MG}=(1-f)\epsilon_B+f\epsilon_A \tag{6.25}$$

The axis orientation is assumed perpendicular to the incident field with $L_m=0$. If the particles are oriented parallel to the incident field, the equation changes to

$$\frac{1}{\epsilon^{MG}}=\frac{1-f}{\epsilon_A}+\frac{f}{\epsilon_B},\ \text{for } L_m=1 \tag{6.26}$$

The Bruggeman case (Polder and van Santen 1946) for ellipsoidal particles yield

$$f\frac{(\epsilon_A-\epsilon^{Br})}{\epsilon^{Br}+L_m(\epsilon_A-\epsilon^{Br})}+\frac{(\epsilon_B-\epsilon^{Br})}{\epsilon^{Br}+L_m(\epsilon_B-\epsilon^{Br})}(1-f)=0 \tag{6.27}$$

Here, the ellipsoids are assumed to be identical in shape and orientation and

$$f=\frac{a_1b_1c_1}{abc}$$

where a, b, c are the lengths of the semi-axes of the random unit cell and a_1, b_1, c_1 refer to the inner ellipsoid.

Figure 20 shows how the shape of particles affects the optical properties of the Ag-SiO_2 composite system (Cohen et al., 1973). The absorption peak shifts towards lower wavelengths as spheres are replaced by cylindrical particles at a given filling factor with no change in the peak position of transmission.

6.2.3 Bounds of EMTs

The complete calculation of the effective dielectric constant requires the knowledge of the dielectric constants and filling factors of the different ingredients, and their detailed geometrical configuration. In case the structural information is not known completely, it is only possible to calculate the

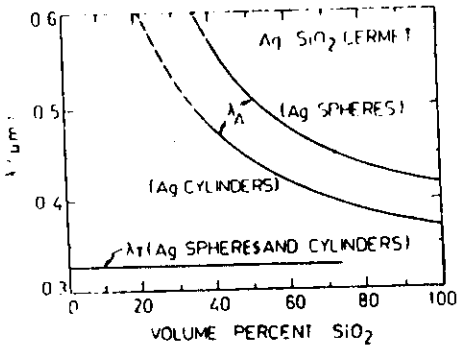

Fig. 20. Dependence of peak absorption wavelength λ_A and peak transmission wavelength λ_T on the shape of Ag particles and volume percent of SiO_2 in Ag-SiO_2 cermet films (Cohen et al., 1973).

effective dielectric constants within certain bounds. These bounds can be theoretically predicted for any practical system. The calculations become complex with increasing number of phases. The simplest case is a two phase system. Hashin and Shtrikman (1962) have calculated bounds for a non-absorbing two phase system. The case of a system with complex dielectric constant has been studied by many workers (Milton 1980, 1981 a,b,c, Schulgsser and Hashin 1976). Bergman (1980, 1981, 1982), has described a two phase (complex) system, in terms of a complex variable defined as

$$F(s)=\frac{\epsilon_B-\epsilon}{\epsilon_B} \tag{6.28}$$

where,

$$\epsilon=\epsilon^{MG}\ \text{or}\ \epsilon^{Br}$$

and

$$S=\frac{\epsilon_B}{\epsilon_A-\epsilon_B} \tag{6.29}$$

Calculations have been carried out for the case of a Co-Al_2O_3 composite (Niklasson 1981) using the reported dielectric constant data for Co (Johnson and Christy 1974) and Al_2O_3 (Harris 1962, Cox et al., 1964). These calculations show that the bounds widen with increasing inaccuracy in the calculated dielectric constant (Fig. 21) and become narrower with decreasing wavelength for a given accuracy.

Figure 21 shows the computed particle radius as a function of the filling factor at a given wavelength $\lambda=1.0\ \mu m$ for different bounds and accuracies. The calculations are limited to $f \leq 0.7$ for the MG case since the separated

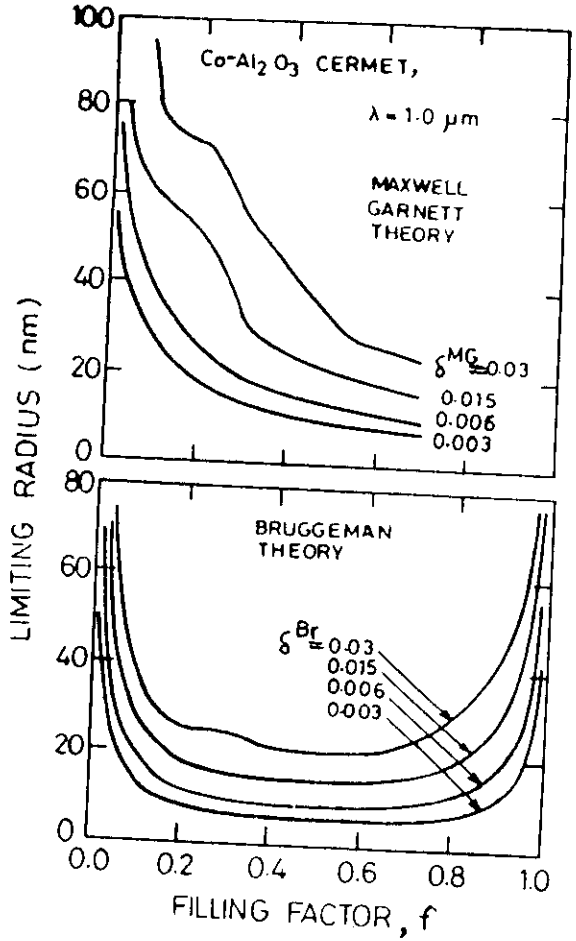

Fig. 21. Limiting radius versus filling factor in Co-Al_2O_3 cermet for the Maxwell Garnett and Bruggeman effective medium theories as computed for a fixed wavelength ($\lambda = 1.0$ μm). The theories are correct to a precision governed by δ^{MG} and δ^{Br} (Niklasson and Granqvist, 1981).

grain structure cannot be maintained to higher filling factors. For the Bruggeman case, both types of grains are assumed to be equal in size. The limiting radius is seen to decrease with increasing filling factor. In the limit of small f, the predictions of the two theories approach each other, as expected. For higher filling factors, the Bruggeman theory is valid upto a smaller limiting radius than for the MG theory.

Figure 22 shows the calculated radius as a function of the filling factor at different wavelengths for a given accuracy (1%, i.e. $\delta = 0.003$). At all wavelengths, though, the overall behaviour is similar to that of Fig. 21. Note that the limiting radius is larger, the longer the wavelength.

6.2.4 Practical Applications of EMTs

The microstructural details of most of the practical coatings is not known precisely. Therefore, one calculates optical constants on the basis of both MG and Bruggeman theories. If the composition of the coating (filling

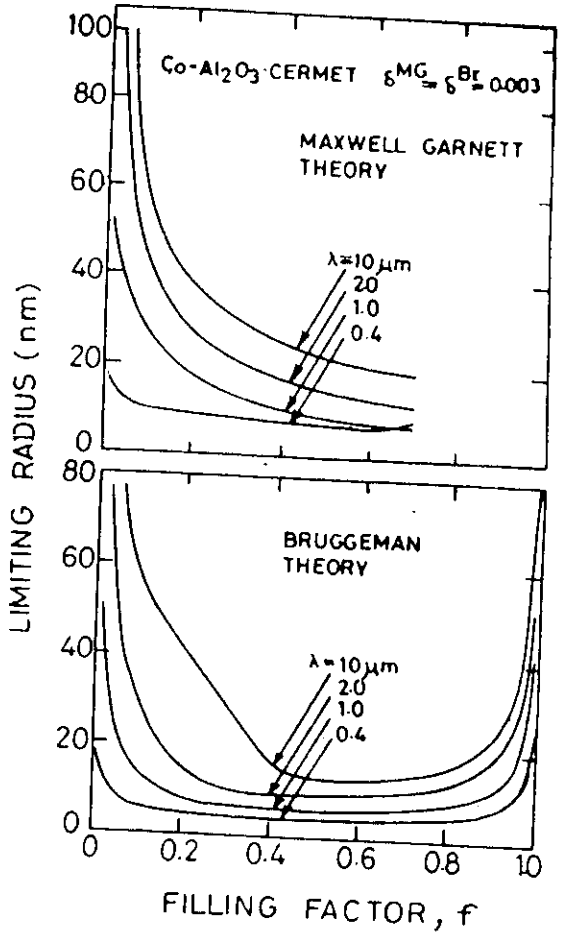

Fig. 22. Limiting radius versus filling factor in Co-Al_2O_3 cermet for the Maxwell Garnett and Bruggeman effective medium theories as computed for four different wavelengths. The theories are correct to a precision governed by fixed magnitude of δ^{MG} and $\delta^{Br}(\delta^{MG} = \delta^{Br} = 0.003)$ (Niklasson and Granqvist, 1981).

factor) varies with thickness, the coating is divided into a number of layers of such thickness that no significant change in filling factor occurs over its thickness. The reflectance of the coating can then be calculated by using the standard matrix multiplication method described earliear (Section 6.1).

Figure 23 shows the calculated and measured spectral reflectance of a Ni pigmented Al_2O_3 composite coating (Andersson et al., 1980). This system has been divided into four layers: (1) pure Al metal substrate; (2) Al_2O_3 barrier; (3) Ni pigmented Al_2O_3 composite; and (4) porous Al_2O_3 region. Using the EMTs to calculate the effective n and k values, the reflectance has been calculated with the help of the matrix multiplication method. This system shows a fair selectivity with λ_c at 1.2 μm for the MG theory model and at 5.0 μm for the Bruggeman model. Comparison with the experimental data shows that the Bruggeman theory gives a better description of the measured data.

The surface roughness can also be taken into consideration for reflectance calculations by assuming that the top few layers are graded with air. Thus, Berthier and Lafait (1979) have calculated the reflectance of black chrome coating by assuming the surface roughness to be due to spherical and conical particles. As seen in Fig. 24, the calculated values show a good agreement with the measured values.

7. DEPOSITION TECHNIQUES

Selective coatings/films can be deposited by one of the many physical and chemical techniques. Physical techniques include evaporation, sputtering and their numerous variations. Here, the coating material is first converted into vapour phase and then condensed atom (molecule)-by-atom (molecule) on a given substrate material. Deposition of atomic/ionic species by pyrolysis, chemical reactions, electroplating, anodization and pigmentation, chemical conversion and solution growth falls in the category of chemical techniques. Extensive reviews of deposition techniques for thin films are available in various books (Chopra 1969, Maissel and Glang 1970, Vossen and Kern 1978, Lowenheim 1978) Chopra and Kaur 1983) Chopra et al., 1982,. In this section, we describe briefly some of the commonly used methods for depositing large area selective coatings onto a variety of commercially available substrates. These substrates include: aluminium, copper, nickel plated copper, nickel plated steel, galvanized iron, stainless steel, molybdenum, tungsten and glass.

(a) *Evaporation*

This is the simplest and most well established technique to deposit thin films wherein the material is converted thermally into atoms/mloecules which are condensed onto a substrate. Among the numerous deposition parameters, the substrate temperature, evaporation rate and vacuum quality affect the microstructure and surface morphology of the coatings significant. If

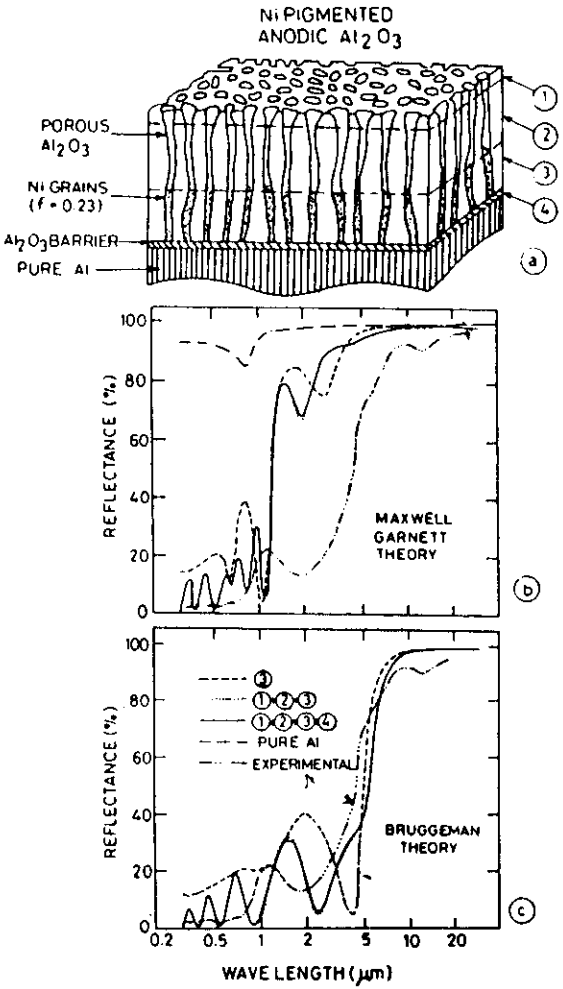

Fig. 23(a) Four layer structure model for Ni pigmented anodic Al_2O_3 containing 0.62 g Ni per m^3. Filling factor for layer 3 is 0.23, (b) and (c) show reflectance behaviour as calculated for individual layers and combination of layers by using Maxwell Garnett and Bruggeman theories respectively. Experimentally measured reflectance curve has been added for comparison with theroy (Granqvist et al., 1979).

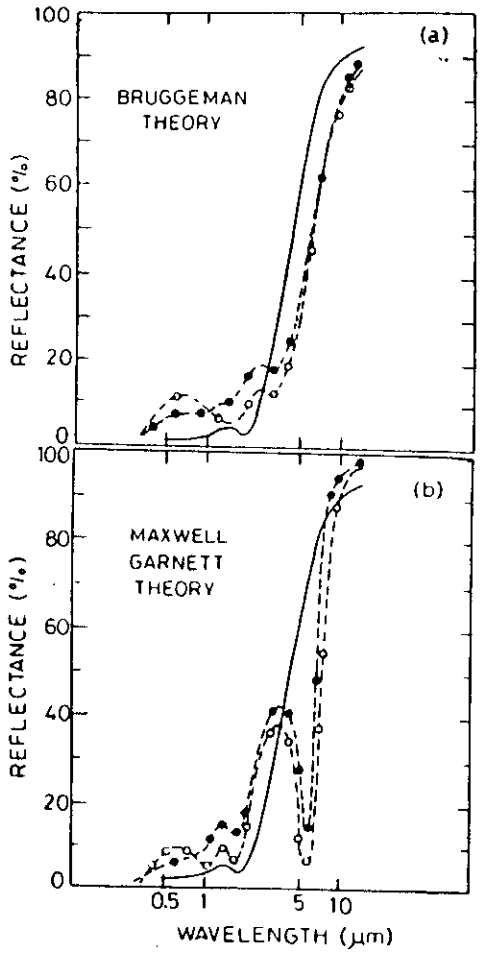

Fig. 24 Calculated reflectance of black chrome coating deposited on copper assuming conical (○) and spherical (●) surface roughness using (a) Bruggeman theory and (b) Maxwell Garnett theory. The calculated curves have been compared with the measured reflectance curve (——) (Berthier and Lafait, 1979).

deposited at very high rates and under poor vacuum conditions, nucleation of the material takes place in the gas phase itself to yield powdery and porous films which exhibit good absorptance due to optical trapping. Black gold is a good example of such a deposition process (O'Neill et al., 1977). Similarly, deposition of films at an angle other than normal can yield under certain conditions columnar films with microvoids which produce light trapping effects.

Thermal evaporation techniques allow precise control over film thickness. Hence, by sequential evaporation with a good control over thickness, multilayer interference stacks of any complexity can be prepared with great precision. A limitation of this technique is that when multicomponent alloys or compounds are evaporated, there may be a deviation in the stoichiometry due to different vapour pressures and/or condensation coefficients of the components. A modification of the filament evaporation process, where this deviation is reduced, is the flash evaporation or arc evaporation techniques. The vacuum evaporation techniques require elaborate and expensive vacuum systems to obtain large area coatings and are thus not well suited for large scale production except for very specialized materials.

(b) *Sputtering*

The ejection of the atoms from the surface of a material (the target) by bombardment with energetic particles is called sputtering. The major advantage of this method is that almost any material can be sputter deposited by one or more sputtering variants. DC, rf, magnetron and ion beam sputtering are the commonly used modes. Significantly high rates of deposition comparable to that for vacuum evaporation are possible today by magnetron sputtering.

By introducing a mixture of inert gas and a reactant in gas form, thin films of carbides, nitrides, oxides and hydrides can be produced by this reactive sputtering process. Also by changing the composition of the gas, we can have a gradient index or have interference stacks. Since good thickness control is possible, it is an attractive technique for the fabrication of interference stacks. Multicomponent composite semiconductors can be very conveniently deposited by cosputtering.

An important advantage of the sputtering technique is that the composition of the sputtered film is nearly the same as that of the cathode and that the rate of deposition remains constant with time. Further, this method is ideally suited to obtain coatings on complex shapes and geometries. This technique can yield hard and adherent films.

(c) *Chemical Vapour Deposition*

In this technique, the formation of the film is due to the heterogeneous reaction taking place at or near the substrate surface. The reactants are in gaseous form and leave a solid product behind. The nature of the film deposited is strongly influenced by the nature of the chemical reaction. By varying the composition of the carrier gas as the film grows, the nature of the deposit can be varied continuously resulting in a profile of refractive index.

The major advantages of the CVD techniques are:

(1) The process takes place generally at atmospheric pressure so that elaborate vacuum systems are not needed.

(2) The high temperature of deposition helps in the elimination of stresses and delamination of the coating.

(3) Like sputtering technique, hard, adherent and coherent coatings are obtained.

The drawbacks of the process are that it is difficult to control the uniformity of the deposit and the reactive gases used for deposition and volatile reaction products formed are in most cases highly toxic and corrosive. Also the substrate must be inactive to the reaction species and should withstand high reaction temperatures.

(d) *Electroplating*

Electroplating is one of the most widely used methods to deposit oxides and sulphides on metals. Black nickel and black chrome are the two well known selective absorbers prepared on commercial scale by electroplating. In the plating process, parameters like pH of the solution, temperature of the bath, current density and plating time affect the microstructure, topography and composition of the coatings obtained which ultimately affect the selectivity. To illustrate this point, keeping all other parameters constant, the effect of plating time on α and ϵ for cobalt sulphide (Chidambaram et al., 1983) is shown in Fig. 25. Such a large number of variables and their interrelationship being not very well known makes precise control and reproducibility difficult. But the method has the advantage that it is suitable for large area coatings and mass production even though only conducting substrates can be used.

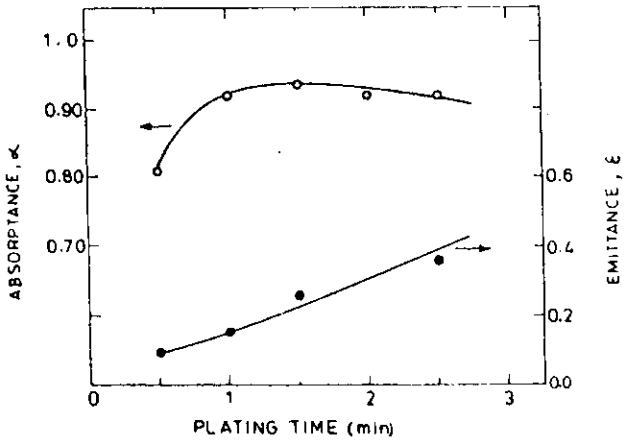

Fig. 25 Variation of absorptance α and emittance ϵ_{100} of electroplated cobalt sulphide on stainless steel with plating time (Chidambaram et al., 1983).

By varying the current density while plating we can obtain a stack of numerous finely divided layers with a continuous gradient of composition resulting in a continuous gradient of refractive index. The structure of the surface can also be textured to have pores and voids.

To deposit oxides, either an oxidising agent is used in the bath, or a metal and an oxide are codeposited where the formation of oxides is due to oxidising ability of the anions. If a plated metal is oxidized, the stability of the coating increases as compared to a plated oxide.

Since electroplating has been one of the most commonly used techniques to prepare a large variety of black coatings, in Table 2 we summarize the bath and plating parameters along with the typical values of α and ϵ obtained for some of the well known coatings.

(e) *Anodization and Pigmentation*

Anodization is an electrolytic oxidation process in which a metal is made the anode in a suitable electrolyte so that when an electric current is passed through the electrolyte, the metal surface is converted to its oxide. Depending upon the solvent action of the selected electrolyte on the anodic oxide and the operating conditions employed, a porous anodic oxide film can be grown on the anode. By carrying out a.c. electrolysis of this anodic film in a metallic salt solution, fine metal particles can be embedded in the pores of the anodic oxide film, giving rise to a black colouration to the coating. In this way, the metal particles can be inhomogeneously dispersed in a dielectric medium.

The operating parameters like composition of the electrolyte, concentration, pH and temperature of the bath, and plating time have to be optimised to get good selectivity. Data in Table 3 illustrates the role of some of these parameters on the α and ϵ values of the nickel pigmented anodized aluminium coatings (Kumar et al., 1983).

(f) *Chemical Conversion*

A conversion coating is the one produced by chemical or electrochemical treatment of metallic surface which gets converted into one of its compounds. In a sense, almost all metals exposed to the atmosphere have on their surfaces "conversion coatings" formed by the chemical reaction of constituents of the atmosphere such as oxide or hydrated oxide on iron, sulphide tarnish on copper and silver, and basic carbonates and sulphates on copper. Among the more widely used conversion-coatings processes are chromating, phosphating, black oxide finishing on iron, copper and its alloys, and various colouring processes for copper, brass, bronze, etc. Oxides of copper and iron on the respective metals have been prepared by the chemical conversion (Gogna and Chopra 1979d) and found to exhibit selective optical behaviour. The coatings form an integral part of the substrate and thus have strong

Table 2

Typical preparation parameters for the deposition of various metal black oxides and sulphides by electroplating method

Coating	Substrate	Bath composition	Deposition conditions	α	ϵ_{100}	Ref.
Black Cobalt	Electroplated nickel	$CoSO_4$: 6.5 g/l	Temp. : 25 C, Current Density : 100-1000 A/m² Time : 5-25 sec.	0.94-0.98	0.25	Smith and Ignatiev (1980)
Black Chrome	Nickel plated copper, aluminium	Chromic acid : 300-400 g/l Na_2SiF_6 : 50-70 g/l Sucrose : 2.4-3.0 g/l	Current Density : 0.3-0.45 A/m² Temp. : 25-35 C	0.94	0.14	Gogna (1980)
Black Nickel	Galvanised iron, aluminium	$NiSO_4$: 50-70 g/l $Ni(NH_4)_6SO_4$: 60-80 g/l NaSCN : 15-25 g/l $ZnSO_4$: 25-36 g/l	pH : 5.6-6 Current Density : 25-45 A/m² Temp. : 30-45 C	0.93	0.08	Gogna et al. (1978)
Cobalt Sulphide	Electroplated nickel, stainless steel	$CoSO_4$: 210 g/l KSCN : 37 g/l	Temp. : 25 C Current Density : 100 A/m² Time : 90 sec.	0.92-0.93	0.25	Smith and Ignatiev (1980) and Chidambaram et al. (1983)

Table 3

Dependence of the α and ϵ_{100} values of the nickel pigmented anodized aluminium selective absorber on the composition of the anodization bath. The nickel pigmentation conditions are kept constant for all specimens (Kumar et al., 1983)

50% H_3PO_4 (w/v), ml.	15% H_2SO_4 (w/v), ml.	α	ϵ_{100}
0	200	0.96	0.46
20	180	0.95	0.45
40	160	0.95	0.44
60	140	0.95	0.41
80	120	0.95	0.39
100	100	0.95	0.34
120	80	0.94	0.32
140	60	0.93	0.29
160	40	0.92	0.23
180	20	0.92	0.11
200	0	0.90	0.06

adhesion. Typical preparation parameters for black Ni, Cu, and Fe are listed in Table 4.

(g) *Immersion Plating/Electroless Conversion*

If a substrate consisting of a less noble metal say M_1 is immersed in a solution containing ions of more noble metal M_2, the more noble metal ions diplace the less noble metal at the substrate surface. The reaction taking place is

$$M_1^0 + M_2^{+n} \rightarrow M_2^0 + M_1^{+n}$$

The metallic ions taking part in this exchange reaction can partly get oxidized in the presence of suitable oxidizing species in the solution. This technique has been used to deposit oxides and sulphides of nickel (Kumar et al., 1980, Cathro 1981, Gogna and Chopra 1979b) and cobalt (Chidambaram et al. 1983) by replacing Zn with Ni/Co using galvanized iron and zincated aluminium substrates. The optical behaviour of the coating is determined by the pH and concentration of the plating bath and dipping time. This is illustrated by Fig. 26 which shows the variation of α and ϵ of cobalt sulphide coatings on galvanized iron as a function of dipping time. In this technique also the coating becomes an integral part of the substrate and behaves as a composite of metal oxide/sulphide and metal particles. Typical plating parameters for black nickel and cobalt coatings are given in Table 4.

(h) *Solution Growth*

This technique is basically a modification of the well known process of chemical precipitation. According to the solubility product principle, a definite

Table 4
Typical preparation parameters for the deposition of various metal black oxides and sulphides by chemical conversion and electroless deposition technique

Coating	Substrate	Bath Composition		Deposition Parameters		α	ϵ_{100}	Ref.
Chemical Conversion:								
Black copper	Polished copper	NaOH	180-100 g/l	Temp.	60-85°C	0.92	0.09	Gogna (1980)
		$NaClO_3$	60-100 g/l	Time	2-15 min			
		Na_2CO_3	20-40 g/l					
Black iron	Stainless steel	$Na_2Cr_2O_7$	100-150 g/l	Temp.	70-85°C	0.90	0.10	Gogna (1980)
		H_2SO_4	350-500 g/l	Time	1-5 min			
Black nickel	Galvanized iron	$NiSO_4$	80-100 g/l	Temp.	30-45°C	0.94	0.15	Gogna and Chopra(1979b)
		$(NH_4)_2SO_4$	10-20 g/l	Time	60 sec.			
				pH	5.6-6			
Electroless Deposition								
Black nickel	Zinc plated steel, galvanized iron. zincated aluminium	$NiSO_4$	50 g/l	Temp.	30°C	0.90-0.94	0.08-0.15	Cathro (1981)
		NH_4SCN	10 g/l	Time	30 sec.			
				pH	6			
Black nickel	Galvanized iron	$NiSO_4$	25 g/l	Temp.	30°C	0.90-0.93	0.07-0.10	Kumar et al. (1980)
		$NaC_2H_3O_2$	9 g/l	Time	1 min			
		NaH_2PO_2	23 g/l	pH	10			
Black cobalt	Galvanized iron	$CoSO_4$	20 g/l	Temp.	20-30°C	0.92	0.15	Chidambaram et al. (1983)
		KSCN	10 g/l	Time	30-90 sec			
				pH	5-6			

Fig. 26 Variation of absorptance α and emittance ϵ_{100} of cobalt sulphide coating prepared by chemical conversion on galvanized iron substrate with dipping time (Chidambaram et al., 1983).

relationship exists between the concentration of ions in a saturated solution of an electrolyte that is in contact with its solid phase. Precipitation occurs when ionic product exceeds solubility product. The film is formed by an ion-by-ion deposition process on a surface dipped in the solution providing nucleation centres. To have a good control over the formation of the precipitate, a complexing agent is used. This stable complex provides a controlled number of free ions. The solution growth technique has been extensively studied in the authors' laboratory (Chopra et al., 1982) and is reviewed elsewhere.

The microstructural properties of the coatings obtained depend on such parameters as pH, temperature of the bath, dipping time and agitation of the solution. The chemical solution growth technique shows characteristic growth kinetics (Fig. 27). Each dipping yields a film of well defined thickness. The deposition of the film by an ion-by-ion reaction process on the substrate surface ensures the stoichiometric composition of the film. By appropriate choice of complexed metal ions, multicomponent films can be deposited. If two non-interfering independent complexing agents are used for complexing the two cations, then the ions dissociate in the aqueous solution to give free metal ions according to the reaction

$$M(A)_n^{+2} \rightleftharpoons M^{+2} + nA$$

$$N(B)_m^{+2} \rightleftharpoons N^{+2} + mB$$

-26-

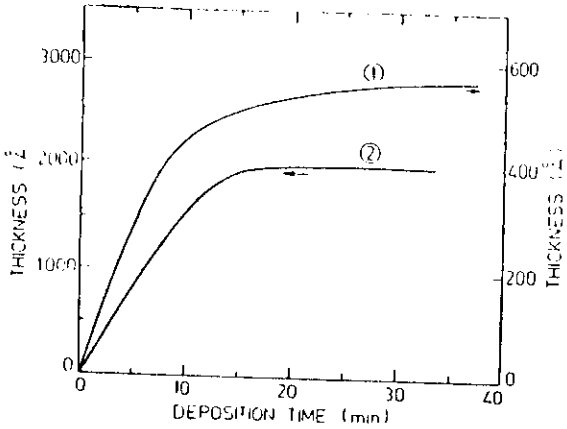

Fig. 27 Variation of film thickness as a function of deposition time for solution grown films of (1) CdS (pH = 12.5, T = 60 C) and (2) PbS (pH = 11 – 12, T = 30°C).

Using this easy and low cost technique oxide films have also been deposited in our laboratory (Chopra et al., 1983). Among other advantages of this method are:

(i) It is a low temperature technique
(ii) It does not need elaborate vacuum equipment
(iii) It can be used to deposit on any substrate.

(i) *Spray Pyrolysis*

Spray pyrolysis involves spraying a solution usually aqueous, containing soluble salts of the constituent atoms of the desired compound onto a heated substrate. Every sprayed droplet reaching the substrate undergoes pyrolytic decomposition and forms a single crystallite or a cluster of crystallites of the product. The other volatile byproducts and the excess solvent escape in the vapour phase. The substate provides the thermal energy for decomposition and subsequent recombination of the constituent species followed by sintering and recrystallization of the clusters of crystallites and thereby resulting in a coherent film. The atomization of the chemical solution into a spray of fine droplets is effected by a spray nozzle with the help of a carrier gas. The solvent serves to carry the reactants and to distribute them uniformly over the substrate area throughout the spray process.

Different parameters like volume of solution sprayed, substrate temperature, solution and gas flow rates, concentration of the solution have to be optimized to get the best combination of α and ϵ. Figure 28 illustrates a typical dependence of the absorptance and emittance of coatings on the volume

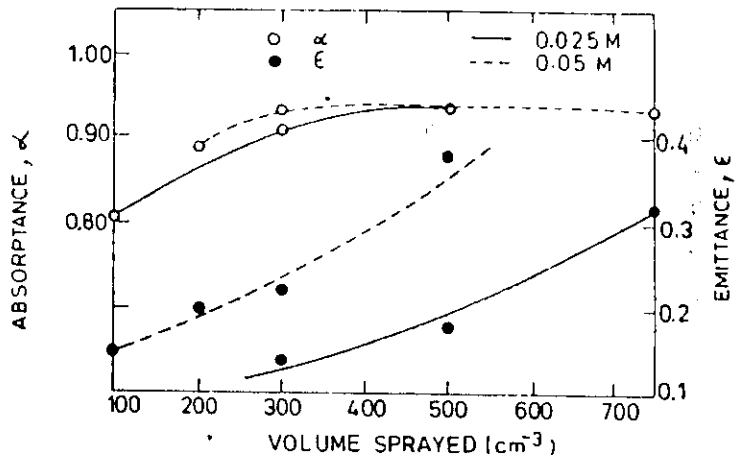

Fig. 28 Variation of absorptance and emittance at 100°C of spray pyrolysed cobalt oxide coating on stainless steel substrate with volume of solution sprayed for two different, 0.025 and 0.05, molar concentrations of the spray solution (Chidambaram et al., 1983).

of spray solution and its concentration and hence film thickness. Note that this method is suitable for those substrate materials which remain inert at the spray temperatures.

(j) *Withdrawal Technique*

This technique involves dipping a substrate in a bath containing the material to be deposited (in a liquid form) and subsequently withdrawing it at a constant rate. According to Landau and Levich (1942), the thickness, t, of the fluid film obtained by this method is given by the expression (Groenveld 1970)

$$t = \text{constant } (\eta v/\rho g)^{1/2}$$

where v is the withdrawal velocity, ρ and η are the density and viscosity of the fluid, respectively and g is the acceleration due to gravity.

Thus, the thickness of the coating is determined by the viscosity (solid concentration) of the liquid and the withdrawal velocity of the substrate. Thin uniform and smooth coatings of commercial black paint possessing moderate selectivity have been obtained by optimizing the thinner to paint ratio and withdrawal speed (Malhotra et al., 1981). The same technique has also been used to prepare carbon pigmented SiO_2 colloid selective surfaces (McKenzie and Zybert, 1981). Thus it is a very useful and economic technique to apply selective paint coatings on any substrate in a controlled manner. The technique is superior to conventional spray technique for paints where a large quantity of material is wasted and the control of thickness is poor.

In concluding this section, let us emphasize again that each deposition technique has its own characteristic parameters and yields films of a specific microstructure. As a consequence, the optical properties of films of the same material (particularly multicomponent alloys/compounds) deposited by different techniques are not necessarily the same. Which technique is more appropriately suited for a particular selective coating is to be determined by technical and economic considerations. The comprehensive Table 1 listing various selective coatings also lists their deposition techniques employed for the purpose.

8. CHARACTERIZATION TECHNIQUES

In order to understand the optical selectivity behaviour and structural stability of coatings, it is necessary to have information on their surface topography, structure, composition and its depth profile, optical and thermal properties. Various techniques and instruments employed to characterize these coatings are described in standard texts (Chopra 1969, Maissel and Glang 1970, Hirsh 1965, Kane and Larrabee 1974, Czanderna 1975, Carlson 1975, Richmond 1963) and are summarized in the following sections.

(a) *Thickness and Surface Roughness*

One of the most important measurements is that of the thickness of the coating. Commonly, the thickness is measured by using the Talystep instrument in which a sharp-tipped diamond stylus moves over a geometrical step between a coated and an uncoated regions of the substrate. The vertical displacement of the stylus on passing this step is amplified and recorded to yield the thickness. Thickness from down to ~ 20 Å to a few microns with an accuracy of $\pm 5\%$ can be measured by this technique. In practice, since coatings are deposited on commercially available metal substrates which have a surface roughness much larger than the coating thickness, specially polished metallic or glass substrates have to be used for this measurement. In doing so, one must assume that the rate of deposition is the same on a smooth and a rough surface, which may not be always valid. In addition to the film thickness, the same instrument can be used to measure the rms surface roughness of the coatings, an important parameter of interest in rough and textured surfaces for optical trapping.

In the case of multilayer selective coatings prepared by vacuum deposition techniques, the thicknesses of the individual layers can be measured in-situ during deposition by employing a quartz-crystal-monitor. The thickness is measured in terms of a frequency shift of an AT cut quartz crystal due to the mass of the deposit. The crystal has to be pre-calibrated for a given set of deposition conditions and the material being deposited. Frequency shift of 1 Hz/sec corresponding to a fraction of angstorm per second can be measured

with this instrument. In case of interference coatings in multilayer stacks, an optical thickness monitor in transmission or reflection mode is generally employed.

(b) *Topography and Structure*

Surface topography of coatings is directly observable in a scanning electron microscope. Transmission electron microscopy of replicas of the surface of coatings also provides useful information on the topographical details. For rough and non-specular surfaces, the angular dependence of reflectance yields rms roughness value.

The microstructure, distribution of grain sizes and inclusions, and crystallographic structure of coatings can be determined with the help of transmission electron microscopy and diffraction techniques. However, for this purpose, the coatings must be thinned down to < 1000 Å. Selected area diffraction of crystallites/inclusions, segregated regions yield information regarding their crystallographic structure and orientation. For thick specimens (> 0.5 μm), reflection electron diffraction and x-ray diffraction are used for the determination of the crystal structure and orientation effects.

(c) *Composition*

Composition on the surface and in bulk and its variation along the thickness of the coating can be determined by the Auger Electron Spectroscopy (AES) technique. In this technique, an electron beam incident on the specimen interacts with the atoms involving three atomic energy levels in the process and yields the so-called Auger electrons leaving the atoms doubly ionized. The energy of these Auger electrons is characteristic of the atom and the energy levels of the atom involved in the Auger process. The Auger transition probability and hence the Auger electron yield decreases with increasing atomic number. Due to the small range of escape depth of Auger electrons, the technique has a high (~ 30 Å) depth resolution. Therefore it is ideally suited for obtaining the depth profile of the constituents (i.e., the concetration of elements along the thickness of the specimen). Whereas the technique can detect the presence and relative concentrations of the elements to concentrations as low as 0.1 at. %, the accuracy of absolute atomic concentration determination is limited to a few percent because of the uncertainty in the sensitivity factors of the elements. A detection limit of 10^{-4} at. %(1 ppm) can be achieved with a Secondary Ion Mass Spectroscopy (SIMS) technique. With this technique it is also possible to establish the chemical state of the elements present in the specimen. On the other hand, the AES technique gives information on the presence of different elements only. For obtaining the chemical state and chemical mapping of the constituents, the better suited technique is that of Electron Spectroscopy for Chemical Analysis (ESCA). In this technique, an x-ray photon knocks-off an electron from the K-shell.

The measurement of the kinetic energy of the resulting electron yields the value of the binding energy of the electron. Since the binding energy of an atom depends on the environment in which it is sitting, the chemical state of the atom can be identified by the ESCA technique. Thus presence of various chemical compounds in the coating can be estimated. The chemical map provides the distribution of the various chemical species present in the film.

(d) *Absorptance and Emittance Measurements*

The measurement techniques for solar absorptance and hemispherical emittance can be classified into three categories: (1) Reflectance, (2) Radiometric, and (3) Calorimetric. The principles, accuracy and limitations of the techniques in terms of spectral and surface characteristics are described in the following (Dutta et al., 1980, Richmond 1979).

(1) *Reflectance Technique*

Reflectance measurement as a function of wavelength yields absorptance and emittance values directly while angular and wavelength dependence of reflectance provides valuable information on the surface topography if the coatings are rough.

(i) *Surface Roughness and Topography:* When light is reflected from a rough surface, both specular and diffuse optical scattering take place. The fraction scattered diffusely depends on the ratio of the roughness to the wavelength. If the rms roughness is small compared to the wavelength, the reflectance is primarily specular and corresponds to that of a smooth surface. If the surface roughness is large compared to the incident wavelength, reflection takes place in different directions. The angular dependence of the reflectivity of a rough surface for different wavelengths provides a useful technique for characterizing the rms roughness. The experimental set-up for such measurements is simple and straightforward, as shown in Fig. 29a. Polarization studies can provide additional information.

Figure 30 shows the angular dispersion of the normalized reflectance at an angle of incidence of 40°. The angular spread in the reflected beam is due to the scattering. The spread in the specular aluminium coating is because of the instrument function. It is clearly seen from this figure that the angular spread of scattering for black chrome is higher than that of dull nickel. The larger roughness of the black chrome is also indicated by the higher solar absorptance of this coating (Gogna and Chopra 1979c).

Figure 31 shows scattering for electroplated black chrome at two angles of incidence 20° and 60° and for two wavelengths 2.3 and 10 μm for a sample with rms roughness of 1.8 μm. It is clear that scattering decreases either with higher angle of incidence or with higher incident wavelength. As expected, the curve for $\lambda = 10\ \mu$m and 60° angle of incidence shows minimum scattering

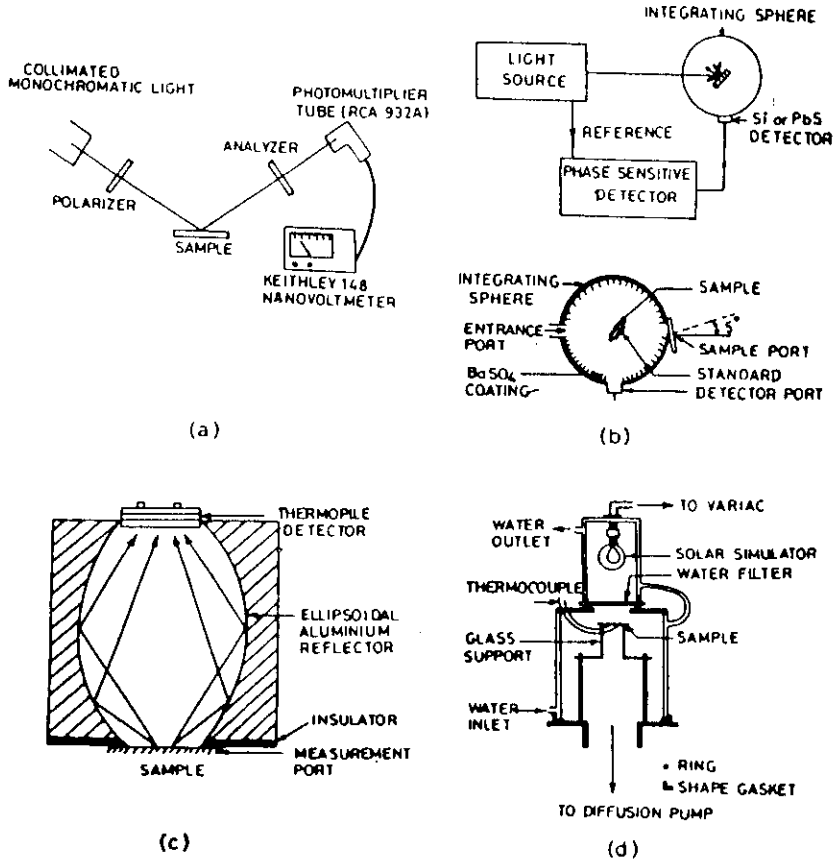

Fig. 29 Schematic diagrams showing the experimental set ups for (a) measurement of angular and wavelength dispersion of refletcance for the surface roughness characterization, (b) integrating sphere reflectometer (alphameter) for evaluation of solar absorptance, (c) ellipsoidal emissometer for thermal emittance characterization of solar absorber panels, and (d) calorimetric set up for the absolute measurement of absorptance emittance and stagnation temperature under dynamic conditions (Dutta et al., (1980).

and approaches that for a specular sample. However, there is an increase in scattering at $\lambda = 2.3\ \mu$m and 45° angle of incidence in comparison to angles of incidence on either side of 45°. This is due to the fact that roughness is of the order of wavelength (Behaghel 1979).

Information obtained from the above technique can be used to design selective surfaces by deliberately roughing the surface of a specular coating. For example, Lafait et al. (1981) has demonstrated that the selectivity of a specular TiN can be enhanced from $\frac{\alpha}{\epsilon} = \frac{0.42}{0.09}$ to $\frac{0.95}{0.34}$ on creating an rms surface roughness of 0.2 μ m.

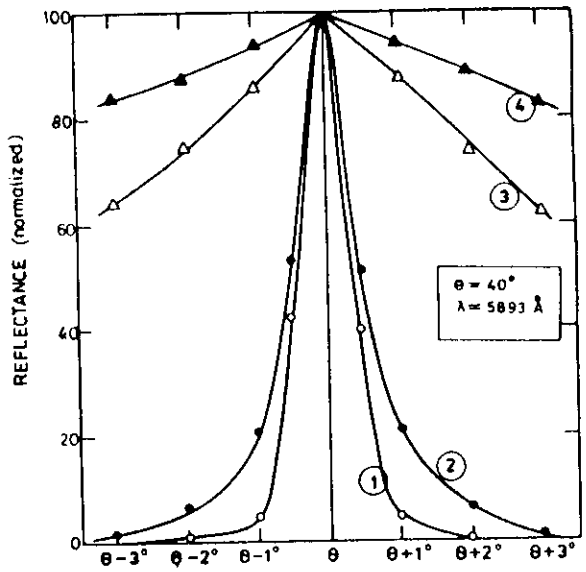

Fig. 30 Angular dispersion of reflectance for sodium light incident at an angle of 40° on specular aluminium coating (○), bright nickel plated steel (●), dull nickel plated steel (Δ) and electroplated black chrome coating (▲) (Gogna et al., 1979c).

(ii) *Absorptance:* The reflectance is measured on a double beam spectrophotometer as a function of wavelength in the range 0.3 to 2.5 μm against a freshly smoked MgO standard reflector. Due to the presence of both specular and diffuse components, it is generally essential to measure the integrated total reflectance of the selective coatings using an integrating sphere reflectance accessory. The averaging over given solar spectrum is carried out using numerical integration (Olson 1963) or by drawing the reflectance curve in distorted wavelength graph (Bradford and Hass 1963) and taking the area under the cuvre with the help of planimeter. In the later case, the wavelength interval is proportional to the solar energy falling within that interval. This method is called spectrophotometric method.

Integrating reflectometers of different designs have been developed to measure the solar reflectance and transmittance directly without the need of computation. These reflectometers use white light source for illumination of the sample and need either the sample of known absorptance or MgO standard for evaluation of the α of the specimen by comparison method. Pettit et al. (1978) have evaluated commercially available instruments and suggested modifications to improve the accuracy of measurements. An improved integrating sphere reflectometer fabricated in our laboratory (Fig. 29b) uses

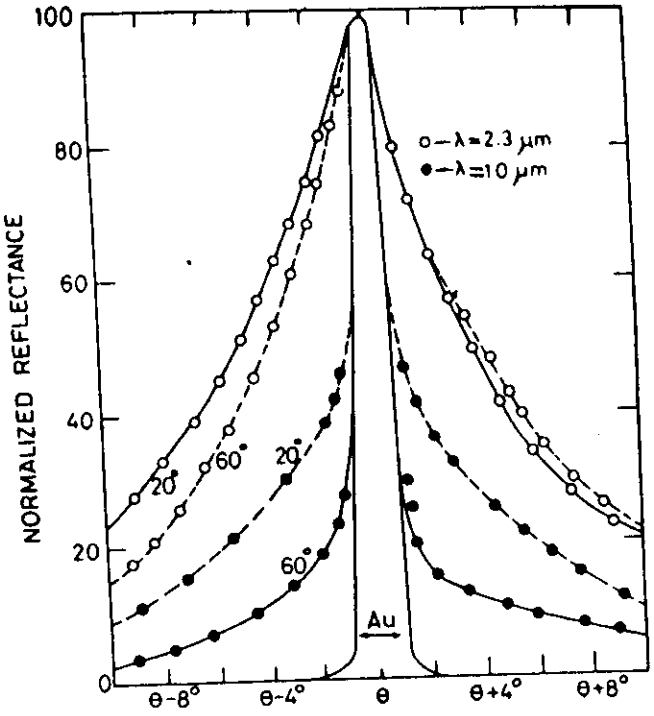

Fig. 31 Angular dispersion of reflectance of electroplated black chrome coating (surface roughness = 1.8 μm) at 20° and 60° angles of incidence using two different wavelengths, 2.3 μm (○) and 10 μm (●). The instrument function is shown in terms of dispersion of reflectance from a specular gold film (Behaghel et al., 1979).

tungsten lamp as the light source. The sample is either fixed at the surface of the sphere for evaluation of α or at the centre of the sphere for the angular hemispherical reflectance measurements. The white light source could be replaced by a monochromator to study the wavelength dependence. Silicon photocell and PbS detector with a silicon window have been used to cover the complete solar spectrum range. A pyroelectric detector having a flat response in the solar spectrum is a better choice except that the signal output is low. The signal from the detector is fed to a lock-in-amplifier locked to the chopping frequency of the incident light beam. The effective solar reflectance is calculated by comparing with the reflectance of a flat response Mg Oreflector. It may be mentioned that although the emission spectrum of the tungsten source does not match the solar spectrum, the integrated absorptance values obtained from the reflectometer are found to be in good agreement with those

calculated from the spectrophotometric method provided that the reflectance behaviour of the sample and the standard do not show any well pronounced variation.

(iii) *Emittance:* For the direct evaluation of the thermal emittance by spectrophotometric method one needs to measure the total reflectance in the infrared range of ~ 2 to 20 μm. Non-availability of integrating sphere reflectometers in this range of spectrum poses a problem for this direct measurement. However, one could measure the specular reflectance and compute ϵ by averaging over the black body spectrum at a given temperature, by numerical integration method. Since at higher λ and low surface roughness the total reflectance is almost same as specular component (Section 8(d)(i)) the ϵ calculated from specular reflectance data provides a good estimate of total thermal emittance.

In practice, heat cavity reflectometers can also be used for evaluation of total thermal emittance at any given temperature (Hembach et al., 1963; Behaghel et al. 1979). The sample is inserted into a black body cavity and illuminated from all directions by the radiation from black body walls or from the hot source kept inside the sphere. The thermal energy reflected in a specific direction is compared with that reflected or emitted by the cavity wall. The sample temperature is controlled and kept constant by circulating water through sample holder so that the effect of sample radiation can be minimized.

(2) *Radiometric Technique*

Direct radiometric measurements (Gaumer et al. 1963, Balickenderfer, 1976) are made by measuring the radiance of a heated sample and of a black body radiator at the same temperature and under the same spectral and geometric conditions and calculating the emittance as a ratio of the two radiances. If the radiation emitted in the complete hemisphere is measured then total hemispherical emittance can be obtained. We have designed a simple emissometer (Fig. 29c) to measure the total hemispherical emittance. It consists of an ellipsoidal concentrator machined from a solid aluminium cylinder. The internal surface is polished to get high surface reflectance. The radiation emitted from the sample/black body (or a ϵ standard) into hemisphere when the same is kept at one of the two focii of the ellipsoid, gets focussed onto the thermopile detector kept at the other focal point. A thermopile detector is used because of its flat spectral response. The signals from the sample and black body are measured and then the emittance calculated by taking their ratio.

(3) *Calorimetric Technique*

The total hemispherical emittance and solar absorptance can be accurately measured using calorimetric set-up (Balickenderfer 1976, Gaumer 1963). Here, the radiant heat transfer from thermally isolated sample is measured in terms

of the heat lost or heat gained from the surrounding. The rate of heat transfer is evalutated in terms of three modes: (a) temperature change and heat capacity of the sample (Balickenderfer 1976, Gaumer 1963, Willrath and Gammon 1978), (b) heat input required to maintain the sample in thermal equilibrium (Curtis 1966), and (c) heat flow from or to a sink (Meinel and Meinel 1976). In those modes, since the sample is kept thermally isolated, the heat transfer to the surrounding is mainly by radiation and the other losses are negligible.

(i) *Dynamic Method:* Figure 29d shows the schematic of a calorimetric set up. In this method, the sample is heated by the absorption of photon flux from a solar simulator and cools by radiation. The solar absorptance, hemispherical emittance and their ratio can be calculated from the measured rates of heating and cooling and the equilibrium temperature of the specimen by using the following simple heat balance equations.

When the sample is exposed to solar radiation the absorptance, α, is given by

$$\alpha = \frac{mC_p}{A_1 I_s}\left(\frac{dT}{dt}\right)_h \tag{8.1}$$

where m is the mass of the sample, C_p, its specific heat, and $\left(\frac{dT}{dt}\right)_h$ its heating rate. A_1 is the irradiated area of the sample and I_s is the irradiation intensity. In this equation the radiation losses are neglected by assuming that $T \simeq T_2$, the ambient temperature.

When radiation source is turned-off, the sample cools and we have

$$\epsilon = \frac{mC_p}{A_2\sigma(T^4 - T_2^4)}\left(\frac{dT}{dt}\right)_c \tag{8.2}$$

where $\left(\frac{dT}{dt}\right)_c$ is the cooling rate at temperature T of the sample, T_2 is the temperature of the surrounding, A_2 is the total area of the sample and σ is the Stefan-Boltzmann constant.

Under constant irradiance from solar simulator an equilibrium is reached when heating and cooling rates are equal and sample attains a stagnation temperature, T_1. Then we have

$$\frac{\alpha}{\epsilon} = \frac{A_2\sigma(T_1^4 - T_2^4)}{I_s A_1} \tag{8.3}$$

The most important advantage of the method is that it yields absolute values without the need for any comparison standard. Also ϵ and $\frac{\alpha}{\epsilon}$ as a function of temperature could be obtained.

(ii) *Steady State Method:* In this method the sample is maintained at a constant temperature with an external heating source. The specimen temperature and the power required to maintain the temperature are measured. With this data, hemispherical emittance can be calculated by means of the Stefan-Boltzmann law.

The specimen heater with resistive heating is attached to the sample and a good thermal contact between the two is ensured. This assembly is placed in a heat shield so that there is no heat loss by radiation from the back and edges. A thermocouple is attached to the specimen for the measurement of temperature. The heater and thermocouple leads are so arranged that only a negligible amount of power is lost via conduction through them. The sample-heater assembly is placed in a vacuum chamber in which exists a provision to illuminate the sample from outside. The hemispherical emittance of the sample is calculated by comparing the power required to maintain at same temperature the samples of unknown and known emittance.

The absorptance is determined in a two-stage measurement. The power required to maintain the sample at the same temperature is measured under two conditions: with and without simulated solar flux incident on the sample. The difference between the two power measurements is the rate at which the incident solar energy is being absorbed. Thus by knowing the incident energy, the absorptance can be calculated.

(iii) *Heat Flow Method:* The sample is placed on a heat-sink-block of copper, whose temperature can be varied. The sample is interfaced with the block by means of a high conductivity lubricant/paste. A heat flow sensor is placed between the sample and the block. The complete assembly is placed in a double walled vacuum chamber in which a window is provided to allow solar flux to impinge on the sample. The chamber wall is maintained at ambient temperature through water circulation. When solar flux is allowed to be incident on the sample, its temperature rises and reaches to an equilibrium determined by the rate of water flow through the copper block. Under equilibrium

$$\alpha I_s = \epsilon\sigma(T^4 - T_2^4) + Q \text{ (water)} \qquad (8.4)$$

If we adjust the water flow such as to hold the sample at the same temperature as that of the chamber (i.e. $T^4 = T_2$), the emitance of the sample can be neglected and α can be measured directly from the rate at which the heat flows from the sample into the block.

To measure ϵ, the incident solar flux is cut-off and sample raised to a temperature higher than the chamber temperature, T_2, so that heat radiates out from the sample. The emittance is calculated from the rate at which heat flows from the block into the sample.

We conclude this section by pointing out that every method for the measurements of optical and thermal properties of selective coatings has its own merits and drawbacks. The accuracy of spectral reflectance measurements (used for calculating solar absorptance) depends on the spectrophotometer used. With great care it is possible to achieve $\simeq 1\%$ overall accuracy. This method is applicable to all types of specimens irrespective of the spectral characteristics of the sample. The α measured with an integrating sphere reflectometer using white light source is highly dependent on the spectral characteristics of the sample. The heat cavity reflectometer has the limitation that the sample must be cut to a specific size and should be a reasonably good thermal conductor. Radiometric method and the calorimetric technique under steady state need a standard for comparison. The calorimetric technique in the transient mode gives absolute values, but requires a sample with identical coatings on both the sides. The spectral characteristics of the sample do not affect the measurement and the coating parameters (ϵ in particular) could be obtained under conditions more close to those under actual operation. However, a great care must be exercised to reduce the conduction and convection losses.

9. DEGRADATION PROCESSES

Photothermal converters function at temperatures ranging from 100°C for flat plate collectors to over 600°C for two axis tracking parabolic dish concentrators and central receivers. Daily diurnal cycles, cloud passage, loss of coolant and exposure to humidity and atmospheric gases may seriously affect the life and performance of these coatings. The coatings are also exposed to U.V. flux that may initiate photochemical changes.

The physical and chemical mechanisms leading to the degradation of selective coatings have not yet been fully investigated although a considerable amount of research is going on in this field at present (Gogna 1980, Hahn and Seraphin 1978, Seraphin 1982). A selective surface may degrade by one of the following processes.

(a) *Substrate Degradation*

Lack of homogeneity and structural integrity at the coating/substrate interface may result due to the formation of intermetallic compounds between the metallic constituents of the lower part of the coating and the substrate metal or within the substrate. This may lead to severe microcracking in the deposit.

(b) *Thermochemical Changes*

The coating may undergo thermal decomposition resulting in the volatilization of hydrated metallic compounds or thermally decomposable complexes. It may react with the atmospheric gases like O_2, CO_2, water vapours undergoing oxidation or carbonization. The resulting products, if volatile, would escape out or remain in the coating causing changes in the fill factors

of the metallic and dielectric constituents and thus changing the effective dielectric constant of the medium which consequently leads to changes in the optical properties of the coating.

(c) *Diffusion Effects*

A graded index (metal-dielectric) material or a multilayer stack may undergo interdiffusion of the coating constituents to a homogeneous distribution of the components. Thus the absorptance would change to the values typical of a homogeneous coating. One or more components of the coating may also diffuse into the substrate or vice versa leading to an increase in the effective thickness of the coating. At higher temperatures, the substrate material may diffuse out to the surface and undergo atmospheric oxidation. Such combined processes of diffusion of substrate material and its consequent oxdation may convert an initially smooth film to a particulate type of film. Such particulate transformation of the coating may wash out the interference peaks of an as-deposited coating.

(d) *Topographical Changes*

Heat treatments may change the particle shape and size leading to changes in the reflectance profile of the coating. Heating may convert non-spherical particles to more spherical particles due to surface tension effects which reduces the particles surface energies.

(e) *Phase Transformations*

Heating may lead to a phase transformation of some constituents of the coating. For example, on heating a black chrome coating at or above 400°C, the initial amorphous form of the oxide Cr_2O_3 is converted into polycrystalline form.

We will now describe the degradation of some important selective coatings in the light of the processes given in the preceding.

(1) *Black Chrome:* Spitz and coworkers have carried out a detailed structural and compositional analysis of their black chrome films annealed at 350 C in air (Ritchie et al. 1979/1980). From the SEM, TEM and the electron diffraction studies of as-deposited and annealed films, they observed distinct structural and compositional changes on annealing for 24 h and 135 h. As-deposited films consist of oriented needle like metallic chromium particles embedded in an unidentified amorphous phase. Several other oxides of Cr, namely, CrO_2, CrO, Cr_3O_4 and Cr_2O_3 are also present in the form of fine grains. Annealing for 24 h results in the transformation of needle like grains into spherical grains and most of the amorphous phase and various chromium oxides transform to the stable Cr_2O_3 phase. 135 h anneal results in a complete transformation of needle like particles to spherical ones and only Cr and Cr_2O_3 are present in the film. Also the orientation of Cr particles changes from (111) to (100). No material loss from the film or material gain from oxygen adsorption is observed. The solar absorptance of the as-deposited film changes from 0.98 to 0.88 for 24 h anneal and to 0.84 for 135 h anneal and the room temperature emittance changes from 0.20 for as-deposited film to 0.11 and 0.08 respectively. It seems that the change in shape of chromium particles on annealing at 350°C is the most important morphological change accompanying the degradation in solar absorptance.

According to Lampert (1979a), the black chrome consists of three different regions: (1) thin Cr_2O_3 top layer; (2) a graded intermediate Cr_2O_3-Cr cermet; and (3) a Cr-Cr_2O_3 cermet dominated with Cr. The Cr_2O_3 either is in amorphous or very fine crystallite form. The coating degrades above 400°C in air and 500°C in vacuum. The major mode of degradation being the diffusion controlled oxidation. Diffusion of O_2 is enhanced by outgassing of CO and CO_2 resulting in cracks in the film. Thus, preferential diffusion paths are provided. During the oxidation process metallic chromium gets depleted and growth of Cr_2O_3 takes place at the surface. With time, coating densifies with elimination of porous structure and the absorption is dominated by the metal substrate.

Zajac and Ignatiev (1979, 1982) have also investigated mechanisms leading to high temperature degradation of black chrome. They have postulated three basic modes of degradation.

(i) Creation of voids due to the escape of volatile constituents, if any, of the film and the surface decomposition of $Cr(OH)_3$ of the film at temperatures less than 300°C according to reaction.

$$2\,Cr(OH)_3 \rightarrow Cr_2O_3 + 3H_2O\uparrow$$

(ii) Oxidation of Cr to Cr_2O_3 in the temperature range of 300-500°C with associated changes in the optical properties.

(iii) At temperatures above 500°C, the underlying Ni deposit starts diffusing out to the top surface and associated with its oxidation results in a major degradation of the system.

The SEM and AES depth profile data of high temperature (> 500°C) degraded black chrome coating, has shown the existence of a rough NiO layer at the top surface below which lies a layer of linear gradation from NiO to Ni. A good agreement between the reflectance calculated according to the model and the experimental data has been established. This suggests that the high temperature degradation of black chrome prepared on nickel coated metal substrates is primarily a Ni substrate dominated process. Thus replacement of nickel with other high temperature stable materials could increase the stability of black chrome.

(2) *Black Nickel:* The main reason of optical degradation of black nickel coating even at relatively lower temperatures (≈200°C) is due to the carbonization of the oxides and sulphides of nickel. To overcome low temperature

degradations, the outer surface is passivated by a process such as chromatizing. High temperature (200 to 500°C) degradations of black nickel probably result from mechanisms similar to the black chrome coatings. In electroless black nickel coatings (Kumar et al. 1980) deposited on galvanized steel, substrate degradation occurs at a temperature ≈ 300°C due to the formation of a Fe_xZn_y compound and the coating starts peeling off.

(3) *Solution Grown Multilayer Stacks:* Extensive studies on the degradation mechanisms of the solution grown multilayer stacks of PbS/CdS, PbSe/CdSe, PbS/SnO_2 and PbS/ZnO selective coatings have been carried out in the authors' laboratory (Reddy et al. 1983). The following has been established: (i) Atmospheric oxidation was responsible for degrading the PbS/CdS coating at temperature > 380°C and PbS/SnO_2 coating at temperatures >400°C. (ii) Inter-diffusion of layers occurred in PbS/ZnO coating at temperatures≈ 400°C and at temperatures ≈440°C in the PbS/CdS system. (iii) PbSe/CdSe coatings degraded due to the thermal decomposition at temperatures >250°C. In (i), the atmospheric oxygen was found to be incorporated in the PbS layer in both the coatings. Also the slightly higher temperature stability of the PbS/SnO_2 coating arises because of the thermal stability of SnO_2. In (iii), the thermal decomposition of the CdSe layer of the PbSe/CdSe system occurs. The AES depth profiles for as-deposited and annealed PbS/CdS stack is shown in Fig. 17.

(4) *Nickel Pigmented Anodized Aluminium:* Anodic alumina is an integral part of the substrate in these coatings. Alumina, being a high temperature stable material and an excellent diffusion barrier of oxygen atoms, resists thermochemical changes and is also chemically inert to atmospheric gases. Further, nickel particles are embedded inside the pores of the anodic alumina, thus avoiding direct exposure to the environmental gases. The coating thus has a higher stability compared to the black chrome and black nickel coatings for medium temperature (200-400°C) applications. Humidity, however, poses a serious problem to the aluminium substrate. Aluminium corrodes slowly at higher temperatures on long term exposures under saline water conditions. Thus, in this case the substrate corrosion is more likely than the coating degradation.

(f) *Passivation Processes*

Selective coatings can in some cases be passivated by post-deposition treatment against degradation. Driver and McCormick (1982) have shown that the black chrome coatings prepared by electrolytic processes show higher stability if films are deposited at low rates in order to minimize deposit stresses and to provide stabilizing oxide layers on the surface particles. For high temperature applications, all black chrome coatings would probably benefit from an initial deposition in excess of the as-plated optically optimum coating followed by a post-deposition annealing to remove the volatile matter.

A novel approach to increase the low temperature (≈ 200°C) stability of black nickel coatings has been reported by van de Leest et al. (1981). Their treatment consists of applying an overcoating by dipping in a neutral chromate solution which passivates the black nickel coating. The passivating treatment results in the deposition of a thin chromium oxide layer, which does not change the optical properties of the initial black nickel deposit. Another passivation process is by electrochemical treatment using a periodic reversal of current. The passivating solution in both the cases are a dilute chromate solution of 10 g CrO_3 per litre solution at a pH = 7. The electrochemical treatment give a better protection. Results of ambient and humidity exposure tests showed that the initial α and ϵ values of 0.95 and 0.23 respectively of a typical black nickel coating changed to 0.38 and 0.20 after 3 days of humidity exposure when no passivating treatment was given. Another coating with an initial $\alpha = 0.96$ and $\epsilon = 0.25$ on chemical passivation and subsequent 3 days humidity exposure gave $\alpha = 0.96$ and $\epsilon = 0.20$. Similarly, a coating with an initial $\alpha = 0.96$ on ambient exposure for one year changed its α to 0.88 while the same coating on electrolytically passivating at a frequency of 0.75 Hz and a current density of 0.4 A/dm² had an $\alpha = 0.94$ after one year's ambient exposure.

It should be noted that the passivation is not possible in case of ordinary bright nickel coatings, but the presence of Zn particles in the electroplated and electroless black nickel coatings and their small particle size contributes to the formation of Cr oxide required for passivation. After passivation, the electrode potential of black nickel coatings shifts to more noble values, which confirms that the new coating obtained is indeed a passive one.

10. APPLICATIONS

10.1 Solar Thermal Conversion

In order to appreciate the role of selective coatings in the performance of collectors for photothermal conversion, let us first examine the factors which determine the conversion efficiency. The conversion efficiency, η, of a collector system is defined as

$$\eta = \frac{\text{Energy extracted from the system}}{\text{Energy input}}$$

$$= \frac{E_e}{A_1 I_s} \tag{10.1}$$

where A_1 is the area of the absorber exposed to the solar flux and I_s the incident solar flux. The extracted energy, E_e, from the system can be written as

$$E_e = (\text{Energy absorbed}) - (\text{Energy lost})$$

$$= (\tau\alpha) A_1 I_s - U_L \tag{10.2}$$

-34-

where $(t\alpha)$ is the effective transmittance absorptance coefficient product for a single covered collector, t is the transmittance of the cover glass and U_L the overall loss of energy from the absorber. U_L is the sum of three parameters that are involved in this process, namely, radiation, conduction and convection losses.

Radiation losses, governed by Stefan-Boltzmann law, are proportional to the emittance of absorber and to the fourth power of the temperature. The other two losses, strongly dependent on the configuration and environment of the system, are linearly proportional to the temperature. The estimation of collector efficiency will become cumbersome and also vary from place to place when we consider the conduction and convection losses. Hence, to illustrate the effective role of the selective absorbers in photo-thermal conversion, we first consider a simple case of collectors, where we assume that the conduction and convection losses are negligible compared to that through radiation process. This assumption is perfectly valid for practical cases also if the collector is operating at high temperatures. In the second part of this section, we choose a practical system where conduction and convection losses will also be considered for η calculation.

For the first case, U_L term in Eq. 10.2 can be replaced with the radiation loss term, so we get

$$E_e = (t\alpha)A_1 I_s - \sigma A_2 \epsilon (T - T_2^4) \tag{10.3}$$

where A_2 is the area of the absorber, ϵ thermal emittance at temperature T of the absorber, T_2 the temperature of the ambient.

From Eqs. 10.1 and 10.3, we have

$$\eta = \frac{E_e}{A_1 I_s} = \frac{(t\alpha)A_1 I_s - \sigma A_2 \epsilon (T^4 - T_2^4)}{A_1 I_s}$$

$$= (t\alpha) - \frac{\sigma A_2 \epsilon}{A_1 I_s}(T^4 - T_2^4) \tag{10.4}$$

since in practice $A_1 = A_2$ and if we are illuminating the absorber with a concentrated solar flux of concentration ratio X, we can write Eq. 10.4 as

$$\eta = (t\alpha) - \frac{\sigma \epsilon}{X I_s}(T^4 - T_2^4) \tag{10.5}$$

In both flat plate and concentrating collectors, we see that to maximize η we must reduce U_L and consequently the radiative losses to the maximum possible extent while at the same time holding the absorptance-transmittance product close to unity. It would seem difficult to meet both these conditions simultaneously. But, this is possible if we examine in Fig. 1 the separation between the energy distribution of solar spectrum ($\approx$ 5800 K black body) and the black body radiation spectrum at 100, 300 and 700°C. It is this shift between the two spectra which makes it possible for a number of materials to have high solar absorptance and low thermal emittance. The cut-off wavelength, λ_c, at which both these spectra intersect, is dependent on the absorber temperature. Figure 1 also shows the dependence of the cut-off wavelength and absorber temperature for various concentration factors. For a selective surface, the cut-off wavelength is defined as the wavelength corresponding to 50% of the reflectance value.

Some features of the performance of photothermal converters depend on α and ϵ separately. Therefore, sometimes (Seraphin 1979) a term "absorptance of merit", α_m, which is nothing but η with no cover ($t = 1$ in Eq. 10.5), is used. From Eq. 10.5, we have

$$\alpha_m = \alpha - \frac{\epsilon\sigma(T^4 - T_2^4)}{X I_s} \tag{10.6}$$

Hence the absorptance of merit gives an upper limit for the conversion efficiency of a solar converter. Figure 32 shows the dependence of the absorptance of merit on the thermal emittance for two solar absorbers—one with $\alpha = 0.95$ and another with $\alpha = 0.90$, for a temperature $T = 500$°C. For $X = 1000$, reducing the emittance to smaller values does not compensate for the difference in α of 0.05. However, for $X = 250$, lowering the emittance by 0.4 for the inferior α value coating renders it equal to the surface with $\alpha = 0.95$. In case of concentration of 100, reduction of only 0.15 in the emittance with $\alpha = 0.90$ makes the coating as effective as the $\alpha = 0.95$ coatings.

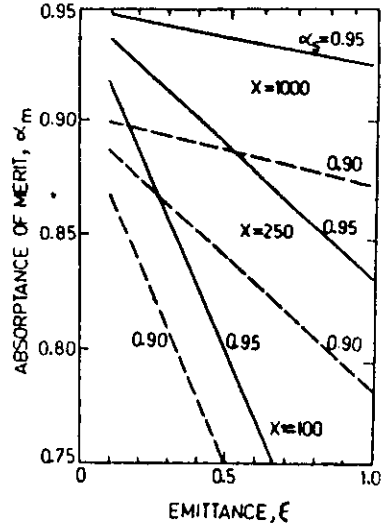

Fig. 32 Absorptance of merit as a function of emittance for solar absorbers of $\alpha = 0.95$ (——) and 0.90 (– – –) at various solar concentrations showing the effectiveness of selective absorber and the relative importance of the magnitudes of α_m and ϵ. The operating temperature of the absorber is 500 C (Seraphin, 1979).

It is clear that by using a selective surface, the collection efficiency can be improved. Winegarner (1975) has calculated the η values of typical flat plate and concentrating collectors with one glass cover. Figure 33 shows the effect of using a solar selective surface for a single glass covered solar absorber operating at 95°C as evaluated by Gogna (1980). Because of the low thermal emittance of the selective absorber as compared to a non-selective one, the thermal losses are reduced from 31.7% to 19.7%. Thus the efficiency of the collector is raised from 43.6% to 53.8%. Similar evaluation for parabolic concentrator type solar collector has been carried out by Winegarner (1975). Figure 34 shows the results as obtained by him.

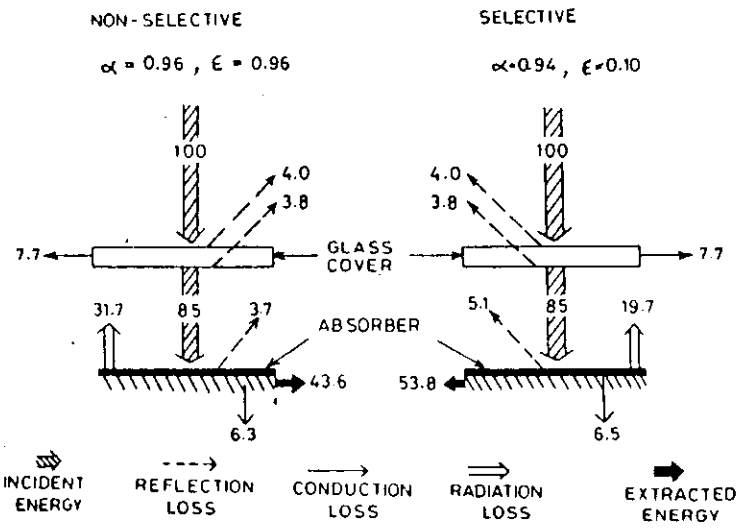

Fig. 33 Estimated net collection efficiency of a given selective absorber compared to a non-selective one for a flat plate collector operating at 95 °C with ambient temperature of 25°C (Gogna, 1980).

Spitz (1977) evaluated the collection-efficiency in terms of collector temperature and concentration. Figure 35 shows graphically the efficiency nomogram constructed by him.

We can measure the output in terms of the mechanical work also by using a Carnot efficiency cycle. The Carnot efficiency, defined as the ratio of the output work to the input heat for a particular thermodynamic cycle, is given by

$$\eta_{(\text{Carnot})} = \frac{W}{Q_h}\,\frac{Q_h - Q_e}{Q_h} = \frac{T_h - T_e}{T_h} \qquad (10.7)$$

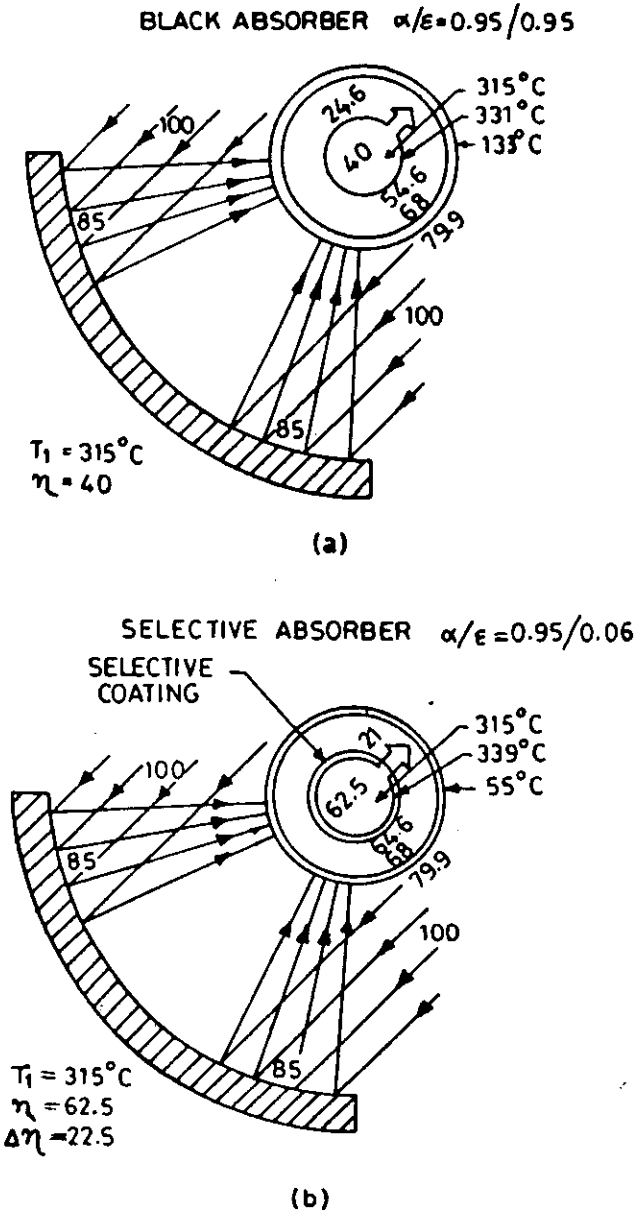

Fig. 34 Estimated net collection efficiency of a given selective absorber compared to a non-selective one for a concentrating parabolic collector operating at 315°C with ambient temperature of 21°C (Winegarner, 1975).

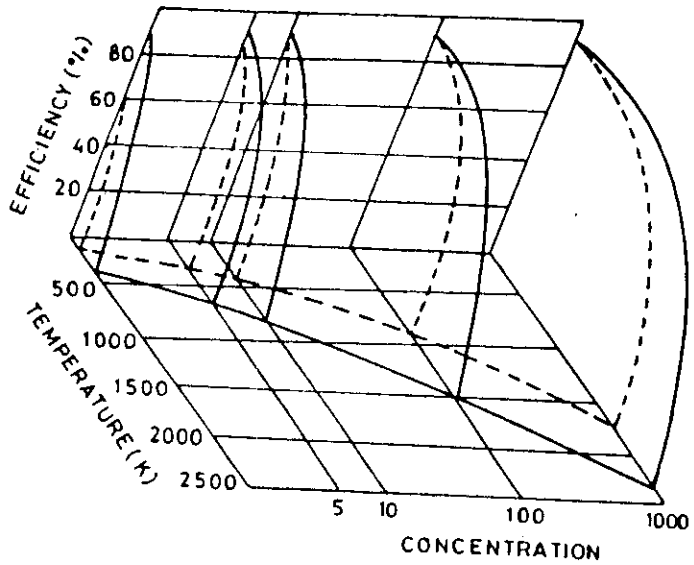

Fig. 35 Conversion efficiency as a function of operating temperature and concentration for a solar collector using a selective absorber with $\alpha = 0.90$, $\epsilon = 0.10$ (——) and black body absorber (– – –) (Spitz, 1977).

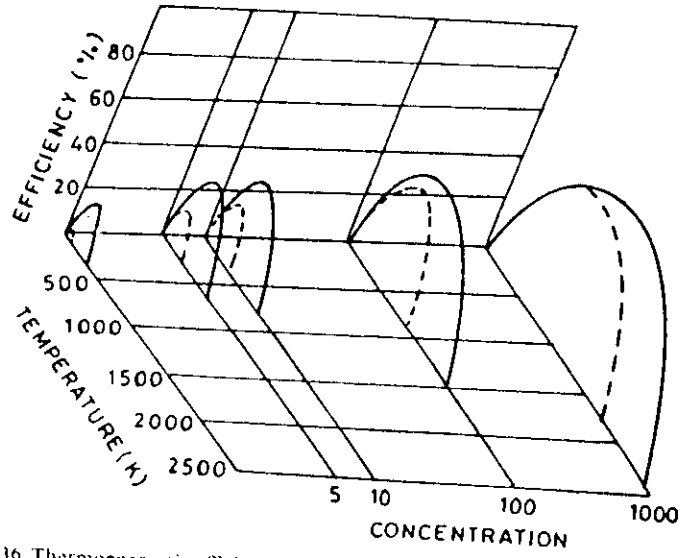

Fig. 36 Thermoenergetic efficiency as a function of operating temperature and concentration for a solar collector executing the Carnot cycle: using a selective absorber (——) with $\alpha = 0.90$, $\epsilon = 0.10$ and a black body absorber (– – –) (Spitz, 1977).

where Q_h is the input heat, Q_e the exhausted heat, T_h input temperature, T_e the exhaust temperature and W the output work. Based on Carnot efficiency (Spitz 1977), the collection efficiency calculated in terms of the mechanical output for a solar collection is shown in Fig. 36.

Now we consider some practical aspects of collectors in the η calculations. As we already mentioned in the beginning, the conduction and convection losses are strongly dependent on the environment (wind velocity, humidity, ambient temperature) and on the configuration of the systems (number of glass covers, space between the covers and the absorber, tilt angle of collector, and the thickness of the insulating layer at the bottom of the absorber). Hottel and Whillier (1955), Hottel and Woertz (1942), Bliss (1959), Whillier (1967) and Gupta and Garg (1967) have discussed the thermodynamic equations governing the efficiency of solar collectors. In practical flat plate collector system, the extracted energy can be redefined as the energy transferred to the flowing liquid. Thus,

$$E_e = \dot{m} C_p (T_0 - T_i) \tag{10.8}$$

where $\dot{m}$ is the mass flow of the heat transfer fluid (usually air or water), C_p the heat capacity of the working fluid, T_0 and T_i are outlet and inlet temperatures of the fluid respectively. Therefore η can be written as, from Eq. 10.2,

$$\eta = \frac{\dot{m} C_p (T_0 - T_i)}{A_1 I_s} = (\alpha t) - \frac{U_L (T_p - T_2)}{I_s} \tag{10.9}$$

where U_L, the energy loss, is a function of $(T_p - T_2)$. T_p is the average plate temperature. The terms on the right hand side in Eq. (10.9) correspond to a straight line equation. The slope of the line is the overall collector heat loss U_L and the ordinate intercept is equal to (αt).

The efficiency can also be plotted as a function of the average fluid temperature $T_f = (T_i + T_0)/2$, and the inlet temperature T_i.

$$\eta = F_P \left[\alpha t - U_L \frac{(T_f - T_2)}{I_s} \right] \tag{10.10}$$

and

$$\eta = F_R \left[\alpha t - U_L \frac{(T_i - T_2)}{I_s} \right] \tag{10.11}$$

F_P in Eq. 10.10 is called the plate efficiency factor and is the ratio of the actual useful energy collected to the useful energy that would have been collected if the entire receiver plate were at the average fluid temperature. Similarly, F_R is the heat removal efficiency factor and is the ratio of the useful energy collected to the useful energy that would have been collected if the entire plate were at the entering fluid temperature. F_P and F_R are independent of the solar intensity, the collector operating temperatures T_f and T_p and the ambient temperature.

For concentrating type solar collectors, Eqs. (10.9), (10.10) and (10.11) are essentially valid. The efficiency of concentrating collector is given by

$$\eta = \frac{\dot{m}C_P(T_0 - T_i)}{XI_tA_1} F_P \left[\alpha_t\beta - \frac{U_L(T_f - T_2)}{XI_t}\right] \qquad (10.12)$$

where β is a cosine factor that is the weighted average of the angles of incidence of the concentrated rays.

The effect of the α, ϵ and number of glass covers on the conversion efficiency has been calculated by Gogna et al. (1980) for a typical flat plate collector. Table 5 shows the values of various parameters used for this evaluation. These values are typical of a clear day in Delhi.

Table 5

Typical configuration and operating parameters used in the calculation of plate efficiency

Solar Insolation, I_t	=800 W/m²
Wind velocity	=2.2 m/s
Absorber temperature	=95° C
Ambient temperature	=25 C
Radiation incident angle	=0 C
Collector tilt angle	=45°
Back thermal insulation thickness (glasswool)	=5 cm
Gap between absorber and cover	=3 cm
Thermal emittance of glass	=0.85
Infrared transmittance of glass	=0.0
Solar transmittance of glass	=0.84

The collection efficiency thus obtained is plotted as a function of thermal emittance in Fig. 37 and as a function of solar absorptance in Fig. 38. It can be clearly seen that emittance has a significant effect on the collection efficiency, particularly for a single cover collector. In the case of collection efficiency as a function of solar absorptance, it is seen that the η change is significant in the cases of both single and double covers.

In practice, the η of a single cover system is more affected by the convection heat losses (through the atmosphere) rather than by the optical properties of the absorber surface. However, for two cover systems, the solar transmittance losses are high due to the reflection and absorptance at each cover. Also, the two cover systems substantially reduce the heat losses and increase the efficiency.

Experimental Results

The thermal performance characteristics of a flat plate solar collector can be measured with the help of a simple set-up operated either in an open mode or a closed mode. The test rig consists of (1) a variable inclination

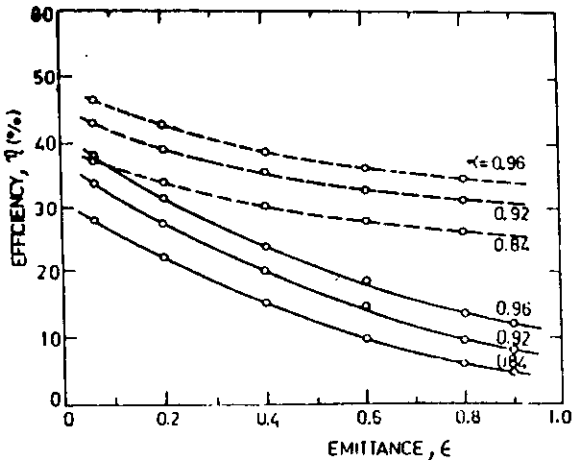

Fig. 37 Calculated conversion efficiency as a function of thermal emittance for solar absorbers of α=0.84, 0.92 and 0.96 using single (——) and double (– – –) glass covers. Operating temperature is 90 C (Gogna, 1980).

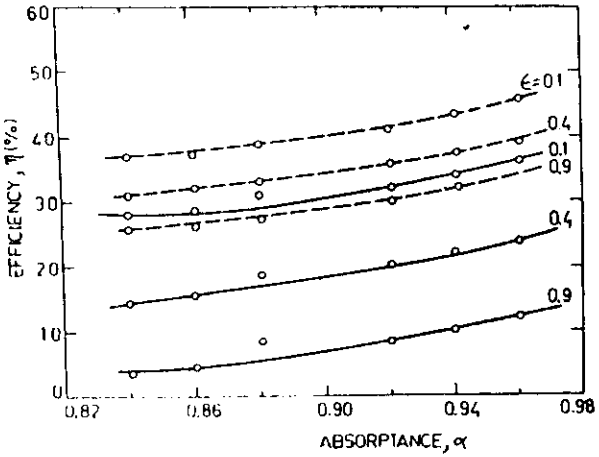

Fig. 38 Calculated conversion efficiency as a function of solar absorptance for absorbers with ϵ=0.1, 0.4 and 0.9 using single (——) and double (– – –) glass covers. Operating temperature is 90 C (Gogna, 1980).

stand to hold the collector and (2) instrumentation to measure insolation, water inlet and outlet temperatures, ambient temperature and water mass flow rate. Using this test rig, the conversion efficiency of a selective coating over that of a non-selective one have been evaluated (Gogna et al. 1980). The black nickel selective coating ($\alpha = 0.93$ and $\epsilon_{100} = 0.1$) used as absorber was prepared by the chemical conversion process. The non-selective collector panel was made by coating a flat black paint ($\alpha = 0.96$, $\epsilon_{100} = 0.90$). The curves of thermal efficiency for both the non-selective and selective coated collectors are shown in Fig. 39. Knowing αt and using Eq. 10.10, the magnitudes of F_R and U_L could be calculated. These values in this case have been found to be 0.84 and 0.92, and 13.0 and 9.2 $Wm^{-2}°C^{-1}$ respectively for non-selective and selective coated collectors. The lower value of U_L and higher F_R, despite a low α, is a consequence of lower ϵ of the selective coating. The most important feature to be observed from Fig. 39 is that a respectable thermal efficiency ($\approx$ 25-30%) is obtained when the selective coated collector is operated around 95-100°C. In sharp contrast, the non-selective coated collector has an efficiency of only 8%.

10.2 Antireflection Coatings

As already described in Section 4.3, reflection losses are reduced by antireflection coatings and are thus required to enhance the efficiency of both solar cells and solar thermal conversion systems. An AR coating thus becomes an important part of the convertor design. The material chosen for an AR coating depends upon the optical properties of the outermost surface considered and nature of the application that needs it. The applications of the AR coatings can be divided into three categories: (a) solar cell, (b) solar thermal collector and (c) cover glass for a solar collector.

(a) *Solar Cell*

Materials used in solar cells such as Si, GaAs, and CdTe have high indices of refraction and consequently have high reflection losses. For example, bare polished silicon ($n = 3.85$ at $\lambda = 0.8$ μm) reflects an average of 35% of the incident solar radiation in the 0.3-1.2 μm region. The optical properties of the AR coating materials to be used in this application must satisfy two requirements: they must havea perfect transparency in the wavelength range of sensitivity of the solar cell (e.g. 0.4-1.1 μm for Si) and should produce a maximum reflection reduction in this spectral range. A number of such dielectric materials are listed in Table 6.

As discussed in Section 4.3, properly designed single layer and multilayer structures can be used as AR coatings. The best advantage of single layers is in the case of obtaining the AR coating. For example, for Si, neglecting dispersion, a quarterwave AR layer requires a material of refractive index 1.96 (i.e. $\sqrt{3.85}$). Such a material happens to be silicon nitride. The thickness d of Si_3N_4 which gives zero reflectance at a given λ_{min} is determined by

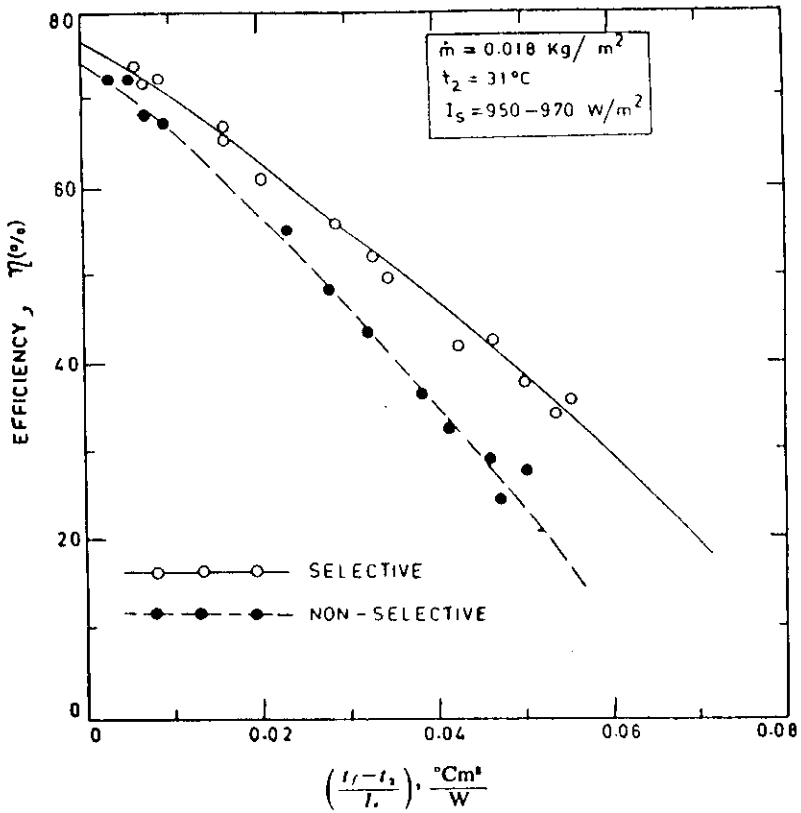

Fig. 39 Experimentally measured conversion efficiency curves for single glass covered flat plate collector: (○) with selective black nickel coating ($\alpha = 0.93$, $\epsilon = 0.09$) prepared by chemical conversion and (●) with non-selective black paint coating ($\alpha = 0.96$, $\epsilon = 0.9$). Inset show the operating parameters of the collector(Gogna et. al., 1980).

$\lambda_{min} = 4$ nd. A quarter wave Si_3N_4 coating with λ_{min} at 0.55 μm reduces the reflectance of Si surface to an average of 12% in the spectral range of 0.4-1.1 μm. Another useful single layer material is SiO with refractive index of 1.8-1.9. However, this material has some absorption losses in the visible region. A substitute for SiO is CeO_2 which has a low absorption in visible but a higher refractive index of 2.2. Koltun (1981) has reported that ~0.15 μm layer of SiO is the optimum layer on Si solar cell under AM0 illumination. This layer produces a 45%increase in the short circuit current, J_{sc} of the cell and also largely modifies its spectral response (Fig. 40). The optimum optical thickness required has a range of values which is an advantage from production point of view as well as for satisfying other requirements such as mechanical strength and integrated absorption coefficient of the coating.

Table 6

Refractive index in visible and IR regions and wavelength region of transparency of some dielectric materials useful for preparation of single/multiple layer AR coatings

Material	Refractive index		Region of Transparency, μm
	Visible	Infrared	
Aluminium Oxide (Al_2O_3)	1.59	1.59	0.3-1
Ceric Oxide (CeO_2)	2.2	2.2	0.4-16
Cryolite (Na_3AlF_6)	1.35	—	0.2-14
Germanium (Ge)	4.2	4.0	1.7-100
Indium Oxide (In_2O_3)	1.8	—	0.3-1.5
Magnesium Fluoride (MgF_2)	1.38	1.35	0.21-10
Silicon (Si)	3.85	3.5	1.1-10
Silicon Monoxide (SiO)	2.0	1.7	0.5-8
Silicon Dioxide (SiO_2)	1.46	1.44	0.2-8
Silicon Oxide (SiO_x)	1.52	—	0.3-8
Titanium Dioxide (TiO_2)	2.2	—	0.35-12
Tin Oxide (SnO_2)	2.0	2.0	0.3-1.7
Zinc Oxide (ZnO)	2.0	—	0.4-2.0

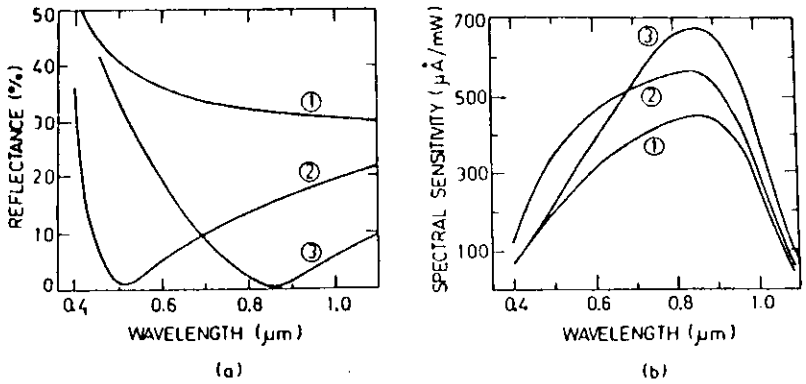

Fig. 40 Wavelength dependence of (a) reflectance and (b) absolute spectral sensitivity of a silicon solar cell with an AR coating of SiO. (1) without AR coating (2) with SiO coating of optical thickness 0.125 μm and (3) with SiO coating of optical thickness 0.2125 μm. It should be noted that with change in optical thickness of SiO, the position of reflectance minima changes and consequently the spectral sensitivity can be enhanced in a selected spectral region (Koltun, 1981).

As already pointed out, single layer AR coatings have a limitation that the reflectance in the vicinity of λ_{min} increases rapidly yielding a high value of average reflectance. The average reflectance can be further reduced by either using multilayer AR coating or by texturizing the surface of the cell

and then depositing the single AR layer. A number of multilayer AR coatings are possible and have been studied by Koltun (1981) for silicon solar cell. Figure 41 shows the reflectance of a silicon solar cell with a number of single and multiple layer AR coatings. Deposition of the two layer $CeO_2 + SiO_2$ or $ZnS + MgF_2$ AR coating on Si solar cell produces a 55% increase in J_{sc}. Curve 4 of Fig. 41 shows the reflectance profile of a glass encapsulated Si solar cell with a five layer AR coating consisting of $TiO_2 + CeO_2 + ZnO_2 + SiO + Al_2O_3$. The increase in the low reflectance region over the complete range of 0.4-1.1 μm by increasing the number of layers is evident from this curve.

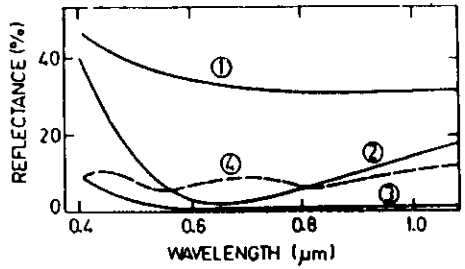

Fig. 41 Reflection profiles showing the reduction in reflection loss of silicon solar cells with 0.15 μm AR coating. (1) without AR coating, (2) CeO_2 or ZnS single layer coating, (3) $CeO_2 + SiO_2$ or $ZnS + MgF_2$ double layer coating, and (4) $TiO_2 + CeO_2 + ZrO_2 + SiO + Al_2O_3$ five layer AR coating along with a layer of transparent adhesive and top glass cover (Koltun, 1981).

(b) *Solar-Thermal Conversion*

The high absorption coefficient for solar radiation of many solar selective coating materials gives rise to high complex refractive index and therefore high reflectance at solar wavelengths. Most of the transparent conducting oxide coatings, which are used as heat mirror coatings, have their refractive indices in the range of 1.75-2.0. Since the refractive index of semiconductors range from 3.0 to 5.0; these oxides can be used as AR coatings for selective absorbers using semiconductor materials. An AR minimum in the visible region can be obtained by properly choosing the thickness of the oxide layer. With appropriate dopant and dopant concentration, the refractive index of the oxide layer can be varied over a range of values so as to optically match a given semiconductor.

The usefulness of SnO_2 and ZnO AR coatings has been investigated in our Laboratory by Reddy et al. (1983) for making solar selective coatings using PbS as an absorber semiconductor deposited on metal substrate. The

thermal emittance of such a system incorporating the AR coating is decided by the combined reflectance behaviour of the oxide layer and the underlying metal substrate. However, only if the IR reflectance of the AR coating is more than that of the underlying metal, the former controls the emittance of the system.

Another way of using AR coating for solar absorber applications is by depositing it over a metallic layer and obtaining a selective AR layer-metal tandem. Metals with good electrical conductivity and low emittance (e.g., Al and Cu) have insufficiently small values of α whereas metals with low electrical conductivity (nickel, tin and iron) have higher α and relatively higher ϵ values than Al and Cu. Now, if we deposit a film of Ni or Sn over Al or Cu, the resulting system will have an α determined by the Ni or Sn coating and an ϵ approaching that of the Al or Cu substrate. When an AR coating is deposited over such a combination, further improvement in the α value will be possible by lowering the reflection losses in the solar region. For example, if we use the optical constants of Ni at $\lambda = 0.589\ \mu$m, we see that an AR layer with a refractive index of $\sim$2.55 is needed. Since the refractive index of 100-400 Å thick Ni film is higher than the bulk Ni, AR layer materials with index lower than 2.55 can also be used. This makes it possible to use materials like Al_2O_3, SiO, SiO_2 and ZrO_2. The energy maximum in the solar spectrum occurs at $\sim$ 0.55 μm, so that the optimum optical thickness, for the AR coating is 0.15 μm and the optimum geometrical thickness will be 0.06 to 0.10 μm for refractive index ranging from 2.5 to 1.5 respectively.

Koltun (1981) has investigated a range of materials which would provide AR coating on a thin ($\sim$ 250-300 Å) layer of Ni on substrates of Cu, Al or its alloys. Table 7 shows the α and ϵ obtained on depositing some of these AR layer-metal tandems.

Table 7

Absorptance and emittance of solar selective absorbers prepared by depositing a variety of AR coatings on copper covered with $\sim$300 Å thick Ni layer. The refractive index and the thickness of the AR layer is also given

Film	n	d(μm)	α	ϵ
MgF_2	1.38	0.15	0.8	0.07
SiO_2	1.45	0.15	0.82	0.07
SiO	1.9	0.15	0.86	0.05
CeO_2	2.2	0.15	0.87	0.05
ZnS	2.3	0.15	0.88	0.05
SiO + MgF_2	1.9 + 1.38	0.15 + 0.75	0.9	0.06
ZnS + MgF_2	2.3 + 1.38	0.15 + 0.75	0.91	0.05

(c) *Cover Glass*

Although the solar reflectance of most glasses does not exceed 5%, its suppression can improve the efficiency of a converter considerably, particularly if several covers are employed. An antireflection coating can reduce the reflection losses by taking the AR material of intermediate refractive index between air (or vacuum) and glass. The ideal coating for glass should have a refractive index of 1.23, but no material is known to have a refractive index of this value. A common AR material is MgF_2 with $n = 1.38$ which gives a reflectance $\sim$ 1.6% at 0.6 μm.. To get closer to the ideal coating, multilayer dielectric coatings described in Section 4.3 are employed. It should be noted that Winegarner (1975) has shown that, because of the breadth of the solar spectrum, a single layer of MgF_2 is superior to a multilayer system in suppressing the surface reflectance of glass cover on a solar collector. Another approach to obtain a broad low reflectance profile of glass is to chemically treat the glass surface so as to obtain a porous SiO_2 layer on its surface (Lin and Zimmer, 1977). An average reflectance of $\sim$ 0.5% has been obtained by leaching of the glass surface to remove the absorbing metallic oxide constituents of glass.

Low index polymer coatings are other examples of AR coatings on glass. A coating of Teflon FEP dispersion ($n = 1.34$) has been investigated by Goldner and Haskal (1975). In case tedlar sheet is used in place of glass, its transmittance can be improved by dipping it in acetophenone (Lin and Zimmer, 1977).

10.3 Heat Mirrors

As already described (Fig. 2(c)), selective coatings which allow the transmission of the visible part and reflection of the IR part of the solar spectrum are called heat mirrors. Such coatings are obviously of considerable interest in controlling the temperature of closed spaces with windows in buildings and of devices (such as solar cells) and instruments (e.g. in a space satellite) exposed to solar radiations. Also, these selective coatings could be used to keep the heat confined within a closed space with windows in a cold environment, or a solar collector.

The selectivity requirements for different applications are clearly expected to be different. Whereas conservation of space heating would require window materials to reflect back the far IR, emitted from within, the conservation of space refrigeration would require window materials to reflect the near IR (above 0.8 μm) from solar radiations. The later requirements are also applicable to solar cell devices. The single layer selective coatings which may have the desirable properties are those of doped and nonstoichiometric oxides of In, Sn, Cd, Zn and their alloys. Typical reflectance and transmittance spectra of In(90): Sn(10) oxide (called I TO), F-doped tin oxide (called FTO) and In-doped ZnO are shown in Fig. 42 The optical spectra are domi-

nated by the electron transport parameters, particularly due to the onset of plasma resonance. The plasma resonance edge can be shifted continuously by doping (see, Fig. 7. Shanthi et al. 1980) from about one to several microns. The presently available trasparent conducting oxide films are, therefore, well suited for keeping heat radiations confined in a building, but offer little advantage to keep out the heat radiations from the sun. For the later application, it is necessary to develop new materials with reflectance edge around 0.7 μm. In a way, partly transparent films of high conductivity metals (e.g. Al, Cu) provide some desirable features at the expense of reduced visible transmission. Among the promising materials which need to be further studied are ReO_3 and Na_xWO_3 (Fan et al. 1974) and rare earth hexaborides. Multilayer interference coatings (Section 4.3) of a variety of materials can provide excellent IR selectivity at desired wavelengths. Such sophisticated coatings are normally used for special applications such as solar cells.

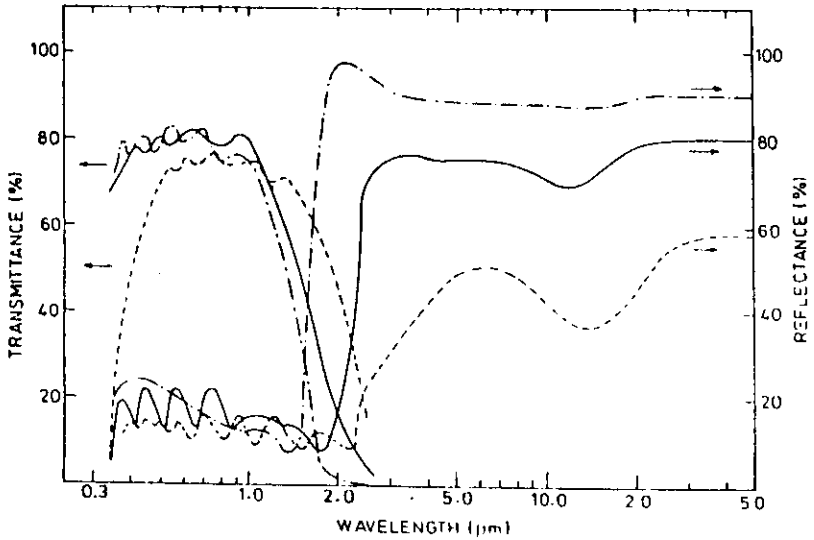

Fig. 42 Spectral reflectance and transmittance of ~ 0.5 μm thick spray pyrolysed indium tin oxide (—·—·—), flourine doped tin oxide (——) and zinc oxide (– – – –) films on glass showing the high transparency visible, near IR region and high reflectivity IR region.

The high IR reflectance of transparent conducting oxides yields low thermal emissivity (Eq. 10.13). A typical variation of the emissivity with resistivity ITO of films is shown in Fig. 43. This variation is represented by an empirical relationship (Frank et al. 1981).

$$\epsilon = 1-(1+0.0053R_{\square})^{-2} \qquad (10.13)$$

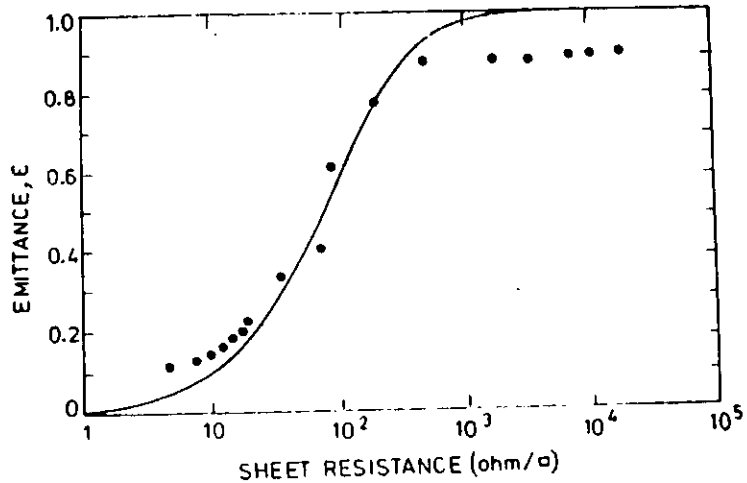

Fig. 43 Variation of thermal emittance at 80°C with the sheet resistance of doped In_2O_3 coating on glass substrate. Solid curve shows the best fit curve according to equation $\epsilon = 1-(1+0.0053R_{\square})^{-2}$ (Frank et al., 1981).

The low emissivity of transparent oxide films can be effectively utilized to increase the efficiency of solar energy conversion in a collector havinga cover glass coated with such a film. The net emissivity of such a system given by

$$\frac{1}{\epsilon_{net}} = \frac{1}{\epsilon_a} + \frac{1}{\epsilon_c} - 1 \qquad (10.14)$$

where ϵ_{net} is the net emittance, ϵ_a and ϵ_c the emittance values of the absorber and cover plate respectively. ϵ_{net} is low whether the absorber is selective or nonselective. However, it is clear that, to compensate for transmission losses in the oxide film, the absorber coating must have as high an absorptance as possible. Thus, a poor absorber in conjunction with an oxide film heat mirror is counterproductive. The necessity of the heat mirror increases with increasing temperature of the absorber such as in the case of concentrator type of collectors because of the highly increased radiation losses. However, the experimental data in this area is rather meagre and unreliable. Finally, selective coatings provide a good method to control the temperarature of instruments inside a satellite. A passive system is based on using coatings of such absorptance and emittance properties as to provide a desired heat balance. If the heat generation or dissipation level changes during the flight of a satellite, it is necessary to employ an active system consisting of mechanically activated surfaces of different and predetermined absorptance/emittance ratios.

10.4 Radiative (Emissive) Cooling

The cooling of surfaces by radiation is a well known phenomenon. To increase the cooling efficiency of the surface, the emittance spectra of the surface and that of the sky have to match. By this we mean that in the 8-13 μm region where the atmosphere is transparent, the emittance of the surface has to be high, so that the radiations are coupled directly to the outside atmosphere thereby increasing the cooling efficiency. The ideal spectral profile for such a surface is shown in Fig. 2(d). With this type of cooling, blackbody can achieve temperatures 10-15°C below ambient.

The infrared transmittance of the sky depends on the meteorological conditions and the zenith angle (Granqvist and Hjortsberg, 1981). For increasing zenith angle, the atmosphere becomes gradually more like a blackbody at all wavelengths. The radiative cooling power and temperature drop below ambient for horizontal surfaces which radiate towards the sky can be evaluated (Granqvist, 1981) for model atmospheres. For a heat transfer coefficient of 1 $Wm^{-2}K^{-1}$, the maximum temperature difference for a device with a non-selective black surface ($\alpha = 1$, $\epsilon = 1$) is 11-21°C and for an IR selective surface is 18-33°C. The desirable optical properties of a surface to exhibit emissive cooling are indicated by the following analysis due to Granqvist et al. (1981).

Considering a plane surface facing the clear sky, we can write the incoming and outgoing radiative powers per unit area as

$$P_{in} = \int_0^\infty \epsilon_a(\lambda)\epsilon_s(\lambda)W(T_a, \lambda)\, d\lambda \qquad (10.15)$$

$$P_{out} = \int_0^\infty \epsilon_s(\lambda)W(T_s, \lambda)\, d\lambda \qquad (10.16)$$

where W is the Planck function, subscripts a and s refer to atmosphere and surface respectively. The radiative cooling power can be written as

$$\begin{aligned} P_{cool} &\equiv P_{out} - P_{in} \\ &\cong \epsilon_s\sigma(T_s^4 - T_a^4) + \int_0^\infty W(T_a, \lambda)[1 - \epsilon_a(\lambda)\epsilon_s(\lambda)]\, d\lambda \\ &\cong \epsilon_s\sigma(T_s^4 - T_a^4) + (1 - \epsilon_{a2})]\epsilon_{s2}\int_8^{13\mu m} W(T_a, \lambda)\, d\lambda \end{aligned} \qquad (10.17)$$

where

$$\epsilon_{s2} = \frac{\int_8^{13\mu m} W(T_a, \lambda)[1 - R(\lambda)]\, d\lambda}{\int_8^{13\mu m} W(T_a, \lambda)\, d\lambda}$$

Here σ is the Stefan-Boltzmann constant, ϵ_{s2} is the average atmospheric emittance.

To achieve good cooling (that is, the largest temperature difference that can be achieved), $\eta = \epsilon_{s2}/\epsilon_s$ must be maximum so that the cooling power is governed by ϵ_{s2}. Such surfaces have been produced by evaporating SiO (Granqvist et al. 1982) on aluminized glass sheet. The profile depends on the thickness as shown in Fig. 44(a). The reflectance minimum in 8-13 μm is due to strong lattice absorption combined with destructive interference. Granqvist has shown that using such surfaces, temperatures ~14°C below the ambient can be obtained. The same authors have prepared Si_3N_4 films on Al coated glass substrates [Fig. 44(b)]. These coatings showed higher values of ϵ_{s2}.

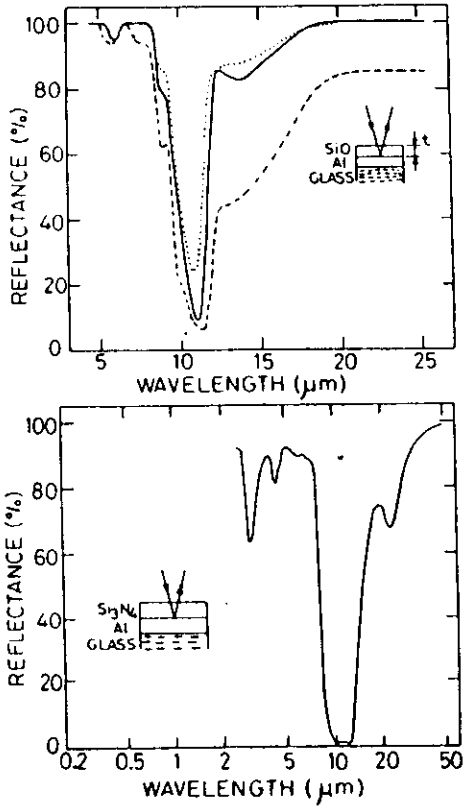

Fig. 44 Measured spectral reflectance of selective surfaces for radiative cooling. (a) SiO on thick aluminium film on glass for different thicknesses of SiO; 0.8 μm (– – – – –), 1.0 μm (———) and 1.2 μm (· · ·) and (b) Si_3N_4 film on thick aluminium coated glass substrate (Granqvist et. al., (1982).

Spitz (1980) has carried out studies on radiative cooling of evaporated Te on polypropylene film. They found that a volume of 12 m^3 containing 60 litres of water could be maintained at 4°C while the ambient temperature varied from 7 to 18°C.

10.5 Selective Coatings for Incandescent Lamps

Heat mirror coatings are also useful in making a considerable saving in the energy required in heating the filament of the incandescent lamp and reducing the unwanted heat radiation in the area illuminated by the lamp. In a conventional lamp, the tungsten filament is at 2650 K and emits about 90% heat and 10% visible radiation. Normally both the heat and light pass through the glass envelope. An ideal solution to improve the efficiency of conversion of electrical energy to light energy is to coat the tungsten filament with a selective heat mirror coating. Materials such as LaB_6 have a high visible transparency but the emissivity is also high at the high operating temperatures. Thus, there is an urgent need for the development of other rare earth hexaboride coatings for such an application.

A more practical solution is to apply a heat mirror selective coating on the glass envelope of the lamp. With the help of such a coating, the thermal part can be reflected back to heat the filament and only the visible part will be transmitted (see the inset of Fig. 46). Thus power consumed to heat the filament is reduced considerably and a cool visible illumination is received. To have an effective heat mirror coating, the cut-off wavelength of the selective heat mirror should be ~0.7 μm. Frank et al. (1981) have studied the usefulness of tin doped In_2O_3 heat mirror coating for this application. Figure 45 shows the spectral transmission and reflection profiles of such a coating having a carrier concentration of 15×10^{20} cm^{-3} ($\lambda_p \sim 1.2$ μm) and an AR overlayer of 0.1 μm thick SiO_2. Also shown in this figure are the 2650 K Planck's spectrum and the visual sensitivity curves. Figure 46 shows a plot of calculated effective visible transmittance, T_{EFF}^{VIS} (by calculating the weighting functions for equal log λ intervals from Fig. 45) and the effective non-transmitted filament radiation $1 - T_{EFF}^{2650\,K}$, which is a measure of the IR reflectance (rejection), as a function of the In_2O_3 layer thickness. Since a gain in one feature causes a loss in the other, an optimum thickness must be used.

Because of the overlap of filament Planck's-spectrum and visual sensitivity curve and unavailability of In_2O_3 layers having λ_p less than 1 μm (owing to the limit imposed by the free electron density obtainable in In_2O_3), it becomes difficult to separate visible and IR radiations. This problem is not there in the case of In_2O_3 layer used in a sodium lamp because of well separated Na emission and 540 K heat radiation spectra. A better coating for an incandescent lamp is that of a TiO_2-Ag-TiO_2 multilayer stack. The transmission and reflection profiles for this stack is also shown in Fig. 45. It is clear that, with the help of this coating, the IR can be completely eliminated. The position

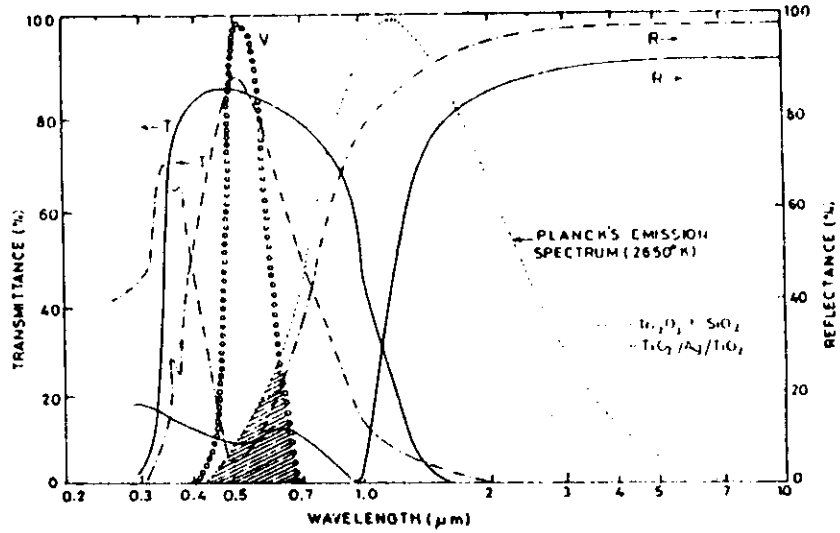

Fig. 45 Spectral variation of transmittance and reflectance of two heat mirror coatings incandescent bulbs. ——, In_2O_3 coating with a protective 0.1μm layer of SiO_2 and —·—·—, TiO_2/Ag/TiO_2 coating. Also shown are the Planck's emission spectrum for 2650 K body (filament) and the visual sensitivity spectrum (V). The shaded area shows the overlap between these two spectra which is a measure of the useful radiation for illumination emitted by the lamp filament. (Frank et al., 1981).

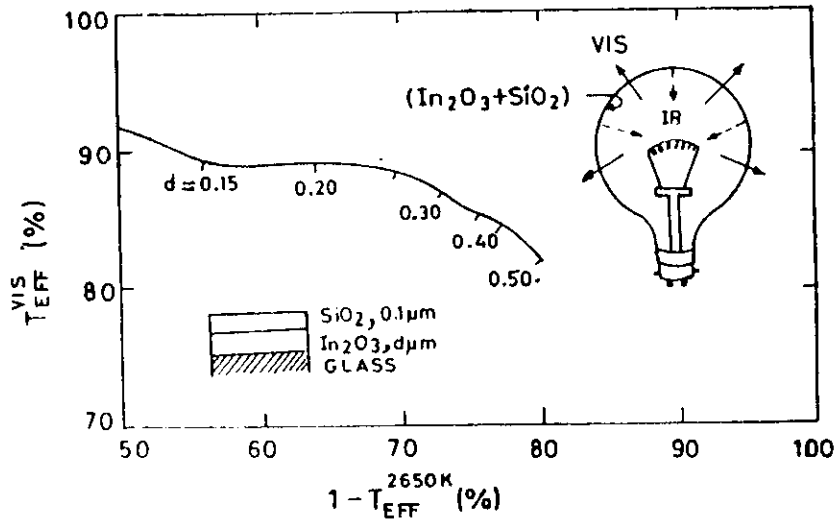

Fig. 46 Dependence of effective visible transmittance and 1-T_{EFF}^{2650} (non-transmitted radiation of filament at 2650 K) on the thickness of the In_2O_3 coating, carrier concentration of $In_2O_3 = 15 \times 10^{20}$ cm^{-3} and the thickness of additional SiO_2 film is 0.1μm (Frank et al., 1981)

of the higher λ transmission edge and reflectance step can be varied by adjusting the thickness of the three layers (Fan 1981). Using this multilayer stack, Spura et al. (1980) have shown a saving of 50% on electricity for the same light output. These heat mirror coatings can be deposited on both inside or outside of the glass envelope with only minor sacrifice in the performance.

11. CONCLUDING REMARKS

(1) Selective coatings of nearly any desired solar spectral reflectance and transmittance, and thermal emittance characteristics can be designed by standard optical modelling techniques and tailor made in the form of multilayers by a number of deposition processes.

(2) Several effective medium theories have been developed to predict the dielectric functions and optical behaviour of composite structure selective coatings. Also, a number of optical absorption processes taking place in different structures have been identified. The mathematical analysis, however, continues to be empirical in nature. A more fundamental approach to this problem based on fundamental parameters of atomic polarizability and percolation processes need to be developed. Such an approach would necessarily involve very large number of calculations.

(3) Most practical and effective selective coatings have a complex microstructure based on a mixture of tandem, gradient index, and composite structures. Such structures include blacks of chrome, nickel and cobalt, and pigmented aluminium. Solar absorptance $\sim$0.95 and emittance (at 100°C) of $\sim$0.1 are readily available for several coatings on large surfaces.

(4) Numerous coating materials have been studied and utilized. Materials with high ($\cdot$ 300°C) temperature stability are few and far between. Such materials with optimized optical and thermal properties pose a challenge to materials research in the area of new composites or multicomponent compounds.

(5) The surface roughness and topological details, and film microstructure play a very dominant role in determining the properties of selective surfaces. Techniques for measurements of roughness and topographical details need to be improved. Further related theoretical analysis techniques have to be refined.

(6) Among the applications of selective coatings, the efficiency of conversion by solar-thermal collectors is decidedly and markedly improved in the temperature range 100-500°C. Such applications as emissive cooling, improvement of the efficiency of tungsten incandescent lamps and passive cooling of buildings are still in the proving grounds, partly because of the lack of appropriate and economic structures. These problems pose a challenge for future R/D work in the area.

(7) The choice of an effective selective coating, substrate material and deposition process depends on (i) application, (ii) availability and economics of materials and chemicals, (iii) energy input, and (iv) desired system life.

(8) Due to numerous technical, economic and commercial variables, it is not advisable to make cost projections at this stage. However, it should be noted that, at today's costs, typical estimated costs for black nickel and chromium are \$ 2/m^2 and \$ 10/m^2, respectively. Though these costs are higher (by no more than a factor of 2) than that for nonselective black paints, these are still only a fraction of the cost of the total collector system. The significant improvement in the efficiency of conversion made possible by selective coatings thus makes their use absolutely essential and desirable.

(9) Though used in a thermal conversion technology of only medium level sophistication (at least in the 100-300°C range), the selective coating deposition technology is a high level technology. In other words, good and precise control of deposition parameters evolved on the basis of extensive R/D work utilizing a host of very sophisticated analytical facilities is required.

12. ACKNOWLEDGEMENTS

The work reported from our laboratory is based on the following Ph.D. theses of our following students:

(1) Selective Black Surfaces for Photothermal Conversion of Solar Energy —by P.K. Gogna

(2) Chemically Deposited Multilayer Selective Surfaces —by G.B. Reddy

(3) Spectrally Selective Black Cobalt Coatings —by K. Chidambaram

(4) Electroless Deposited Blacks and Metal Pigmented Anodized Aluminium as Solar Selective Coatings —by S.N. Kumar

REFERENCES

Agnihotri O.P. and Gupta B.K. (1981), "Solar Selective Surfaces", (John Wiley & Sons, New York).

Allward J.F., Fong C.Y., Batanouny M.L. and Wooten F., (1975), Phys. Rev., *B12*, 1105.

Andersson A., Hunderi O. and Granqvist C.G., (1980), J. Appl. Phys. *51*, 754.

Aveline A. and Bonilla I.R., (1981), Solar Energy Materials *5*, 211.

Balickenderfer R., Lincoln R.L. and Derdorff D.K., (1976), U.S. Bureau of Mines, Washington. Report No. RI—8167.

Behaghel J.M., Berthier S., Lafait J. and Revory J. (1979), Solar Energy Materials *1*, 201.

Behaghel J.M., Berthier S. and Lafait J. (1981), J. de Phys. (Paris), *42*, 355.

Bergman D.J. (1978), Phys. Rep. *43*, 377.

——— (1979), Phys. Rev. *B 19*, 2359.

——— (1980), Phys. Rev. Lett., *44*, 1285.

——— (1981), Phys. Rev. *B23*, 3058.

——— (1982), Ann. Phys. *138*, 78.

Berthier S. and Lafait J. (1979), J. de Phys. (Paris) *40*, 1093.

Beucherie P. (1980), Electric Power Systems Research *3*, 125.

Bliss R.N. (1959), Solar Energy *3*, 55.

Booth D.C. and Seraphin B.O., (1979), D.O.E. Absorber Surfaces for Solar Receiver Conf., Boulder, Jan. 1979.

Bradford A.P. and Hass G. (1963), J. Opt. Soc. Am., *53*, 1096.

Bruggeman D.A.G. (1935), Ann. Phys. *24*, 636.

Carlson T.A. (1975), "Photoelectron and Auger Spectroscopy" (Plenum Press, New York).

Cathro K.J., (1981), Solar Energy Material *5*, 317.

Chaudhary C. and Sehgal H.K., (1982), Solar Energy *28*, 25.

Chidambaram K., Malhotra L.K. and Chopra K.L., (1982), Thin Solid Films *87*, 365.

Chidambaram K., Malhotra L.K. and Chopra K.L., (1983), (unpublished).

Chopra K.L., (1969), "Thin Film Phenomena", (McGraw-Hill, New York).

Chopra K.L. and Inderjeet Kaur, (1982), "Thin Film Applications", (Plenum Press, New York).

Chopra K.L., Kainthla R.C., Pandya D.K. and Thakoor A.P., (1982), in "Physics of Thin Films", Vol. 12, Ed., G. Hass, M.H. Francombe and J.L. Vossen, (Academic Press, New York).

Chopra K.L., Pachori R.D. and Inderjeet Kaur, (1983) (unpublished).

Cohen R.W., Cody G.D., Coutts M.D. and Abeles B., (1973) Phys. Rev., *B8*, 3689.

Coumo J.J., Zeigler J.F. and Woodall J.M., (1975) Appl. Phys. Lett, *26*, 557.

Cox J.T. and Hass G., (1958) J. Opt. Soc. Am, *48*, 677.

Cox J.T., Hass G. and Ramsey J.B., (1964) J. de Phys. (Paris) *25*, 250.

Craighead H.C., Bartynski R. and Buhrean R. (1979) Solar Energy Materials *1*, 105.

Curtis H.B., (1966) J. Space Craft *3*, 383.

Czanderna A.W., (1975) "Methods of Surface Analysis" (Elsevier Scientific, New York).

Dobrowlski J.A., (1966) Paper presented at 7th General Meeting of the ICO Paris.

Dobrowlski J.A. and Lowe D., (1978) App. Opt. *17*, 3039.

Donnodien A. and Seraphin B.O., (1978) J. Opt. Soc. Am. *68*, 292.

Driver P.M. and McCormick P.G., (1978) Proc. Int. Solar Energy Congress, New Delhi, India. Ed., F. deWinter and M. Cox (Pergamon Press, New York). p. 881.

Driver P.M. and McCormick P.G., (1982) Solar Energy Materials, *6*, 381.

Dutta V., Chidambaram K., Reddy G.B., Mukerjee A.K., Pandya D.K., Malhotra L.K. and Chopra K.L., (1980) Proc. National Solar Energy Convention, Annamalainagar, India (Allied Publishers, New Delhi, 1980), p. 300.

Fan J.C.C., Reed T.B. and Goodenonga J.B., (1974) Proc. of 9th Int. Soc. Energy Conven. Engg. Conf., San Francisco, New York. p. 341.

Fan J.C.C. and Zavracky P.M., (1976) Appl. Phys. Lett. *29*, 478.

Fan J.C.C. and Sprua S.A., (1977) Appl. Phys. Lett. *30*, 511.

Fan J.C.C. (1981) Thin Solid Films *80*; 125.

Feinleib J., Scouler W.J. and Ferretti A., (1968) Phy. Rev., *165*, 765.

Frank G., Kauer E. and Kostlin H., (1981) Thin Solid Films, *77*, 107.

Gadgil S.B., Thangaraj R., Iyer J.V., Sharma A.K., Gupta B.K. and Agnihotri O.P., (1981) Solar Energy Materials *5*, 129.

Gaumer R.E., Hohnstreiter G.F. and Vanderschmidt G.F., (1963) in "Measurement of Thermal Radiation Properties of Solids". NASA-SP-31, Washington DC, p. 117.

Gaumer R.E. and Stewart J.V., (1963) Ibid, p. 127.

Geheva K.A., Chain E.E. and Seraphin B.O., (1980) Solar Energy Materials *3*, 415.

Giaquinta G. and Mancini N.A., (1978) Intl. Symp. Workshop on Solar Energy, Cairo, Egypt.

Gillette R.B., (1960) Solar Energy *4*, 24.

Gittleman J.I., Sichel E.K. and Arie Y., (1979) Solar Energy Materials *1*, 93.

Gogna P.K., Pandya D.K. and Chopra K.L., (1978) Proc. Internat. Solar Energy Congress, New Delhi, Eds. Winter and Cox (Pergamon Press, New York) p. 842.
Gogna P.K. and Chopra K.L., (1979a) Thin Solid Films *57*, 299.
Gogna P.K. and Chopra K.L., (1979b) Solar Energy *23*, 405.
Gogna P.K. and Chopra K.L., (1979c) Thin Solid Films, *63*, 183.
Gogna P.K. and Chopra K.L., (1979d) National Solar Energy Convention, Bombay, India (Allied Publishers, New Delhi).
Gogna P.K., (1980) Ph.D. Thesis Indian Institute of Technology, New Delhi, India.
Gogna P.K. Mullick S.C. and Chopra K.L., (1980) Int. J. Energy Research *4*, 317.
Goldnar R.B. and Haskar H.M., (1975) Appl. Opt. *14*, 2328.
Granqvist C.G. and Hunderi O., (1977) Phys. Rev., *B16*, 3513.
Granqvist C.G. and Hunderi O., (1797) Appl. Phys. Lett. *32*, 798.
Granqvist C.G., Anderson A. and Hunderi O., (1979) Appl. Phys. Lett. *35*, 268.
Granqvist C.G., (1981) Appl. Optics *20*, 2606.
Granqvist C.G. and Hjorstberg A., (1981) J. Appl. Phys. *52*, 4205.
Granqvist C.G., Hjorstberg A. and Erikson T.K., (1982) Thin Solid Films *90*, 187.
Grimmer D.P., Heir K.C., McCerary W.J., (1978) J. Vac. Sci. Technol. *15*, 59.
Groenveld P., (1970) Chem. Engg. Sci. *25*, 1259.
Gupta C.L. and Garg H.P., (1967) Solar Energy *11*, 1.
Gupta B.K., Tiwari F.K., Agnihotri O.P. and Mathur S.S., (1979) Intl. J. Energy Res., *3*, 371.
Hahn R.F. and Seraphin B.O., (1978) in Physics of Thin Films Vol. 10 Ed. G. Hass (Academic Press, New York).
Hanai T., (1960) Kolloid Zeitschr, *171*, 23.
Harris L., (1962) J. Opt. Soc. Am., *52*, 223.
Hari M. and Yonezawa F., (1977) J. Phys. C. Solid State Physics *10*, 229.
Harding G.L., (1976) J. Vac. Sci. Technol., *13*, 1070.
Harding G.L., (1978) J. Vac. Sci. Technol. *15*, 65.
Hashim Z. and Shtrikman S., (1962) J. Appl. Phys. *33*, 3125.
Heavens O.S. (1965) "Optical Properties of Thin Solid Films" (Dover Publ. New York).
Hembach R.J., Hemmerdinge L. and Katz A.J., (1963) in "Measurement of Thermal Radiation Properties of Solids". Ed., J.C. Richmond NASA-SP-31 Washington DC.
Hirsh P.B., Howie A., Nicholson R.B., Pashley D.W. and Whelan M.J., (1965) "Electron Microscopy of Thin Crystals" (Butterworths, London).
Homhaul C., Inal O.T., Murr L.E., Torma A.E. and Gundiler I., (1981) Solar Energy Materials *4*, 309.

Hottel H.C. and Woertz B.B., (1942) ASME Trans. *64*, 91.
Hottel H.C. and Unger T.A., (1959) Solar Energy *3*, 10.
Hottel H.C. and Whillier A., (1955) Trans. Conf. on the use of Solar Energy *2*, 74 (University of Arizona Press).
Horwitz C.M., (1974) Optics Communication *11*, 210.
Johnson P.B. and Christy R.W., (1974) Phys. Rev. *B9*, 5056.
Kane P.F. and Larrabee G.B., (1974) "Characterization of Solid Surfaces", (Plenum Press, New York).
Kerkar M., (1969) "Scattering of Light and other Electromagnetic Radiations" (Academic Press, New York).
Kokoropoulas P., Salam E. and Daniels F., (1959) Solar Energy *3*, 19.
Koltun M.M., (1981) "Selective Optical Surfaces for Solar Energy Converters" (Allerton Press, New York).
Kumar S.N., Malhotra L.K. and Chopra K.L., (1980) Solar Energy Materials *3*, 519.
Kumar S.N., Malhotra L.K. and Chopra K.L. (1983) Solar Energy Materials *7*, 439.
Kruidhoff W. and Van der Leij M., (1980) Solar Energy Materials *2*, 69.
Lafait J., Behaghel J.M., Berthier S. and Rivory J., (1981) J. de Phys. (Paris) *42* C1-133.
Lamb W., Wood D.M. and Asheroft N.W., (1978) AIP Conf. Proc. *40*, 240.
Lamb W., (1980) Phys. Rev. *B22*, 6364.
Lampert C.M. (1979) Solar Energy Materials *1*, 319.
Lampert C.M., (1979a) Ph.D. Thesis (University of California).
Landauer R., (1978) AIP Conf. Proc. *40*, 2.
Landau L.D. and Levich V.C., (1942) Acta Physica Chemica URSS *17*, 41.
Li V.V., Faiziev A., Gazier V.K. and Trukhov V.S., (1977) Appl. Solar Energy *13*, 40.
Liddell H.M., (1981) "Computer Aided Techniques for the Design of Multilayer Filters" (Adam Hilger Ltd., London).
Lin R.J.H. and Zimmer P.B. (1977) Techn. Rept. Co. 0 2930-12 (Honeywell Corporation).
Lofving S. (1981) Solar Energy Materials *5*, 103.
Lowenheim F.A. (1978) "Electroplating Fundamentals of Surface Finishing" (McGraw-Hill, New York).
Maissel L.I. and Glang R. (1970) "Handbook of Thin Film Technology" (McGraw-Hill, New York).
Marchini R. and Gandy R (1978) J. Appl. Phys. *49*, 390.
Martin P.J. Netterfield R.P. and Sainty W.G. (1981) Thin Solid Films *87*, 203.
Mattox D.M. and Kominaik G.J. (1975) J. Vac. Sci. Technol. *12*, 182.
Mattox D.M. (1975) Sandia Labs, NMSAND 75-0361.
Maxwell Garnett J.C. (1904) Phil. Trans. Roy Soc. (London) *A 203*, 385.

Maxwell Garnett J.C. (1906) Phil. Trans. Roy. Soc. (London) *A 205*, 237.
McDonald J. (1971) "Metal-Dielectric Multilayers" Monographs on Applied Optics no. 4 (Adam Hilger, London).
McDonald G.E. (1975) Solar Energy *17*, 119.
McDonald G.E. (1980) Thin Solid Films *72*, 83
McKenzie D.R. (1979) Thin Solid Films *62*, 317.
McKenzie D.R. and Zybert J.J. (1981) Thin Solid Films *85*, 191.
Macleod H.A. (1969) "Thin Film Optical Filters" (Adam Hilger, London)
McMohan T.J. and Jasperson S.N. (1974) App. Opt. *13*, 2750.
Meinel A.B., Mckenney D.B. and Beauckamp W.T. (1975) Tech. Rept., NSF-RANN/SE/GE/41895.
Meinel A.B. and Meinel M.P. (1976) "Applied Solar Energy—An Introduction" (Addison-Wesley, Reading Mass).
Messier R, Krishnaswamy S.V., Gilbert L.R. and Swab P. (1980) J. Appl. Phys., *51*, 1611.
Milton G.W. (1980) App. Phys. Lett. *37*, 300.
Milton G.W. (1981a) Phys. Rev. Lett. *46*, 542.
Milton G.W. (1981b) J. Appl. Phys. *52*. , 5286.
Milton G.W. (1981c) J. Appl. Phys. *52*, 5294.
Niklasson G.A. and Granqvist C.G. (1978) J. Appl. Phys., *49*, 3512.
Niklasson G.A. and Granqvist C.G. (1979) J. Appl. Phys. *50*, 5500.
Niklasson G.A. and Granqvist C.G. (1981) Solar Energy Materials *5*, 173.
Niklasson G.A. and Granqvist C.G. and Hunderi O. (1981) Appl. Opt. *20*, 26.
Niklasson G.A. and Granqvist C.G. (1982) App. Phys. Lett. *41*, 773.
Niklasson G.A. (1982) Ph.D. Thesis Chalmers University of Technology, Gotebarg, Sweden.
Olson O.H. (1963) Appl. Opt. *2*, 109.
O'Neill P., Doland C. and Ignatiev A. (1977) App. Opt., *16*, 2822.
Pandya D.K. and Chopra K.L. (1981) Vacuum-Surfaces-Thin Films Ed. K.L. Chopra and T.C. Goel, (Vanity Books, Delhi).
Pasquetti R. (1975) Ph.D. Thesis, University of Provence, Marseille, France.
Payan R. and Rasigni G. (1964) J. Phys. Radium *25*, 92.
Pegis R.J. (1961) J. Opt. Soc. Am., *51*, 1225.
Peterson R.E. and Ramsey J.R. (1975) J. Vac. Sci. Technol. *12*, 471.
Pettit G.D., Cuomo J.J., Distejano T.H. and Woodall J.M. (1978) IBM Res. Rev. *22*, 372.
Pettit R.B. and Sowell R.R. (1976) J. Vac. Sci. Technol. *13*, 596.
Ping Sheng (1980a) Phys. Rev. Lett. *45*, 60.
(1980b) Phys. Rev. *B22*, 6364.
Polder D. and van Santen J.H. (1946) Physica *12*, 257.
Potdar H.S., Pavaskar N., Mitra A and Sinha A.P.B. (1981) Solar Energy Materials *4*, 291.

Potdar H.S., Hegde R.I., Badrinarayana S. and Pavaskar N. (1982) Solar Energy Materials *6*, 183.
Reddy G.B., Dutta V., Pandya D.K. and Chopra K.L. (1981) Solar Energy Materials *5*, 187.
Reddy G.B., Pandya D.K. and Chopra K.L. (1982) Proc. National Solar Energy Convention, New Delhi (Allied Publishers, New Delhi) p. 8.024.
Reddy G.B., Pandya D.K. and Chopra K.L. (1983) (to be published).
Richmond J.C. (1979) High temperatures—High Pressures *11*, 355.
Ritchie I.T. and Window B. (1977) App. Optics *16*, 1438.
Ritchie I.T., Sharma S.K., Valignant I. and Spitz J. (1979/1980) Solar Energy Materials *2*, 167.
Schmidt R. N. and Park K.C. (1965) Appl. Opt. *4*, 917.
Schulgasser K and Hashin Z. (1976) J. Appl. Phys., *47*, 424.
Seely J.S., Liddell H.M. and Chen T.C. (1973) Opt. Acta *20*, 641.
Seraphin B.O. and Meinel A.B. (1976) "Optical Properties of Solids—New Developments" Ed. B.O. Seraphin (North Holland, Amsterdam).
Seraphin B.O. (1979) "Topics in Applied Physics" Vol. 31 Ed. B.O. Seraphin (Springer-Verlag, New York).
Seraphin B.O. (1982) Thin Solid Films *90*, 395.
Shanthi E., Banerjee A., Dutta V. and Chopra K.L. (1980) J. Appl. Phys. *51*, 6243.
Sievers A.J. (1978) J. Opt. Soc. Am. *68*, 1505.
Sikkens M. (1981) Solar Energy Materials *5*, 55.
Sikkens M. (1982) Solar Energy Materials *6*, 415.
Simenis F., Van der Leij M. and Hoogendoorn C.J. (1979) Solar Energy Materials *1*, 221.
Smith G.B. (1977) J. Phys. D. Appl. Phys. *10*, 139.
(1979) Phys. Lett. *35*, 668.
Smith G.B. and Ignatiev A. (1980) Solar Energy Materials 3, 461.
Smith G.B. and Ignatiev A. (1981) Solar Energy Materials *4*, 119.
Spitz J. (1977) Thin Solid Films *45*, 31.
Spitz J. (1980) Activities Non Nucleaires, Centre d'Etudes Nucleaires de Grenoble, France.
Spura S.A., Fontana R.P., Hurwilt S. Aronson A. Brett. J., Walsh P.J., Thouret W.E. and Thorington L. (1980) Optical Spectra, March 1980 p. 57.
Stroud D. (1975) Phys. Rev. *B12*, 3368.
Swab P., Krishnaswamy S.V. and Messier R. (1980) J. Vac. Sci. Technol. *17*, 362.
Tabor H. (1967) "Low Temperature Engineering Applications of Solar Energy" Ed. R.C. Jordan (ASHRAE, New York).
Trotter D.M. Jr. and Sievers A.J. (1979) Appl. Phys. Lett. *35*, 374; J. Opt. Soc. Am. *69*, 1400.

Thornton J.A., Penfold A.S., Lamb, J.L. (1980) Thin Solid Films *72*, 101.
van der Leij M. (1978) J. Electrochem. Soc., *125*, 1361.
van de Leest R.E., van der Werf and Kriji G. (1981) Solar Energy *26*, 551.
Vaidyanathan J., Gadgil S.B., Sharma A.K., Gupta B.K. and Agnihotri O.P. (1981) Solar Energy Materials *6*, 113.
Vossen J.L. and Kern W. (1978) "Thin Film Processes" (Academic Press, New York)
Whillier A. (1967) "Low Temperature Engineering Applications of Solar Energy" Ed. R.C. Jordan (ASHRAE. New York).
Williams W.S. (1957) Prog. Solid State Chem. *6*, 11.
Williams D.A., Lappin R.A. and Duffie J.A. (1963) J. Eng. Power *85A*, 213.
Willrath H. and Gammon R.B. (1978) Solar Energy *21*, 193.
Winegarner R.M. (1975) Optical Spectra June.
Window B., Ritchie I.T. and Cathro K.J. (1978) App. Opt. *17*, 2637.
Zajac G. and Ignatiev A. (1979) J. Vac. Sci. Technol. *16*, 233.
Zajac G. and Ignatiev A. (1982) Thin Solid Films *91*, 131.